University of Nottingham
UK | CHINA | MALAYSIA

# Assessing *Cupriavidus necator* H16 as a chassis for the production of PQQ-dependent enzymes using membrane bound glucose dehydrogenase.

Thesis submitted to the University of Nottingham for the degree of Master of Research
November 2025

Andrei Mihai Birtalan
20380544

Supervisors: Dr Klaus Winzer, Dr Katalin Kovacs

School of life sciences, Faculty of Medicine and Health sciences
University of Nottingham

# Declaration:

Unless otherwise acknowledged, the work presented in this thesis is my own.
No part has been submitted for another degree at the University of Nottingham
or any other institute of learning.

Andrei Birtalan 2025

# Acknowledgements:

To my supervisors, Dr Klaus Winzer, and Dr Katalin Kovacs. Thank you for your endless guidance, thorough support.

To Kwadwo Nketia Opoku, thank you for your counsel and aid in the lab, you made a daunting experience as easy as it can be.

Abstract

Rising global temperature caused by greenhouse gas emissions has reached an environmental tipping point signifying the uphill struggle presented by undoing centuries of explosive economic and societal growth fuelled by the fossil fuel industry and the titanic amounts of greenhouse gas emissions released. A major contributor to this is the chemical industry which has adopted a linear model, utilising non-renewable fossil fuel stocks as the basis for the majority of chemical production worldwide including plastics, pharmaceuticals, and solvents. An emerging and promising solution for this problem is the employment of microbial cell factories capable of producing chemicals from feedstocks such as biomass, industrial off gasses, municipal waste, and atmospheric $CO_2$. *Cupriavidus necator* H16 provides an attractive model platform due to its metabolic robustness and redundancy making it conducive of modifications and subsequent optimisation of metabolic pathways; as well as a rapidly expanding synthetic biology toolkit. The diverse *C. necator* H16 genome possesses a pyrroloquinoline quinone biosynthesis operon under an unknown promoter, as well as putative quinoproteins, making this a promising chassis for quinoprotein pathways in order to expand available feedstocks.

This study aimed to evaluate *C. necator* H16 as a chassis for quinoprotein production, and PQQ dependent metabolic pathways, through the coupling of the native PQQ biosynthetic operon with a medium strength synthetic promoter, and using membrane bound-PQQ dependent glucose dehydrogenase (mGDH) from *Gluconacetobacter diazotrophicus* as a non-toxic, proof of concept, which is also easily selectable due to the inability of *C. necator* to utilise glucose except when specific mutations arise spontaneously in the N-acetylglucosamine phosphotransferase system to confer glucose utilisation. If possible, the resultant strain would be subjected to adaptive laboratory evolution to elucidate potential bottlenecks and strategies for further optimisation. Firstly, the prevalence of glucose utilisation arising spontaneously was determined in a medium relevant to this study, mGDH was successfully introduced into *C. necator* on a broad-host range vector for simplicity, and by chromosomal insertion to replace the locus of possible mutations providing glucose utilisation. The PQQ biosynthetic operon was coupled with the P21 synthetic promoter; alongside this as a back-up for supplying intracellular PQQ, a putative PQQ import system was identified but shown to not be constitutively active. Active mGDH was not observed in any strain presumably due to species specific hurdles such as DNA sequence or chaperone incompatibilities.

# Table of Contents

Abbreviations:

ADH: Alcohol dehydrogenase

ALE: Adaptive Laboratory Evolution

CBB: Calvin-Benson-Bassham cycle

CFU: Colony Forming Unit

Cl: Cleared lysate

CTQ: Cysteine tryptophylquinoline

ED: Entner Doudoroff

FAD: Flavin Adenine Nucleotide

GHG: Greenhouse Gas

HPLC: High performance liquid chromatography

MCF: Microbial cell factory

MDH: Methanol dehydrogenase

MF: membrane fraction

mGDH: PQQ-dependent membrane bound glucose dehydrogenase

MOPS: 3-(N-morpholino)propanesulfonic acid

$NAD^+$: Nicotinamide Adenine Dinucleotide

PBS: Phosphate buffered saline

PCR: Polymerase chain reaction

PHA: Polyhydroxyalkanoate

PHB: Polyhydroxybutyrate

PQQ: Pyrroloquinoline quinone

$PTS_{nag}$: N-acetylglucosamine phosphotransferase system

RBS: Ribosome binding site

RFP: Red fluorescence protein

SF: Soluble fraction

TTQ: Tryptophan tryptophylquinoline

WC: Whole cell

# 1. Introduction

Global warming due to greenhouse gas (GHG) emissions is a problem (1). Global average surface temperature has risen by 1.46°C since the pre-industrial average (1800-1900 C.E.), resulting in cascading effects including erratic and enhanced weather patterns, sub average global snow cover, and the 7$^{th}$ lowest recorded sea-ice coverage in 2024 (2). This prolonged state ensued global sea levels to rise 10.1 cm between 1993 and 2023 alone contributing to coastal erosion, land poisoning due to saltwater intrusion, and flooding (3). Less sea ice and increased surface temperature also meant an increase of 1.2°C in the average sea temperature in the same period (3, 4). Numbers paint an impersonal and almost abstract picture not truly conveying the issue in this case, to conceptualise the problem it may help to look at it in terms of significant observable consequences which are difficult to explain with any reasoning other than climate change, so called tipping points (5).

According to a report by the University of Exeter, we are currently experiencing the first of a few climate tipping points, this has taken the form of the fourth, and largest, mass coral bleaching event currently affecting 80 % of all reefs (5). This is a direct consequence of human mediated global warming pushing sea temperatures above 1.2°C since pre-industrial era; with the international Paris Climate agreement to limit global warming by 1.5°C being far above the thermal tolerance limit of coral reefs meaning even if international goals are hit, all coral reefs except isolated patches are likely to die out (5). Coral reefs impact the livelihood of up to a billion people, and sustain around 1 million species in terms of habitat or food source, the loss of the reefs would be unlikely to destabilise countries but it will have significant non-reversible effects on these people and animals, however its significance should not be understated as at the very least it is an indication of what will happen to other ecosystems which, while more robust and resilient to changes in temperature and climate, have their own limits of adaptability (5). Current predictions for future tipping points include; rapid forest degradation of the Amazon rainforest due to tripartite pressure coming from human deforestation, rising sea levels affecting the banks of the amazon river, and rising surface temperature disturbing complex ecosystems (5); and accelerated glacial melting impacting local populations through flooding and decreased industry, as well as potential negative effects on fish breeding populations, specifically salmon, in glacially influenced environments (5).

The situation is not hopeless. Policies are getting introduced to curb GHG emission where possible; significant improvements in renewable energy, and energy storage have released some of the burden of energy away from fossil fuels, one of the largest contributors to GHG emissions at over 70 % of global emissions (5, 6). The second largest contributor is the agricultural industry in the form of fertiliser manufacture, and general farm practices at 12 % (6, 7). The third being the chemical industry, which was afforded rapid development in the industrial age off the back of the booming oil industry, which lead to the development of revolutionary materials and an attitude of 'improving lives through chemistry', fostering reliance on petrochemicals (6, 8, 9). Unavoidably, the primary petrochemicals contain carbon which when released through end-of-life processes contribute 65 % to 73 % of the overall carbon footprint (9). The remaining ≈ 30 % is represented by energy requirements during production and so improvements to the energy sector would reduce this, however even still the chemical sector contributes approximately 6.3 % of GHG annually (6). This industry presents special challenges when improving GHG emissions, other sectors would usually push for decarbonisation, a concept which fundamentally misaligns with the organic chemistry underpinning most of the chemicals industry, which is by definition carbon based (8). As such, the focus shifted on limiting the amount of carbon released overall, employing the idea of renewable carbon which aims to utilise industrially novel carbon sources for chemical manufacturing, such as $CO_2$ or existing plastics (9). Ultimately the goal would be a circular economy where the waste of one process is used as the input of another resulting in a closed material loop requiring minimal input barring extra energy to overcome the thermodynamic limitations of breaking down and building up molecules (10, 11).

## 1.1. Synthetic biology and global warming.

The strategies employed to move the modern global chemical industry away from a reliance on fossil fuels involves unlocking certain carbon sources such as biomass or atmospheric $CO_2$ for use in manufacturing (9). Essentially applying the same principle as in other manufacturing industries where a renewable source is more sustainable than a non-renewable source, however in this case the utilisation of these sources presents some added challenges inherent to industrial chemistry, namely the requirement for high quality and often pure starting material (8, 9). The philosophy of green chemistry and renewable carbon is multifaceted but focuses on prevention of emissions at the source through proper design and foresight, central to this is the concept of an atom economy which strives for synthesis routes developed to use the least amount of atoms

to achieve the final product, contributing to synthesis are also the tenets of energy efficiency and safer solvents throughout synthesis, to that end catalytic reactions are often favoured due to energy efficiency and selectivity (12).

Of the many methods being explored to aid this multifaceted problem, a promising avenue is that of bio-manufacturing which relies on the use of biological systems for the production of desired chemicals (13). This has inherent benefits over traditional chemistry in many applications mainly due to the safety afforded by biological systems which function at 'normal' temperatures and pressures, with the availability of enzymes being so numerous that most reactions of interest can be replicated by a metabolic pathway to deliver target chemicals with high stereoselectivity where relevant (14–16). Key to a circular carbon economy would be pollutant to product applications, highly suited to this would be the employment of microbial cell factories (MCF) which act as highly efficient platforms for the production of a specific chemicals such as biofuels of pharmaceuticals (13–16).

The field of biotechnology ultimately began with the domestication of certain bacteria, and application in cheese, wine, and solvent fermentation (17, 18). At that point the process beyond the addition of a starter culture, or simple fermentation, was not fully understood. The genomic era changed that, the discovery of enzymes and the monumental research carried out in order to elucidate metabolisms, and the relationship between DNA and the inner machinations of the cell has afforded us an understanding of these bioprocesses to the point that editing was a real possibility (19). The evolution of biochemistry into the massively interconnected discipline it is today furthered this knowledge, providing intimate detail in the control of gene expression, and protein production, and the impact genetic modifications can have on an organism in terms of metabolic flux. Allowing us to not only modify, but also optimise to produce industrially competitive methods of production for target chemicals (13, 15). The culmination of this is the field of synthetic biology, which aims to employ the engineering principles of design-build-test-learn, and modularity, to bio-engineering in order to optimise the process of creating these bespoke organisms in the first place (13, 15, 16).

One of the aspects which makes MCF attractive for bio-manufacturing is the huge metabolic diversity providing engineers a wide variety of 'components' to choose from (13). Of course, heterologous expression is rarely a 'plug and play' procedure, requiring considerations like codon optimisation, and gene expression control to prevent overproduction of an enzyme which

may be detrimental to optimal metabolic flux (i.e. by redirecting limiting resources away from homeostatic processes) (20). This was a problem recognised early on resulting in the development of the bio-brick system which aimed to divide genetic elements such as promoter sequence, ribosome binding site (RBS) and coding sequence, into standard, interchangeable parts assembled on plasmids for easy reconstitution and subsequent genetic modifications (20).

Genes and the target pathways form only half of the considerations, arguably the most important deliberation would be the choice of platform organism. As mentioned, the versatility of bacteria means there are practically endless choices, each optimised to fill an ecological niche which could be repurposed for human benefit (13). This versatility, however, also presents difficulties, as each novel type of organism must undergo a process of domestication and development of biological tools for efficient modifications (13). Organisms with established synthetic biology toolkits which are industrially attractive include: glucose utilising strains such as *Escherichia coli*, and *Bacillus subtilis*; lignocellulosic organisms such as *Clostridium thermocellum*; and $CO_2$ fixing organisms such as *Cupriavidus necator* and *Clostridium autoethanogenum* (13). The latter of which already enjoys industrial applications in the production of ethanol using synthetic gas (syngas) as a feedstock (21).

As mentioned earlier, establishing a circular carbon economy involves treating pollutants as products. The genomic era has enabled the feasible rational modification of organisms using either standardised synthetic biology methods, or simple heterologous expression and subsequent optimisation, including adaptive laboratory evolution (ALE) (14–16, 19, 20). As such, organisms can be modified either to assimilate pollutants and produce their natural products, or if they already assimilate pollutants (i.e. *C. necator* utilising $CO_2$), then editing downstream metabolism to utilise this carbon source for the production of non-native chemicals.

## 1.2. *Cupriavidus necator* H16

The taxonomic classification of *Cupriavidus necator* initially underwent many iterations but was ultimately described according to the 1987 *C. necator* N-1 isolate (22). Prior renditions for e.g. the H16 strain began with *Hydrogenomas eutrophus* before reclassification through *Alcaligenes eutropha, Ralstonia eutropha,* and *Wautersia eutropha* (23–25). Ultimately the organism was named for its predatory behaviour ("necator" meaning slayer (26)) and resistance to copper, with copper strongly stimulating growth initiation (22). *C. necator* H16 differs from the type strain, *C. necator* N-1, by its possession of the pHG1 mega-plasmid which, among other things, encodes for the biosynthesis of various hydrogenases allowing *C. necator* to grow autotrophically using $H_2$ as an energy and electron source, with $CO_2$ fixed through a complete Calvin-Benson-Basham (CBB) cycle (27–29). What makes *C. necator* interesting is its identity as a chemolithoautotroph capable of autotrophic, heterotrophic, and mixotrophic growth; the extensive and highly redundant genome results in an organism capable of aerobic or anaerobic growth on a wide variety of organic, aromatic, and inorganic substrates, using oxygen, nitrite or nitrate as terminal electron acceptors (30–33). Metabolites are mainly generated autotrophically and mixotrophically through the CBB cycle (34–36), or through the Entner-Doudoroff pathway from fructose, *N*-acetylglucosamine, and gluconic acid; though *C. necator* is capable of heterotrophic growth on many volatile fatty acids, amino acids, and aromatic compounds (28, 37, 38). A comprehensive list of viable substrates for *C. necator* H16 has been reported (39). A simplified schematic of *C. necator* H16 metabolism is shown in *Figure 1.1*

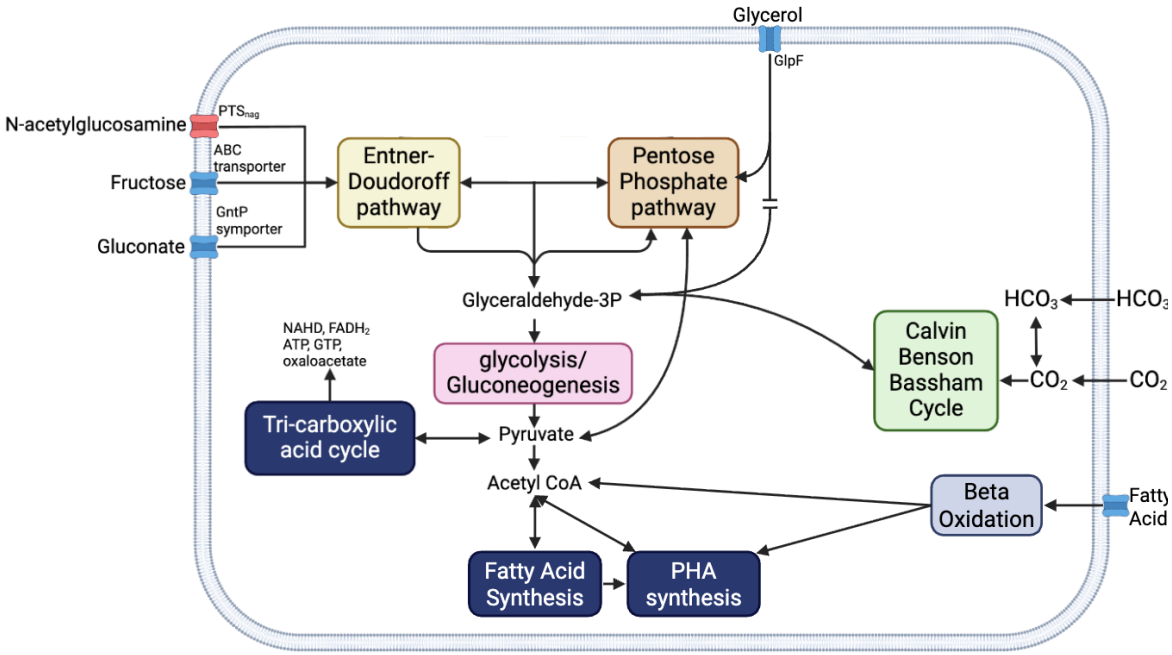


*Figure 1.1*: **Simplified schematic of *C. necator* H16 central metabolism.** Blue membrane proteins represent importers of interest; red membrane protein represents the *N*-acetylglucosamine importer (NagE) capable of conferring glucose assimilation once mutated (40). Protein abbreviations: GntP (WP_011615955.1, WP_010813171.1, WP_010814138.1): Gluconate:$H^+$ permease/symporter family (41); GlpF (WP_011616257.1)- putative glycerol facilitator belonging to the aquaporin family (42, 43); $PTS_{nag}$: *N*-acetyl glucosamine phosphotransferase system porin (NagE, WP_011614455.1); ABC-transporter (WP_041688111.1): ATP-binding cassette sugar transporter (44).

Under unbalanced nutrient conditions *C. necator* directs carbon flux to the production and storage of the biopolymer poly(3-hydroxybutyrate) (PHB) of which it can accumulate to up to 90% of dry cell mass (45, 46). This is another aspect of interest as PHB is a biocompatible thermoplastic belonging to the polyhydroxyalkanoate (PHA) family of plastics, this being a polyester is thus able to relieve the use of petroleum derived plastics in relevant contexts (47). *C. necator* provides a strong platform strain for industrial PHB synthesis due to its chemolithoautotrophic capabilities allowing varying degrees of PHB production from a very large range of feedstocks (33). This genomic complexity makes *C. necator* H16 conducive to use in waste stream valorisation for the creation of a circular carbon economy whereby the resource input, waste output, and energy leakage are slowed and minimised, achievable through the optimisation of processes, recycling, and valorisation of waste streams (48). In such a

system technologies are developed and implemented with the goal of continuing the usefulness of a resource past the initial use, a very basic but descriptive non-microbiological example is the manufacture of chip-board from the waste generated in traditional sawmills (49). More relevantly would be the linking of MCF's to sources of organic waste for the production of PHA, an example would be TianAn biopolymers (Ningbo, China) producing a PHA derivative polyhydroxybutyrate-co-3-hydroxyvalerate using bacterial fermentation with dextrose derived from crops as a feedstock (50). Another promising although not yet commercial avenue is the use of waste streams such as sewage and food waste as feedstocks for bacterial fermentation of PHA (51). Research has been directed to improving the efficiency of this process through the rational engineering of existing or novel platform strains; expansion of feedstocks utilisable for this process; and expansion of the range of end-products (52, 53). Moreover, microplastics have been identified as a major risk factor for human health and environmental damage (54); unmodified, biosynthesised PHA is readily degraded in all investigated bio-active environments including aerobic, anaerobic, soil, marine, and freshwater environments (55).

*C. necator* H16 has been identified as a potential chassis not only for applications producing PHA, but also for the production of non-native products through the expression of exogenous genes and pathways, and re-directing of carbon flux in central metabolism. *C. necator* is convenient in such applications firstly due to the versatile and redundant genome resulting in robust growth, and secondly due to advances in the microbiological and synthetic biology tools available for its manipulation (33, 56–59).

### 1.2.1. Synthetic biology tools for use in *Cupriavidus necator* H16.

As mentioned, *C. necator* H16 has been heavily researched, initially for its robust growth, accumulation of PHB, and substrate versatility. This lead to the creation of a range of synthetic biology tools for the editing and manipulation of *C. necator* genome and metabolism. To note would be the pMTL7000 series of modular plasmid vectors which have collated a range of genetic elements into a modular system for general cloning applications (60). The entire 18 element kit is contained on 6 plasmids which can be re-combined using 4 unique, highly specific restriction enzymes. The resultant vector is comprised of a *C. necator* replicon, selectable marker, *E. coli* replicon, and an application specific module which can be easily modified for use in heterologous expression of genes, genetic manipulation via suicide plasmid mediated gene knock out/in, creation of reporter constructs etc (61).

Besides cloning genes, synthetic manipulation of organisms often requires fine control of gene expression levels, particularly when optimising redox balance and carbon flux for metabolic manipulations. Such control can be awarded through customisation of promoter sequences, ribosome binding sites (RBS), and other regulatory mRNA structures. To this end, constitutive and inducible promoters, and RBS, either native or heterologous but known to function in *C. necator* H16 were mutated and systematically analysed using a fluorescent protein reporter construct (62, 63). This generated a library of promoters, inducible and constitutive, with a wide range of transcriptional activities. And a library of RBS which can be used to fine tune protein production of genes contained in an operon controlled by a single promoter. Ultimately this provides options for fine control over gene expression and protein production for future expression systems (59, 63).

Of course, genetic engineering is also hindered by the ability to introduce relevant vectors into the organism, to this end many efforts have been dedicated to expanding the methods available for *C. necator*. Initially the main method involved bacterial conjugation using an appropriate donor strain such as *E. coli* S17-1 harbouring a mobile shuttle vector (64). This relied on the vector containing an origin of transfer (*oriT*) which can be mobilised in microorganisms containing the RK2 mobilisation machinery. *C. necator* endogenously harbours gentamicin resistance allowing for easy counterselection against *E. coli* (63–65). Later on, an electroporation protocol was developed which greatly decreased the time taken for transformation, however this suffered from low efficiency (66). Later efforts succeeded in improving upon this through protocol optimisation, and genetic manipulation to knock-out specific endonucleases ultimately resulting in an efficient electroporation protocol sufficient for most use cases (57, 60, 67).

Genome elucidation combined with the ever-expanding synthetic biology toolkit allowed for rational engineering approaches whereby existing pathways can be calculatedly modified, and heterologous metabolic pathways can be designed around the existing genome (34, 35). Moreover, it allowed for the creation of detailed metabolic models measuring carbon flux, again greatly aiding rational engineering efforts by allowing the prediction of the effects a certain modification may have on the metabolism as a whole (36, 39).

### *1.2.2.* Expanding enzyme classes available within *C. necator*

Expanding the classes of enzymes accessible within an organism will help with the diversity of feedstocks and products, and may help with modulating metabolic flux (68). Many enzyme catalysed reactions utilise a specific co-factor such as $NAD^+$ and $FAD^+$. Creating pathways which utilise non-canonical redox co-factors provides a theoretically straightforward method of creating orthogonal genetic circuits with minimal impact on central metabolism due to their decoupling from central redox states. This however is currently highly complex due to limitations in creating custom enzymes capable of utilising the non-canonical redox cofactors, and then linking enough of these to form a metabolic pathway with optimal carbon flux (68, 69).

As outlined, *C. necator* is a highly versatile and robust organism, with recent advances having created a relatively expansive synthetic biology toolkit for its genetic modification (59). Current solutions climate problems in part caused by an over-reliance on oil by the chemical industry include the valorisation of canonical waste products. An example of this would be the reduction of $CO_2$ using renewable energy for the production of methanol (70). In terms of $C_1$ compounds, this is favoured over $CO_2$ as being a liquid means medium supplementation is much simpler than gas fermentation (68). However, synthetic methylotrophy presents its own problems regarding toxicity of intermediates. The reduction of methanol by dehydrogenases results in the formation of formaldehyde with known DNA damaging properties (68). Unlike for most compounds, the NAD-dependent dehydrogenases are the minority in methylotrophic bacteria, the exact reason is unknown but likely to do with the production of toxic $H_2O_2$ and thermodynamically unfavourable enzyme kinetics requiring high concentration of methanol for sufficient growth, something which is avoided industrially to minimise the loss of substrate by evaporation (68, 71, 72). Instead, the prevalent class of enzymes in native methylotrophs are the pyrroloquinoline quinone (PQQ) dependent methanol dehydrogenase (MDH) which provide a midpoint between generating reducing potentials, and adequate enzyme kinetics (68). PQQ MDH produces approximately 1 ATP/MeOH whereas $NAD^+$ MDH produces 2.5 ATP/MeOH, however a different redox profile means the forward reaction towards formate is thermodynamically favourable and as such synthetic methylotrophs may be capable of faster growth, at lower MeOH concentrations (68).

*C. necator* is potentially an attractive chassis for quinoprotein pathways as it already possesses a complete putative PQQ biosynthesis gene cluster, with the H16 strain containing putative quinoproteins (based on homology searches as part of this study, see Figure 1.2), and a different strain harbouring a confirmed active quinoprotein for the reduction of tetrahydrofurfuryl alcohol (73). Establishing synthetic methylotrophy requires fine tuning of multiple metabolic processes to optimise rapid removal of toxic by-products, introduction of just the quinoprotein MDH would result in toxic by-product accumulation making it difficult to select for positive mutants. As such, a different quinoprotein was the focus of this study (see 1.4) for establishing a quinoprotein chassis. PQQ-dependent membrane-bound glucose dehydrogenase (mGDH) provides a non-toxic marker for functional quinoprotein production and is well studied with a published structure (see Figure 1.2) (74). Moreover, this is easily selectable in *C. necator* H16 due to the organisms inability to utilise glucose (40, 75, 76).

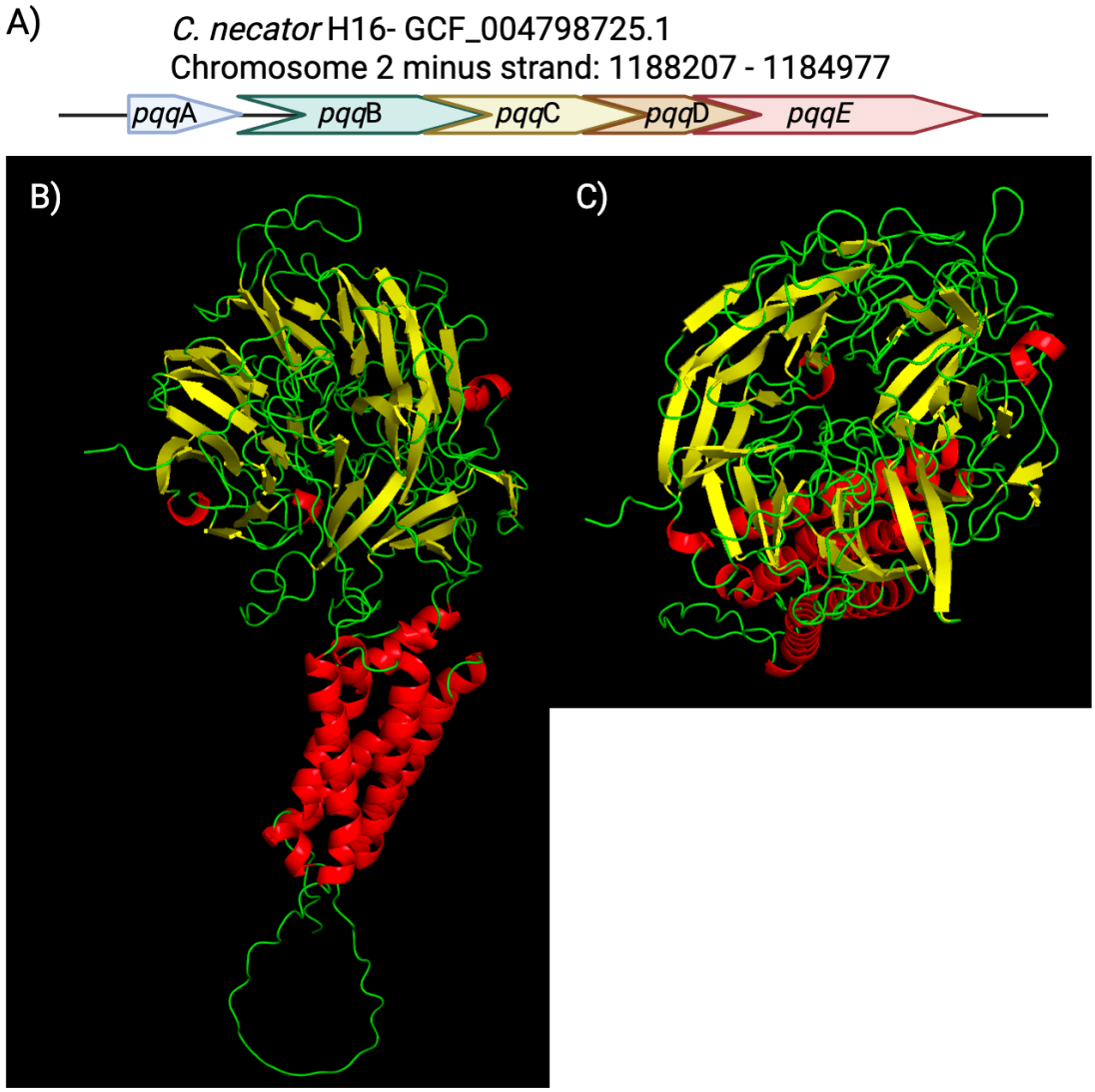


*Figure 1.2*: ***C. necator* H16 *pqq*ABCDE arrangement, and mGDH (A0A7W4FD41) from *G. diazotrophicus* Pal5.** A) Arrangement of *pqqABCDE* in *C. necator* H16 on the negative strand of chromosome 2 (GCF_004798725.1). The structure of mGDH from *G. diazotrophicus* Pal5 (gene: *gcd*- A0A7W4FD41) shown from the side (B) and from the top (C) highlighting α-helices and β-sheets in red and yellow, the high concentration of α-helices represents the transmembrane domain, whilst the domain with high concentration of β-sheets represents the PQQ interacting catalytic domain (74, 77)

## 1.3. Glucose utilisation in *C. necator* H16

As mentioned (1.2) , *C. necator* H16 is host to a varied metabolism capable of utilising a range of substrates including fructose, $CO_2/H_2$, and to a lesser extent glycerol (see Figure 1.1). What *C. necator* H16 is unable to utilise however, is glucose due to a lack of specific transporter (40, 75, 76, 78, 79). The first mutants to utilise glucose was discovered in 1965 with subsequent mutants being elucidated by UV mutagenesis, and spontaneous generation (75, 76). The two mutations conferring this ability were found to be on the *N*-acetylglucosamine phosphotransferase system ($PTS_{nag}$), the first was a missense mutation on *nagR*, this encoded a GntR type transcriptional regulator, involved in various sugar related metabolic functions, which transcriptionally repressed various loci in the absence of the downstream *N*-acetylglucosamine metabolite glucosamine-6-phosphate (80, 81). This de-represses the *nagE* locus, encoding the membrane spanning component of the $PTS_{nag}$ which already exhibits low affinity to glucose and thus limited growth can be observed. Though all mutants obtained through selection on a glucose minimal medium also possessed a second mutation in this *nagE*, a substitution either alanine replaced by threonine at 153; or glycine replaced by arginine at position 265 (40, 79). Both of these mutations achieved an increase in the affinity for glucose leading to much greater transport into the cell.

Previous attempts at reconstituting glucose utilisation in *C. necator* included inserting the aforementioned *nagER* mutations, though the absence of *nagR* negatively affected metabolic homeostasis leading to sub-par growth (82, 83). Building on this, later attempts introduced heterologously expressed galactose permease (*galP*) and glucokinase (*glk*) facilitating entry and phosphorylation of glucose upon entry, which resulted in a marked improvement in growth shown by the production of high PHB titres (82).

The PQQ dependent membrane bound glucose dehydrogenase mGDH catalyses the oxidation of glucose to gluconolactone, and subsequent transfer of electrons into the bacterial electron transport chain via ubiquinone (84–87). Gluconolactone spontaneously converts to gluconate in the presence of water, which is a favourable substrate for *C. necator* H16 and readily taken up for subsequent metabolism through the Entner-Doudoroff pathway (ED, See Figure 1.3; (36). This provides a yet untested method of introducing glucose utilisation into *C. necator* H16 and offers the advantage of partial detachment from the central redox balance on account of the co-factor utilised being PQQ (68).

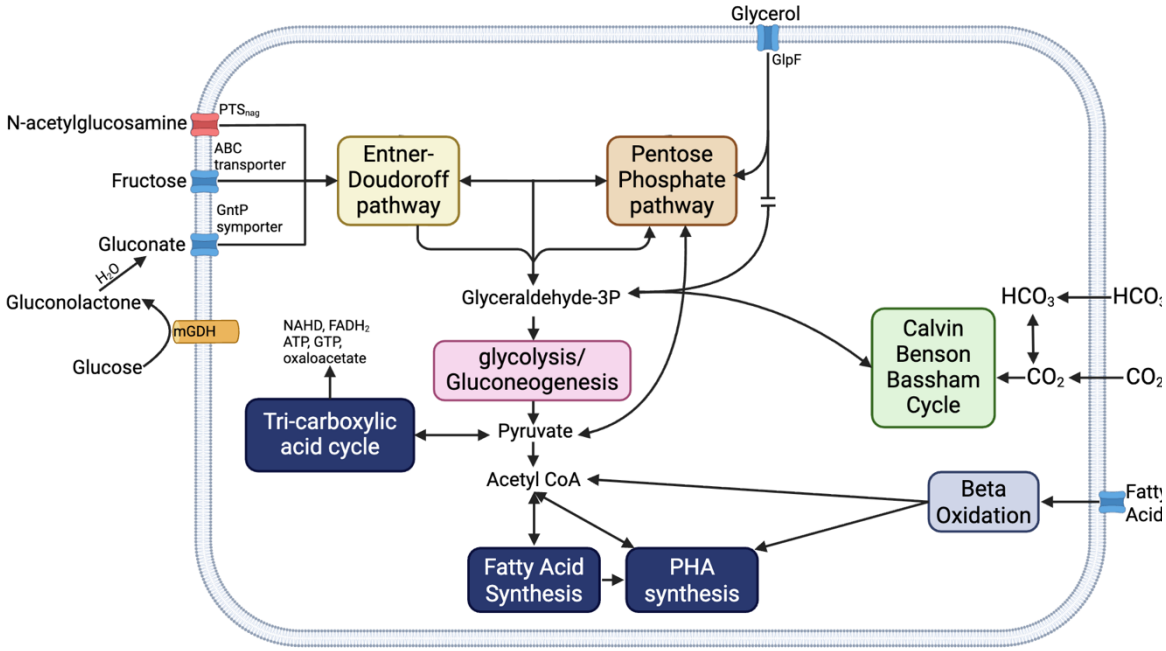


Figure 1.3: **Simplified schematic of *C. necator* H16 carbon metabolism including planned mGDH.** Adapted from Figure 1.1. mGDH is shown on the left in orange. Protein abbreviations: GntP (WP_011615955.1, WP_010813171.1, WP_010814138.1): Gluconate:$H^+$ permease/symporter family (41); GlpF (WP_011616257.1)- putative glycerol facilitator belonging to the aquaporin family (42, 43); $PTS_{nag}$: *N*-acetyl glucosamine phosphotransferase system porin (NagE, WP_011614455.1); ABC-transporter (WP_041688111.1): ATP-binding cassette sugar transporter (44).

As it has been observed that *C. necator* H16 can spontaneously acquire mutations conferring glucose utilisation when cultured in a glucose medium (75), and these have been exclusively found within *nagE/R* of the $PTS_{nag}$, it was decided that for the introduction of mGDH this system must be disrupted to prevent off-target glucose utilisation pathways from arising.

## 1.4. Pyrroloquinoline quinone and quinoproteins

Quinoprotein history began with the observation of several bacterial methanol and D-glucose dehydrogenases, utilising a novel co-factor lacking both flavin or pyridine-nucleotide characteristics (88–90). Initial characterisation efforts were hampered by the inability to acquire enough biomass for the extraction of enough pure enzyme and co-factor for structural and stoichiometric analysis, although various groups characterised aspects of the novel co-

factor providing evidence this was a novel family of enzymes (91, 92). It was found that the co-factor was easily dissociable under acidic (pH < 3) and basic (pH > 12) conditions, and through boiling (92), the purified compound was shown to be dark red, highly polar, acidic, and with a distinct green fluorescence. Apo-enzyme was obtainable through chromatography at low pH, which could be re-constituted using preparations of the co-factor (generally the cleared supernatant of boiled holoenzyme) (89, 92).

Around this time, single-cell protein for use in animal feed was optimised for industrial production leading to the construction of industrial bio-reactors growing the methylotroph *Methylophilus methylotrophus* with the resultant animal feed named pruteen by the company ICI (London, United Kingdom). The bacterium contains a PQQ-dependent methanol dehydrogenase (MDH). Improvements to the procedure for the purification of both enzyme and co-factor (84) combined with the large amount of biomass now obtainable, meant sufficient purified material was now obtainable for further analysis of the novel co-factor and enzyme group (93). It was shown that this molecule contained an o-quinone moiety with 2 nitrogen molecules within its structure (84, 94). Subsequent x-ray diffraction analysis showed the co-factor to be 4,6-dioxo-1H-pyrollo[2,3-f]quinoline-2,9,7-tricarboxilic acid (see Figure 1.4) (95).

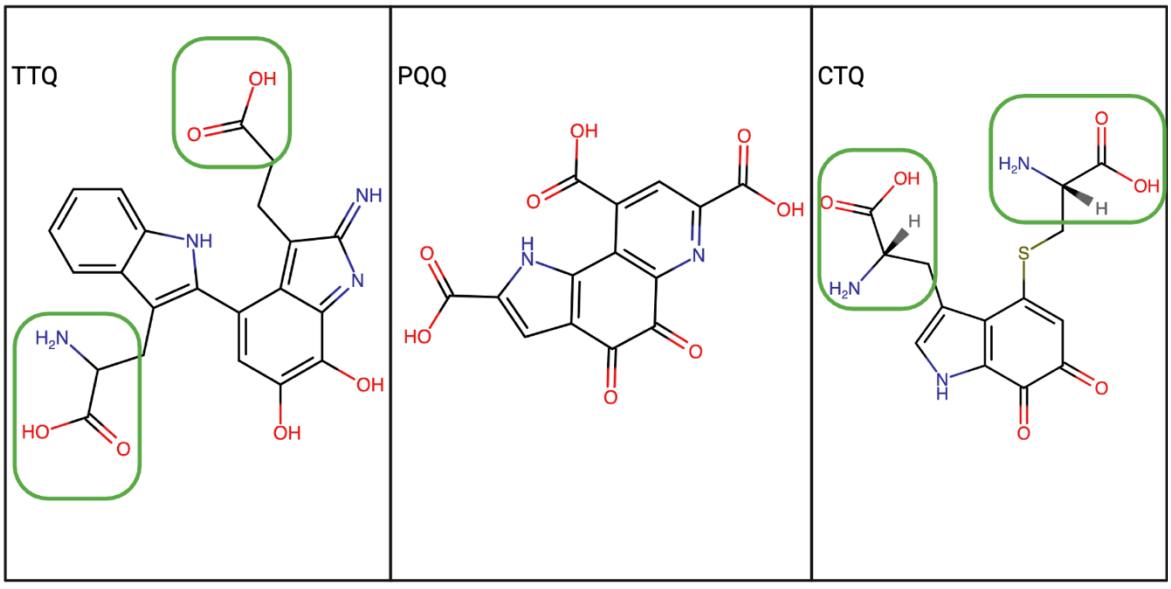


*Figure 1.4*: **Chemical structures of Tryptophan tryptophylquinoline (TTQ)** (96)**; Pyrroloquinoline quinone (PQQ)** (95)**; Cysteine tryptophylquinoline (CTQ)** (97)**.** TTQ and CTQ are shown as free molecules, with the locations where the polypeptide chain would be attached encircled in green.

This was initially named methoxatin due to the source and focus of study being methylotrophic bacteria, and due to apprehensions about the quinone identity of the co-factor with groups arguing the structure was being modified during isolation (93). Re-constitution assays using the apo-enzyme glucose dehydrogenase and co-factor preparation from MDH indicated the co-factor to be identical between the enzymes studied thus confirming them to be the same family, and also indicated that purification of the co-factor did not result in structural modification (94). Furthermore, studies investigating the activity of MDH when re-constituted with PQQ analogues and derivatives proved the o-quinone group to the vital for activity; the importance of the o-quinone moiety for enzymatic function and the prevalence of the co-factor in enzymes other than MDH resulted in its-renaming to pyrroloquinoline quinone (PQQ) based on the chemical structure, with enzymes containing PQQ designated 'quinoproteins' (94).

The definition of quinoproteins was expanded to include later discovered- covalently bound quinone co-factors such as: (Topa-quinone, TPQ) from copper containing amine oxidase; tryptophan tryptophylquinoline (TTQ) from methylamine dehydrogenase; 6-hydroxy-phenylalanine; and cysteine tryptophylquinoline (CTQ) from amine dehydrogenase (Latter two structures shown in Figure 1.4) (98–100). Like PQQ, these are amino acid-derived and rely on an essential quinone moiety for enzymatic activity. However, unlike PQQ which is synthesised separately to the quinoprotein and non-covalently bound, TTQ, TPQ, and CTQ are derived from modifications to tyrosine or tryptophan sidechains within the protein itself, and remain covalently bound once synthesised (98–101).

### 1.4.1. Physiological role of PQQ-quinoproteins in bacteria

Since its discovery, PQQ biosynthesis and use has been found to be widespread and PQQ-dependent enzymes have come to be known as the third major class of oxidoreductases alongside FAD and NAD(P) dependent dehydrogenases, responsible for the initial oxidation of various compounds which are then further oxidised, assimilated into cell material, or released into the environment .

#### 1.4.1.1. PQQ biosynthesis in Gram-negative bacteria

As would be expected for a prevalent co-factor, PQQ biosynthesis capabilities are prevalent amongst bacteria, with alpha and beta-proteobacteria making up more than 80% of the species believed to possess this pathway based on the presence of the highly conserved, and vital element, PqqA (see Figure 1.5) (102).

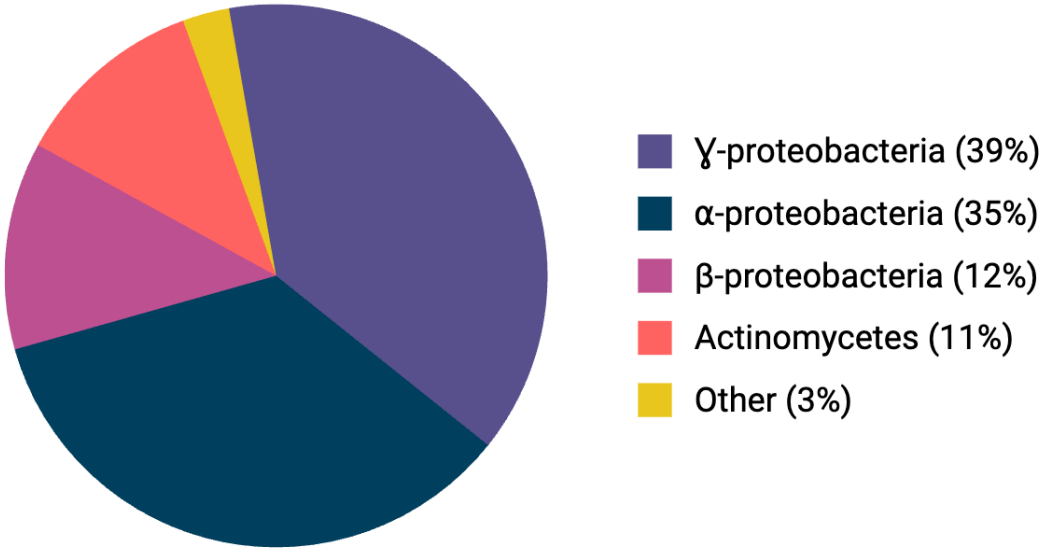


*Figure 1.5*: **Distribution of organisms believed to contain the PQQ biosynthesis pathway.** Data represents number of proteomes in the PFAM 38.0 database (https://pfam.xfam.org/) containing PqqA (PF0842) since PqqA is indispensable in PQQ biosynthesis. To note under 'other' are the classes of bacteria: *Cyanobacteria* (14 entries) and *Bacilli* (18 entries).

The biosynthesis of PQQ was found to be controlled by the genes *pqqABCDEF/G,* conserved across PQQ producing bacteria (103–112). *pqqABCE* are most often found contained on an operon, with *pqqF/G* (encoding a protease) often found under the control of a separate promoter, and in some species missing entirely indicating non-essentiality towards PQQ biosynthesis, or possible redundancy in some organisms with the presence of an unidentified protease, see Figure 1.6 for schematic of possible *pqq* operon arrangements (112, 113).

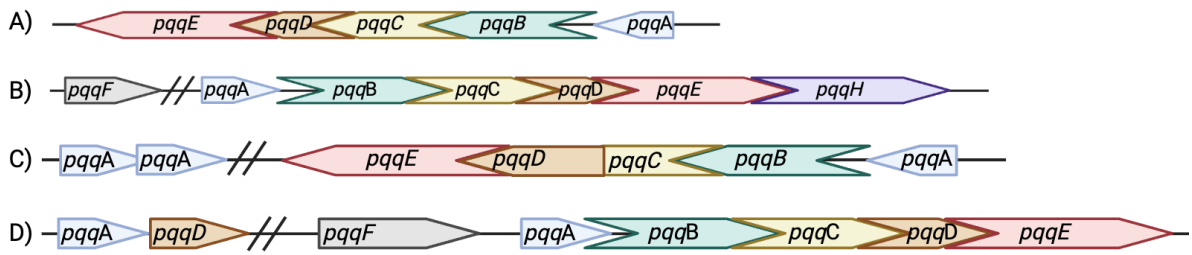


*Figure 1.6*: **Examples of possible PQQ biosynthesis operon arrangements.** A) *C. necator* and *G. diazotrophicus* present the same arrangement of *pqqABCDE*, missing a distinct *pqqF*. B) *Pseudomonas aeruginosa* PA01 presents as *pqqABCDEH* with *pqqF* distal to the core operon. C) Methylorubrum extorquens DM4 contains multiple independent copies of *pqqA* at significant distance from the core operon. *pqqD* is fused to *pqqC* D) *Pseudomonas fulva* NY5087 has a copy of *pqqAD* distal to the core operon, with the main operon having *pqqF* immediately upstream of *pqqABCDE*. Direction of arrow represents orientation of gene. All information on gene location and orientation was obtained from the NCBI genome data set (https://www.ncbi.nlm.nih.gov/datasets/genome/)

PQQ biosynthesis begins with the expression of the *pqqABCDE* operon and production of the associated proteins. *pqqA* is translated into a short 20-30 amino-acid chain containing highly conserved glutamate and tyrosine residues (see Figure 1.7), identified by site directed mutagenesis studies to be the most likely candidates for PQQ pre-cursors (107). The enzyme initiating PQQ biosynthesis is Pqq*E*, due to the presence of a CxxxCxxC motif coordinating [4Fe-4S] cluster near the N-terminus, this was identified as belonging to the radical S-adenosyl-methionine (SAM) family of proteins which cleaves SAM to form methionine and the highly reactive 5'-deoxyadenosyl radical (5'-dAdo·) (114, 115). 5'-dAdo· then abstracts a hydrogen from an otherwise inert site to generate 5-deoxyadenosine and a substrate radical primed for further chemistry (116). Further investigation into PqqE via Mössbauer spectroscopy (117) and electronic paramagnetic resonance (114, 118, 119) elucidated a SPASM domain (120). Mutagenesis studies show interference with the SPASM domain can modulate radical SAM (RS) activity at the N-terminus, but that alteration removed PqqA crosslink capabilities (121). Despite enzymatic activity, a mixture of PqqA, PqqE, SAM, and external reductant alone caused no change in PqqA; this was only observed with the addition of PqqD which was elucidated as being a chaperone type protein facilitating the interaction between PqqA, PqqE and SAM (114, 118, 122). PqqD is often found as an independent protein, but has also been observed as a C-terminal fusion of PqqC or N-terminal fusion with PqqE (See figure 1.6) (123).

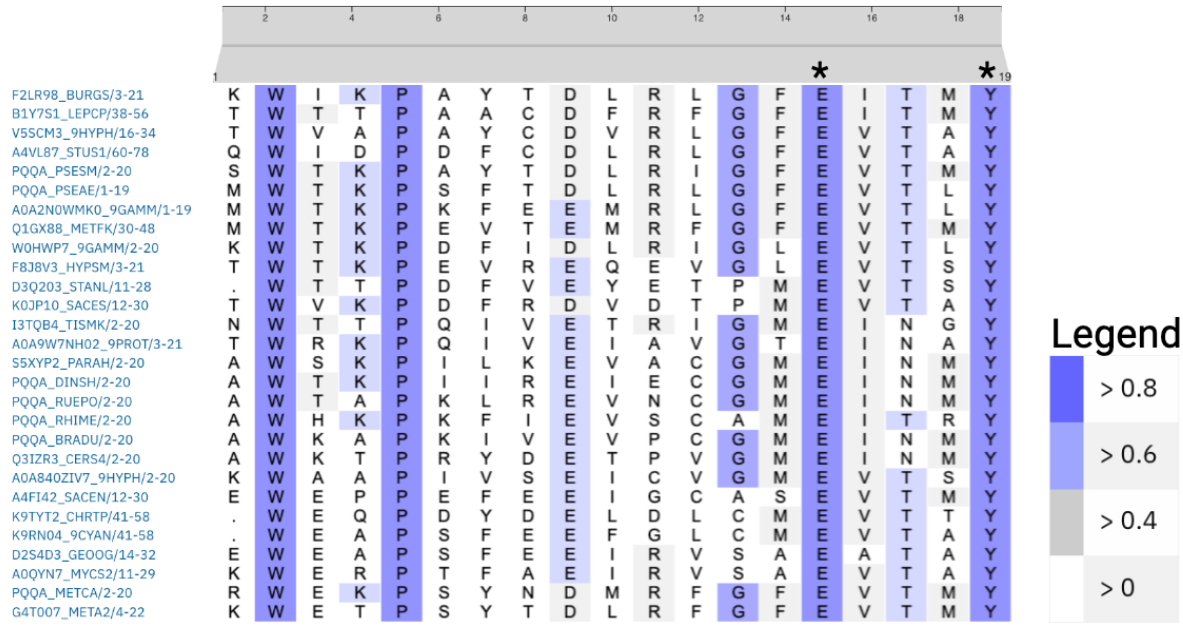


*Figure 1.7*: **Pfam alignments of PqqA highlighting conserved residues.** 28 'seed' sequences forming a representative sample of all PqqA entries in Pfam 38.0 (124). More conserved residues shown in darker purple as shown in the legend. The experimentally determined pre-cursor residues for PQQ are glutamic acid and tyrosine designated with asterisks (107).

The next step following Glu-Tyr crosslink in PqqA via the PqqADE complex is hydrolysation by PqqF/G 'trimming' the C and N-terminal amino acids, although further action by a yet-unidentified protease is likely required to form the Glu-Tyr di-amino acid substrate for the subsequent modification by PqqB (125). PqqF is often found active as a monomer sometimes within encoded within the core PQQ operon, other times under independent control, although in some organisms PqqF is only functional in complex with PqqG; and in others, there is no obvious PqqF/G homologue (103, 112, 123, 125). PqqF is often found under independent control of the *pqqABCDE* operon, in *Pseudomonas aeruginosa pqqF* is constitutively transcribed at low levels, with no uptick in production when the *pqqABCDE* operon is also transcribed. This potentially hints at its involvement in processed other than PQQ biosynthesis, which may explain why some organisms have an apparent lack of PqqF, instead suggesting reliance on a 'multifunctional' enzyme (126).

PqqB belongs to the Metallo-β-lactamase superfamily which generally catalyse the hydrolysis of small molecules utilising various metal centres (127). Studies on the enzymatic activity of PqqB used Cys-DOPA as an analogue for the proposed Gly-Tyr di-amino acid substrate, metal ion reconstitution assays found promiscuous yet stable association to a range of metal ions excluding iron (127). However, interestingly, catalytic activity in the form of $O_2$ dependent aromatic ring hydroxylation of Cys-DOPA, only occurred upon incubation of PqqB with iron, whereas PqqB associated with copper, zinc, manganese, or magnesium was inactive under the same conditions (128). Furthermore, the hydroxylated Cys-DOPA was observed to undergo spontaneous cyclisation to form an analogue of the PqqC substrate: 3a-(2-amino-2-carboxyethyl)-4,5-dioxo-4,5,6,7,8,9-hexahydroquinoline-7,9-dicarboxylic acid (AHQQ) (129). This resulted in the proposed mechanism whereby PqqB facilitates the stepwise insertion of 2 oxygen molecules onto the tyrosine ring via interaction with the coordinated iron molecule forming an isoquinoloid intermediate (128, 130). Whether the rearrangement of this intermediate into AHQQ is spontaneous or enzymatically guided is unclear and requires further work for definite conclusions (128).

Finally, PqqC catalyses an 8 electron and 8 proton oxidation of the intermediate AHQQ, independent of any organic or metallic co-factors (131). Catalysis is instead promoted by substrate binding to the positively charged active site pocket formed of 14 essential residues, this triggers a considerable conformational change, closing the pocket and re-arranging residues into optimal coordination positions forming extensive hydrogen bonds with AHQQ (131, 132). The proposed mechanism first sees the substrate bound PqqC facilitate the cyclisation of the 5 membered ring to form the tricyclic system observed in PQQ, followed by successive base-mediated tautomerisations forming quinol intermediates capable of direct electron transfer to $H_2O_2$ or $O_2$, ultimately forming PQQ (102, 131) .

#### 1.4.1.2. Other PQQ interacting enzymes

As seen, PQQ biosynthesis is a complex procedure requiring a large protein and energy investment for the production of the machinery and the co-factor itself (102). PQQ is often transported to the periplasm either freely or associated with a protein as this is where the majority of quinoproteins are harboured (102, 112, 133). While the machinery involved in PQQ biosynthesis have been elucidated, little light has been shed on the intra-/intercellular transport of PQQ, although this has been shown to be ecologically relevant; as widespread as PQQ biosynthesis is in bacteria, genomes harbouring quinoproteins are more numerous with many

organisms lacking PQQ biosynthesis capabilities while still encoding and producing quinoproteins under certain conditions, making use of the commonly observed secretion of PQQ into the environment (87, 133–135).

Firstly, intracellular transport of PQQ from the cytoplasm to the periplasm is likely to occur either via some sort of transporter due to the large molecular weight and polarity of PQQ, or as part of complete holo-enzymes assembled in the cytoplasm; while the mechanism remains unclear, *pqqB* overexpression in *Gluconacetobacter oxydans* WSH-003 led to a marked increase in PQQ production but also in the expression of three genes which when overexpressed resulted in a 2-3 fold increase in extracellular PQQ, leading to the hypothesis that PqqB facilitates PQQ transport across the inner membrane (133). Structural analysis of PqqB yields no hydrophobic stretches indicating it is unlikely PqqB directly transports PQQ, but more likely interacts and modulates an unidentified transporter (133).

Secondly, PQQ secretion has been observed in various species, and is likely explained by PQQ lying under the diffusion limit for outer-membrane porins causing it to 'leak' out of the cell (95, 133, 135–137). As the production of PQQ is quite energy taxing, it would be in the best interest of many bacteria to harness recovery mechanisms to limit the loss of PQQ; the first protein employed in this role was discovered in the alpha-proteobacterium *Methylobacterium extorquens* AM1 and designated PqqT (signifying PQQ transport) (136). This presented as a solute binding protein with a high binding affinity for PQQ ( $K_d$: 50 nm) which it bound 1:1, localised to the periplasm but not associated to any membrane (136, 138). The mechanism by which PqqT introduces PQQ into regulatory and activatory pathways for quinoprotein apo-enzymes are unknown, however it has been shown that in *M. extorquens* AM1, PqqT production is upregulated in the presence of lanthanides (Ln) (136, 139).

Despite the existence of PqqT capturing free PQQ in the periplasm, *M. extorquens* AM1 was still observed to secrete PQQ into the environment (140). This could be explained by the observation of bacteria which lack PQQ biosynthesis machinery but are known to utilise quinoproteins, thus indicating PQQ may be released as a 'common' good molecule, modulating the environment or behaviour of certain organisms at the behest of others, for example *E. coli* scavenging PQQ to reconstitute the membrane bound apo-enzyme mGDH for the release of gluconate, shown to be utilised for inorganic phosphate solubilisation and plant growth promotion (86, 135, 141–143).

The extremely low concentrations of PQQ observed in nature suggests there may be an import system for extracellular PQQ; despite PQQ being able to diffuse through the outer-membrane, an extracellular PQQ concentration greater than that generally observed in nature would be required for adequate utilisation (87, 95, 135, 137, 144). To this end, a very high affinity transporter was first identified in *E. coli* K12 which harbours a gene encoding the membrane bound quinoprotein glucose dehydrogenase (mGDH), is unable to endogenously produce PQQ (135, 143). This was designated PqqU, and identified as belonging to the Ton-B dependent family of siderophore receptors usually responsible for the import of vitamin B12 and iron siderophores, PqqU forms a complex with the membrane protein ExbB and ExbD allowing the complex to use the proton motive force across the inner membrane for high affinity transport (135, 145). In *E. coli* K12, glucose is usually metabolised starting with the phosphotransferase system (PTS) facilitating the phosphorylation and import of glucose into the cell, but a PTS deficient strain still saw growth on glucose when the medium was supplemented with PQQ at concentrations as low as 1 nM (135). An *E. coli* K12 strain deficient in both the PTS and PqqU showed a dose dependent response to PQQ supplementation in glucose minimal medium, with 100 nM PQQ leading to an extended lag phase (18 hr) compared to 3000 nM PQQ (5 hr) but with no effect on the maximum OD (135). Together with kinetic studies, this indicates that PqqU functions as an import/scavenging system for situations where environmental PQQ is scarce ($K_d$ <1 nM, (146).

Further characterisation of PqqU brough to attention a set of conserved residues essential for binding of PQQ, these were found to be unique to PqqU and could be used to map its prevalence across a phylogenetic tree (146). Of the species identified as potentially carrying PqqU, only 23% showed possible PQQ biosynthesis highlighting the communal reliance on PQQ that seems to have fostered (146). Interestingly, only 67% of the identified species also harboured a PQQ dependent dehydrogenase, the rest which also did not possess PQQ biosynthesis capabilities harboured no known quinoproteins, suggesting either undiscovered quinoproteins or alternative uses for the co-factor (146).

## 1.5. Aims of This Study

This study aimed to assess the suitability of *C. necator* H16 for quinoprotein production in order to expand its substrate spectrum, and for engineering of PQQ dependent pathways in order to minimise the effects of heterologous pathway insertion on core redox balance by employing a co-factor independent of the predominant NAD(P) and FAD (68). This was to be tested through the heterologous expression of the mGDH encoding gene from *G. diazotrophicus*, thus complementing its incomplete glucose assimilation pathway by converting extracellular D-glucose into a favourable substrate, gluconate (36). Incorporating the well-studied mGDH aimed to provide an easily selectable, non-toxic marker, as a proof-of-concept for the suitability of exogenous quinoproteins (84, 86, 147, 148). However, *C. necator* H16 is known to spontaneously acquire glucose assimilation through mutations to the $PTS_{nag}$ system (40, 75, 76). Therefore, the incidence of this occurring under conditions relevant to this study should be assessed to inform on the requirement of alterations to prohibit this from occurring.

Production of active quinoproteins also required PQQ, of which the biosynthesis operon of the cofactor is found within *C. necator* H16, however under the control of an unknown promoter with unknown activity. Therefore, the biosynthesis operon would have to be coupled with a constitutively active promoter. Alternatively, the feasibility of medium supplementation with PQQ was to be assessed by exploring potential PQQ import systems.

Specific objectives for this study are:

- Evaluating the incidence of spontaneous glucose utilisation mutations arising under conditions relevant to this study.
- Introduction of the mGDH encoding gene from *G. diazotrophicus* Pal5 into *C. necator* H16 on a broad-host range vector, and via genomic integration
- Establishment of PQQ biosynthesis by introducing a medium strength synthetic promoter (P21) upstream of the native *pqqA* (62).
- Exploration and characterisation of potential PQQ import systems within *C. necator* identified via homology and conserved residues of importers known to be prevalent in gram-negative bacteria (146).
- Adaptive laboratory evolution of mGDH harbouring strains for the identification of bottlenecks and information towards future studies and optimisations.

# 2. Materials and Methods

Unless otherwise stated, all chemicals were obtained from Sigma Aldrich (Missouri, USA), and all restriction enzymes were obtained from New England Biolabs (Massachusetts, USA).

## 2.1. Microbiological methods

### 2.1.1. Strains, oligonucleotides, and plasmids.

All plasmids, oligonucleotides, and bacterial strains used and created in this analysis are shown in table 2.1, 2.2, and 2.3 respectively.

*Table 2.1:* List of plasmids used in this study.

| Plasmid Name | Function | Source |
|---|---|---|
| pMTL71301 | Broad host range vector for constitutive heterologous expression. pBBR1 *tetR* resistance marker, pBBR1 replicon, *mob*+ mobilisation gene. | (60) |
| pMTL70641_*sacB* | Modular suicide vector for gene knock in/out, in *C. necator* H16. pBR322 *tetA* resistance marker, pBR322 *oriT* replicon, *sacB* selection marker. | (60) |
| pMTL71301_$P_{psts}$_*rfp* | Broad host range *rfp* reporter plasmid (*pstS* promoter activity) used to create transcriptional and translational reporter fusions. pBBR1 *tetR* resistance marker, pBBR1 replicon, *mob*+ mobilisation gene. | (60) |
| pMTL71301_ $P_{pqqU}$_*rfp* | Broad host range vector containing translationally linked *pqqU- rfp* reporter. | This study |
| pMTL71301_*phaC*_mGDH | Broad host range vector harbouring the mGDH encoding gene from *G. diazotrophicus* under control of the *phaC* promoter. Carries tetracycline resistance marker | This study |
| pMTL70641_*sacB3*_mGDH_Δ*nagE* | Suicide vector for the replacement of the *nagE* locus with the mGDH-encoding gene from *G. diazotrophicus.* Carries | This study |

| | | |
|---|---|---|
| | *sacB* gene and tetracycline resistance marker | |
| pMTL70641_*sacB3*_P21 | Suicide vector for the insertion of a constitutively active synthetic promoter (P21) upstream of *pqqA*. Carries *sacB* gene and tetracycline resistance marker | This study |

All Oligonucleotides were ordered from Integrated DNA technologies (Iowa, USA) in the form of standard 25 nM DNA oligonucleotides. Primers came lyophilized and were resuspended nuclease free water (Qiagen, Hilden, Germany) to a concentration of 100 µM. Aliquots of this were diluted tenfold (10 µM) to make working solutions. Stocks and working solutions of oligonucleotides were stored at -20°C. Unless otherwise stated, primers with the suffix 'HiFi_' were designed using the NEBuilder assembly tool (https://nebuilder.neb.com/#!/).

*Table 2.2:* List of Oligonucleotides used in this study.

| Oligonucleotide name | Function | Sequence (5'→3') |
|---|---|---|
| HiFi_71301_*phaC*_fwd | Amplification of the *phaC* promoter from *C. necator* (HiFi) | AATTTTTTTATCAGGAAACAGCTATGACCGCGGCCGCTCATCCTTCTCGCCTATGCTCTG |
| HiFi_71301_*phaC*_rev | Amplification of the *phaC* promoter from *C. necator* (HiFi) | CCCCGGGTACCGAGCTCGAATTCGTAATCATGGTCATATGTTGATTGTCTCTCTGCCGTC |
| HiFi_71301_mGDH_fwd | Amplification of the mGDH encoding gene (excluding terminator sequence) from *G. diazotrophicus* (HiFi) | CGGCAGAGAGACAATCAACAATGAATATTAAACAAGGGTTGCGGCC |
| HiFi_71301_mGDH_rev | Amplification of the mGDH encoding gene (excluding terminator sequence) from *G. diazotrophicus* (HiFi) | TAAAACGACGGCCAGTGCCAGGTATGCTCAGTGGGCTTC |
| HiFi_71301_p*pqqU*_fwd | Amplification of the *pqqU* promoter region from *C. necator* (HiFi) | CAGGAAACAGCTATGACCGCGGCCGCGTGAGCGTCCATGCAATC |
| HiFi_71301_p*pqqU*_rev | Amplification of the *pqqU* promoter region from *C. necator* (HiFi) | AACGTCTTCGCTACTCGCCATATGCGGGATGCGGGGGATACC |

| | | |
|---|---|---|
| HiFi_70641_mGDH_LHA_fwd | Amplification of left homology arm for *nagE* deletion and insertion of the *G. diazotrophicus* mGDH encoding gene for HiFi construction of pMTL70641_*sacB*_mGDH_Δ*nagE* | TTTATCAGGAAACAGCTATGACCGCCGTGCCTATTGAGGTGGCCG |
| HiFi_70641_mGDH_LHA_rev | Amplification of left homology arm for *nagE* deletion and insertion of the *G. diazotrophicus* mGDH encoding gene for HiFi construction of pMTL70641_*sacB3*_mGDH_Δ*nagE* | GGGCCGCAACCCTTGTTTAATATTCATCTTCATTGGCGTTCTCCGAA |
| HiFi_70641_mGDH_fwd | Amplification of the *G. diazotrophicus* mGDH encoding gene with terminator region for pMTL70641_*sacB3*_mGDH_Δ*nagE* (HiFi) | TTCGGAGAACGCCAATGAAGATGAATATTAAACAAGGGTTGCGGCCC |
| HiFi_70641_mGDH_rev | Amplification of the *G. diazotrophicus* mGDH encoding gene for HiFi assembly of pMTL70641_*sacB3*_mGDH_Δ*nagE* | GTTGCCGATGGGGAAGGTCGACCGCCGGATGAATGTCTTCACATATCCGATAGATAGG |
| HiFi_70641_mGDH_RHA_fwd | Amplification of the right homology arm for *nagE* deletion and insertion of the *G. diazotrophicus* mGDH encoding gene for HiFi assembly of pMTL70641_*sacB3*_mGDH_Δ*nagE* | CCTATCTATCGGATATGTGAAGACATTCATCCGGCGGTCGACCTTCCCCATCGGCAAC |
| HiFi_70641_mGDH_RHA_rev | Amplification of the right homology arm for *nagE* deletion and insertion of the *G. diazotrophicus* mGDH encoding gene for HiFi assembly of pMTL70641_*sacB3*_mGDH_Δ*nagE* | GCCAAGCTTGCATGTCTGCAGGCCTCGACGAGAAGGTGGCATTGCGCGAGTTGAAC |
| HiFi_70641_p21_LHA_fwd | Amplification of left homology arm for pMTL70641_*sacB3*_P21 HiFi assembly (integration of P21 upstream of *pqqA*) | TGCCAAGCTTGCATGTCTGCAGGCCCGTGGGCATCACCGCTGCCAGCCCG |
| HiFi_70641_p21_LHA_rev | Amplification of left homology arm for pMTL70641_*sacB*_P21 HiFi assembly (integration of P21 upstream of *pqqA*) | ACATACTCTACGAGCCGGATGATTAATTGTCAATGGTTAGTGAATATCGTTGTGCAGCGG |

| | | |
|---|---|---|
| N_70641_p21_LHA_Nfwd | For first step of nested PCR for amplification of left homology arm for pMTL70641_*sacB*_P21 | CGGTGTAGGCGGGGGTGGTCCAGCGCATGTCTCTCTCC |
| N_70641_p21_LHA_Nrev | For first step of nested PCR for amplification of left homology arm for pMTL70641_*sacB*_P21 | CCACGTACACGCCTGGCTGCAGCCGCT |
| HiFi_70641_p21_RHA_fwd | Amplification of right homology arm for pMTL70641_*sacB*_P21 HiFi assembly (integration of P21 upstream of *pqqA*) | CAATTAATCATCCGGCTCGTAGAGTATGTGGAGTATATGCCACCCAAGGAGAGAGACATG |
| HiFi_70641_p21_RHA_rev | Amplification of right homology arm for pMTL70641_*sacB*_P21 HiFi assembly (integration of P21 upstream of *pqqA*) | CAGGAAACAGCTATGACCGCCGAGAAGCCAGGCGCCTGCATCTC |
| *LuxL*_fwd | Targeting the *luxI* homologous gene in *G. diazotrophicus* | TCATGCGGGAGAAATGGGAC |
| *luxL*_rev | Targeting the *luxI* homologous gene in *G. diazotrophicus* | AGTGCTTCTTTGGACCTCGG |
| *nagR*_fwd | Targeting *nagR* gene on *C. necator* | GTTGCCGCCAGAGGAAGATCCG |
| *nagR*_rev | Targeting *nagR* gene on *C. necator* | CGTAAAGCGAAGCGATGGCGATG |
| *nagE*_fwd | Targeting *nagE* gene on *C. necator* | CCCAGTACACCCTGGCCATTGAC |
| *nagE*_rev | Targeting *nagE* gene on *C. necator* | AGAAGCTGACGCCGTACTGGTTG |
| UL_mGDh fwd | Screening upstream linked integration of the *G. diazotrophicus* mGDH encoding gene | GAATTCACGCCGTCCGACC |
| UL_mGDH rev | Screening upstream linked integration of the *G. diazotrophicus* mGDH encoding gene | GGCAATGAGGTAGTAGAGCGAT |
| DL_mGDH fwd | Screening downstream linked integration of the *G. diazotrophicus* mGDH encoding gene | CGGGCCTATCTATCGGATATGTG |

| | | |
|---|---|---|
| DL_mGDH rev | Screening downstream linked integration of the *G. diazotrophicus* mGDH encoding gene | CCGTCAGAACAGGTGGATG ATG |
| UL_p21 fwd | Screening upstream linked integration of the P21 promoter | AGTTGTCATAGGGCGATTTC CAT |
| UL_P21 rev | Screening upstream linked integration of the P21 promoter | AATCATCCGGCTCGTAGAGT ATG |
| DL_P21 fwd | Screening downstream linked integration of the P21 promoter | CATACTCTACGAGCCGGATG ATT |
| DL_P21 rev | Screening downstream linked integration of the P21 promoter | ATGCGTGTTGACCACCCAAC |
| Seq_mGDH_fwd | For Sanger sequencing of the *G. diazotrophicus* mGDH encoding gene | GACACCGTGTATCTGTGCTC |
| Seq_mGDH_mid_fwd | For Sanger sequencing of the *G. diazotrophicus* mGDH encoding gene | ATGTTCCACCAGCTTCGC |
| Seq_mGDH_rev | For Sanger sequencing of the *G. diazotrophicus* mGDH encoding gene | CATTGGTGGGCAGGAAGAT G |
| Seq_$P_{pqqU}$- rev | For sanger sequencing of pMTL71301_$P_{pqqU}$_*rfp* | ACCCACTCACTACAGCAGAG CC |
| P21_Flank-fwd | For the amplification of region encompassing P21 and homology arms used for suicide plasmid | TCGGGCGAGTCTTCCACCAG |
| P21-Flank-rev | For the amplification of region encompassing P21 and homology arms used for suicide plasmid | CTCAGGTGGACCAGGGTCG G |
| Seq_P21-fwd | For Sanger sequencing of chromosomally inserted P21 | AGCGGTATCGCCGTCAGTGT |
| Seq_P21-rev | For Sanger sequencing of chromosomally inserted P21 | AACAGCGCGAGCACATCGT C |
| M13_fwd | For Sanger sequencing of plasmids | CAGGAAACAGCTATGACC |
| M13_rev | For Sanger sequencing of plasmids | GTAAAACGACGGCCAG |
| 71301_*tet*_fwd | Targeting tetracycline cassette on pMTL71301 | ATCGTCACCCTTTCTCGGTC |
| 71301_*tet*_rev | Targeting tetracycline cassette on pMTL71301 | CCACCCGTTCCACGTTGTTA |

| | | |
|---|---|---|
| 70641_*tet*_fwd | Targeting tetracycline cassette on pMTL70641 | TTGCTAACGCAGTCAGGCACCG |
| 70641_*tet*_rev | Targeting tetracycline cassette on pMTL70641 | TGAATCCGTTAGCGAGGTGCCG |

*Table 2.3:* List of bacterial strains made and used in this study

| Strain name | Description | Source |
|---|---|---|
| *Gluconacetobacter diazotrophicus* PAI5 | Wild type strain, used as source of mGDH encoding gene; and control variable for assays | German Collection of Microorganisms and Cell Cultures GmbH (DSMZ), Braunschweig, Germany |
| *Cupriavidus necator* H16 (DSM 428) | Wild type strain | German Collection of Microorganisms and Cell Cultures GmbH (DSMZ), Braunschweig, Germany |
| *C. necator* Δ*nagR* | H16 derivative with *nagR* gene deleted | Mohammed Ehsaan University of Nottingham CRG |
| *C. necator* Δ*nagR_nagE*_G265R | H16 derivative with *nagR* gene deleted and point mutation in *nagE* | Christopher Stead University of Nottingham CRG |
| *C. necator* H16::p21*_pqqA_ΔnagR* | H16 derivative with *nagR* gene deleted, and P21 synthetic promoter inserted upstream of *pqqA* | This study |
| *C. necator* H16::mGDH_Δ*nagE* | H16 derivative with the *G. diazotrophicus* mGDH-encoding gene knocked in, replacing the *nagE* locus | This study |
| *C. necator* 71301*_pqqU_rfp* | *C. necator* H16 carrying pMTL71301_$P_{pqqU}$_*rfp* | This study |
| *Escherichia coli* DH5a | Used for cloning and storage of plasmids: *fhuA2Δ(argF-lacZ)U169 phoA glnV44 Φ80Δ(lacZ)M15 gyrA96 recA1 relA1 endA1 thi-1 hsdR1* | New England biolabs C2987I |

| | | |
|---|---|---|
| *E. coli* S17-1 | Conjugal donor strain: *recA thi pro hsdR- hsdM+* RP4::2-Tc::Mu::Km Tn7 *λpir*, TpR, SmR | Internal culture collection |

### 2.1.2. Antibiotics

Ampicillin (powder) was stored at 4°C, gentamicin and tetracycline (powder) were stored at room temperature.

*Table 2.4*: List of antibiotic stocks used in this study, the solvent used, and both stock and working concentrations.

| Antibiotic | Solvent | Stock concentration (mg $ml^{-1}$) | Working concentration (μg $ml^{-1}$) |
|---|---|---|---|
| Tetracycline | 70% EtOH | 12.5 | 12.5 |
| Gentamicin | $H_2O$ | 10 | 10 |
| Ampicillin | $H_2O$ | 100 | 10 |

### 2.1.3. Bacterial media

#### 2.1.3.1. Solid Media plates

All media for plates were made by the addition of 15 g $l^{-1}$ agar no.1 (Oxoid, Thermo Fisher Scientific, Massachusetts, USA) prior to autoclaving.

#### 2.1.3.2. Lysogeny Broth (LB)

Lysogeny broth (LB) consisted of 10 g $l^{-1}$ tryptone (Oxoid™, Thermo Fisher Scientific), 5 g $l^{-1}$ yeast extract (Oxoid™, Thermo Fisher Scientific), and 5 g $l^{-1}$ NaCl. It was adjusted to a pH 7 using NaOH, sterilised by autoclaving and stored at room temperature.

#### 2.1.3.3. Low salt LB-3-(N-morpholino)propanesulfonic acid medium (LSLB, MOPS)

LSLB MOPS consisted of 10 g $l^{-1}$ tryptone (Oxoid™, Thermo Fisher Scientific), 5 g $l^{-1}$ yeast extract (Oxoid™, Thermo Fisher Scientific), 2.5 g $l^{-1}$ NaCl and 10.46 g $l^{-1}$ MOPS. pH was adjusted to 7 before sterilisation via autoclaving, and storage at room temperature.

#### 2.1.3.4. SL7 Trace Element Solution

The SL7 Trace element solution was adopted from the DSMZ Phototrophic medium (DSM 1129). It contained: 1 ml $l^{-1}$ HCl (25%, v/v), 70 mg $l^{-1}$ $ZnCl_2$, 100 mg $l^{-1}$ $MnCl_2 \times 4H_2O$, 60 mg $l^{-1}$ $H_3BO_3$, 200 mg $l^{-1}$ $CoCl_2 \times 6H_2O$, 20 mg $l^{-1}$ $CuCl_2 \times 2H_2O$ 20 mg $l^{-1}$, 20 mg $l^{-1}$ $NiCl_2 \times 6H_2O$, 40 mg $l^{-1}$ $Na_2MoO_4 \times 2H_2O$ (149). This was sterilised by filtration (0.22 μm) and stored at room temperature.

#### 2.1.3.5. SL7 Minimal Media (MM)

This medium was adapted from Biebl, H. and Pfennig, N. (1981) and consisted of 9 g $l^{-1}$ $Na_2HPO_4$,1.5 g $l^{-1}KH_2PO_4$, 1.0 g $l^{-1}$ $NH_4Cl$, 0.2 g $l^{-1}$ $MgSO_4 \times 7H_2O$, 0.02 g $l^{-1}$ $CaCl_2$, 1.2 mg $l^{-1}$ Fe (III) citrate, 1 ml $l^{-1}$ SL7 trace element solution (150). Stocks of each constituent was made and sterilised by filtration (0.22 μm) and added to double distilled water ($dH_2O$). This was supplemented with up to 20 mM fructose (F-MM) or glucose (G-MM), using filter sterilised (0.22 μm) stocks.

$MgSO_4$, $CaCl_2$, and Ferric citrate stocks were stored at 4°C.

#### 2.1.3.6. DYGS medium

DYGS medium consisting of 2 g $l^{-1}$ glucose, 2 g $l^{-1}$ yeast extract, 1.5 g $l^{-1}$ peptone, 0.5 g $l^{-1}$ potassium phosphate dibasic, 0.5 g $l^{-1}$ $MgSO_4 \times 7H_2O$, 1.5 g $l^{-1}$ glutamic acid was adjusted to pH 5 using acetic acid before sterilisation by autoclaving and storage at room temperature.

### 2.1.4. Growth conditions

*E. coli* and *C. necator* were routinely grown aerobically in LB (2.1.3.2) at 37°C or 30°C respectively, liquid cultures were kept shaking at 200 RPM in 50 ml falcon tubes (Greiner, Bio-one) or 250 ml membrane filtered shake flasks (Duran®).

Additionally, *C. necator* was cultivated in SL7 MM (2.1.3.5) at 30°C, with liquid cultures shaken at 200 RPM.

*G. diazotrophicus* was grown aerobically in DYGS (2.1.3.6) at 30°C, with liquid cultures shaken at 200 RPM.

For all strains, liquid cultures were no more than 20% of the container volume to allow for good aeration. Pre-cultures were grown as appropriate from single colony in 5 ml suitable

medium overnight and used to inoculate main cultures to the $OD_{600}$ (2.5.1) required by the experiment. Biological replicates were obtained from stocks (2.1.5) plated onto suitable solid medium, or from dilutions ($10^{-3}$ to$10^{-6}$) plated from single colony pre-cultures.

### 2.1.5. Long term bacterial storage

Key type strains, mutants, and plasmid carriers were stored using the bead stock system from Microbank™(Pro-lab diagnostics, Bromborough, England). 800 µl of an overnight cell culture was added to the bead-containing tubes, followed by 5-10 inversions, and aspiration of the majority of the liquid before storage at -80°C.

Evolved strains, and backups of generated mutants were stored in a glycerol stock, made by adding 500 µl of an overnight cell culture to 500 µl glycerol (50% v/v) in a 2 ml cryotube before storage at -80°C.

### 2.1.6. Preparation of chemically competent *E. coli* cells

Pre-cultures (2.1.4) of relevant *E. coli* S17-1 were used to inoculate 50 ml LB in 250 ml membrane filtered shake flasks (Duran®) to an $OD_{600}$ 0.1 and grown aerobically at 37°C with shaking (200 RPM). $OD_{600}$ measurements were taken hourly until a value of 0.7-0.8 was reached. The culture was chilled on ice for 20 min, before centrifugation at 3000g in a chilled rotor (4°C) for 15 min. The supernatant was discarded, and the pellet resuspended in 50 ml ice cold 0.1 M $CaCl_2$. After centrifuging as before the pellet was resuspended in 25 ml ice cold 0.1M $CaCl_2$ 15% (v/v) glycerol. After a final centrifugation the cells were resuspended in 1 ml ice cold 0.1 M $CaCl_2$ 15% (v/v) glycerol. Cells were to be used immediately or snap frozen in 50 µl aliquots and stored at -80°C. Chemically competent *E. coli* DH5a were obtained from new England Biolabs (NEB® 5- alpha competent *E. coli* High efficiency, New England Biolabs).

### 2.1.7. Transformation of chemically competent *E. coli*

Aliquots of chemically competent cells were thawed on ice, 1-5 µl (up to 250 ng ) of the desired plasmid was added and mixed via pipetting and incubated for 1 h on ice. Cells were heat-shocked at 42°C or 45 s and brought back on ice for 5 min before the addition of 950 µl SOC (Invitrogen™) and transfer into a 1.5 ml Eppendorf tube. This was incubated at 37°C with shaking (200 RPM) for 1 h. Following outgrowth, 100 µl of the culture was spread onto solid

LB agar and LB agar +antibiotic before incubating overnight at 37°C. Colonies present on the selective plate were screened for plasmid presence via colony PCR, or miniprep followed by double digest.

### 2.1.8. Transformation of *C. necator* via electroporation

Electrically competent *C. necator* were made following a protocol from an earlier study (67). In short, *C. necator* pre-cultures (2.1.4) were used to inoculate 50ml LB in a membrane filtered shake flask (Duran®, Wertheim, Germany) to an $OD_{600}$ 0.1 and grown at 30°C until an $OD_{600}$ of 0.4-0.6 was reached. This was transferred to a 50 ml falcon tube (Grenier, Bio-one) and chilled on ice for 15 min before centrifugation at 6500 ×g in a chilled rotor (4°C) for 2 min. The supernatant was discarded and the cell pellet resuspended in 25 ml ice cold 50 mM $CaCl_2$, before incubating on ice for 15 min. Following centrifugation as before, the pellet was resuspended in 25 ml ice cold 0.2 M sucrose, and again in 15 ml ice cold 0.2 M sucrose before a final resuspension in 0.5 ml ice cold 0.2 M sucrose. 150 µl aliquots were used for transformation. Electrically competent *C. necator* was always prepared same day of use, and never stored.

For transformation the cuvettes and electroporator arm were pre-chilled on ice. Electrically competent *C. necator* was thawed on ice before adding up to 250 ng plasmid DNA, ensuring this was no more than 2% of the reaction mixture. The mixture in transferred to a 2 mM cuvette and incubated on ice 5 min; Electroporation was carried out using a Biorad™ GenePulser (2.5 kV, 25 µf, 200 Ω) proceeded by immediate addition of 900 µl SOC (Invitrogen™) supplemented with 20 mM fructose. The cells were then transferred to a 30 ml universal tube for outgrowth at 30°C for 2 h. Following outgrowth, the solution was centrifuged and re-suspended in 100 µl LB, then spread on LB + antibiotic plates before incubation at 30°C for up to 48 h. Colonies present were screened for plasmid presence via colony PCR.

### 2.1.9. Transformation of *C. necator* via bacterial conjugation.

*C. necator* transformation via conjugation was carried out with *E. coli* S17-1, carrying the desired plasmid, as the donor cell.

5 ml LB+ antibiotic was inoculated by single colony from agar plate for both the donor and recipient and cultured until an $OD_{600}$ of 3 was reached for *C. necator* (2.5.1). 1 ml of each

culture was centrifuged at 10,000 ×g for 1 min before discarding the supernatant and resuspending in 500 µl LB. The donor and recipient were combined into one tube and centrifuged as before, followed by resuspension in 50 µl LB. This was spotted onto LB Agar plates and incubated for 16 h at 30°C. Following incubation, the spot was resuspended in 200 µl PBS and plated onto F-MM + 10µg $ml^{-1}$ gentamicin + appropriate antibiotic. Colonies appeared after at least 48 h incubation, some of these were re-suspended in 20 µl PBS and spotted onto F-MM selective plates. Following an 18-h incubation at 30°C the spots were screened via PCR for plasmid presence or integration in the case of pMTL based suicide plasmids.

## 2.2. Molecular Biology

### 2.2.1. Plasmid DNA Isolation

Plasmids were isolated using the QIAprep Spin Miniprep kit (Qiagen) according to the manufacturer's instructions; 5 ml of overnight culture was used.
In order to overcome low copy number, or when greater quantities of plasmid were required, the subsequent protocol was used:

The following buffers were prepared beforehand and stored at room temperature: P1 (6.06 g $l^{-1}$ Tris base, 3.72 g $l^{-1}$ EDTA×$2H_2O$, 100 mg $l^{-1}$ RNAse A, pH 8.0 with HCl. Filter sterilised 0.22 µm), store at 4°C. P2 (8.09 g $l^{-1}$ NaOH, 1 g $l^{-1}$ SDS, Filter sterilised 0.22 µm), store at room temperature. N3 (401.25 g $l^{-1}$ guanidine hydrochloride, 88.35 g $l^{-1}$ potassium acetate, pH 4.8 with glacial acetic acid, Filter sterilised 0.22 µm), store at room temperature.

A preculture of LB+antibiotic was inoculated using a single colony from plate, after an overnight incubation at an appropriate temperature this was used to inoculate 50 ml LB+ antibiotic and left to grow overnight. After centrifuging at 10,000 ×g for 5 min, the supernatant was discarded and the pellet resuspended in 2.5 ml buffer P1. 2.5 ml buffer P2 was added and inverted 6 times. After leaving at room temperature for maximum 5 minutes, the lysate was neutralised by adding buffer N3 and inverting 6 times. The resultant solution was centrifuged at 10,000 ×*g* for 15 min, and the supernatant carefully removed ensuring no solid contamination. 6 ml isopropyl alcohol was added to the supernatant and incubated 30 min at room temperature before centrifugation at 10,000 ×*g* for 20 min. The supernatant was

discarded, and the pellet resuspended in 1 ml ethanol, centrifuged at 10,000 ×*g* for 5 min before discarding the supernatant and resuspending in 100 µl nuclease free water (Qiagen).
Plasmids were stored at -20°C.

### 2.2.2. DNA Quantification and purity assessment

Isolated DNA was analysed using a NanoDrop Lite (Thermo Scientific), quantification was determined by measuring absorption at 260 nm ($OD_{260}$:1=50 µg $ml^{-1}$). Purity was assessed via ratio between absorptions at 260:280, with a value between 1.8-2.0 being considered clean enough for all applications.

### 2.2.3. Isolation of genomic DNA

Genomic DNA was isolated from 5 ml (*G. diazotrophicus*) or 3 ml (*C. necator*) overnight culture using the DNeasy Blood and tissue kit (Qiagen). The protocol was carried out according to manufacturer's instructions.

### 2.2.4. PCR amplification of DNA

Amplification of DNA for use in cloning or sequencing was carried out using the Q5® High-fidelity polymerase MasterMix (New England Biolabs). 25 µl reactions were set up according to manufacturer's instructions, but with the addition of 5% DMSO. Primers were used at a concentration of 10 µM (2.1.1). Tm was determined by using the NEB Tm calculator and subtracting 4°C To account for the addition of DMSO (151). PCR reactions for the amplification of HiFi fragments (2.2.8) used oligonucleotides with significant overhang to the target template, as such the Tm was calculated using the region with homology to the template. Reactions were carried out in a Mastercycler Nexus X2e (Eppendorf), thermocycler settings began with 1 min at 95°C, subsequent cycles 95°C for 15 s, 56-72°C for 30 s, 72°C for 1 min per kb length of target. With a final extension time of 10 min. PCR reactions were routinely carried out in the touchdown style with starting annealing temperature being 10°C higher than calculated, followed by 1°C decreases in annealing for the next 10 cycles, and a further 20 cycles at the target temperature. Samples to be separated by agarose gel electrophoresis were then mixed with 4 µl gel loading dye, purple 6X (New England Biolabs).

### 2.2.5. Agarose Gel Electrophoresis

Agarose gel electrophoresis was used to separate DNA. Routine gels were made up to 1% agarose (w/v) with 100 µl $l^{-1}$ SYBR safe (Thermo Fisher Scientific) in 1x TAE buffer (4.84 g $l^{-1}$ Tris base, 1.142 ml $l^{-1}$ glacial acetic acid, 0.29 g $l^{-1}$ EDTA, pH 8.5) , run at 100-120 V for 30-45 min using a compact gel tank (Biometra, Göttingen, Germany) and a nanoPAC 300P (Cleaver Scientific, Rugby, UK). DNA size was determined against the 1 kb plus DNA ladder (New England Biolabs). DNA was visualized using a GelDock XR+ system(BioRad). Bands to be excised were done so with the aid of a UV transilluminator.

### 2.2.6. DNA purification

DNA excised from agarose gels was purified using the Monarch® DNA gel extraction kit (New England Biolabs) following the manufacturer's instructions.
DNA from PCRs or sub-standard minipreps was cleaned using the Monarch® PCR & DNA cleanup kit (5 µg) (New England Biolabs) following the manufacturer's instructions.

### 2.2.7. Restriction digest

Digestion of DNA was carried out according to the restriction enzyme manufacturer's instructions (New England Biolabs, Thermo fisher Scientific) except for incubation which was routinely done overnight.

### 2.2.8. DNA assembly via HiFi

Plasmid assembly was carried out using the NEBuilder® HiFi DNA assembly Master MiX (New England Biolabs), according to the manufacturer's instructions but at a volume of 10 µl, incubation was carried out in a Mastercycler Nexus X2e (Eppendorf). This allowed for a one-pot seamless ligation of up to 6 DNA fragments. The constructs and primers used for fragment amplification were designed using the NEBuilder assembly tool (https://nebuilder.neb.com/#!/) The DNA fragments used in assemblies for this study were amplified via PCR (2.2.4), isolated by agarose gel electrophoresis (2.2.5), and purified (2.2.6). 5 µl of the completed reaction was used to transform *E. coli* DH5α for validation (2.2.9) and downstream applications.

### 2.2.9. Plasmid validation

Assembled plasmids maintained in *E. coli* DH5α were isolated (2.2.1) and initially checked via restriction digest (2.2.7) and subsequent agarose gel electrophoresis (2.2.5) to create a distinct 'fingerprint'. Once confirmed, samples were prepared to be sent to Eurofins Genomics (Munich, Germany) for Sanger sequencing, to confirm accurate DNA assembly. Once confirmed, the plasmids were transformed into *E. coli* S17-1 (2.1.7) for conjugal transfer into *C. necator*.

### 2.2.10. Colony PCR

For the purposes of validating strains, single and double crossovers, and plasmid presence in mutated strains of *C. necator*, DreamTaq PCR Master Mix (2X) Green (Thermo Fisher Scientific) was used. Reactions were set up to a volume of 10 µl with the additions of 5% DMSO, at the ratio set up by the manufacturer. In short: 5 µl Master mix, 0.5 µl forward primer, 0.5 µl reverse primer, 0.5 µl DMSO, 1 µl DNA or 1 µl of a bacterial colony resuspension, 2.5 µl nuclease free water. Colonies were prepared by resuspending in 40 µl nuclease free water. Thermocycler settings began with 10 min at 99°C subsequent cycles at 95°C for 15 s, 56-72°C for 30 s, 72°C for 1 min per kb length of target. With a final extension time of 10 min. PCR reactions were routinely carried out in the touchdown style with starting annealing temperature being 10°C higher than calculated, followed by 1°C decreases in annealing temperature for the next 10 cycles, and a further 20 cycles at the target temperature. Samples could then be loaded directly onto agarose gels for analysis (2.2.5).

## 2.3. Measuring mGDH activity

### 2.3.1. Determination of DCPIP extinction coefficient

A reaction mixture is prepared as mentioned (2.3.4) but varying the amount of DCPIP being added to give a range of concentrations (from 0 mM to 3 mM in of 0.025 mM increments), the volume of PBS added was altered to accommodate the varying amounts of DCPIP, finally the protein mixture was replaced by PBS. 200 µl samples were dispensed in triplicate into wells of a clear 96 well plate, measurements were taken in a M1000 infinite pro (Tecan, Männedorf, Switzerland) incubating the plate at 30°C. This plate reader does not automatically path-length correct so path length was first determined by measuring the difference in absorbance at 900 nm and 977 nm for 200 µ$H_2O$ and multiplying this by 0.18, giving 0.52 cm (Length (cm)=

$(OD_{900} - OD_{977}) \div 0.18)$ (152). Following path correction, measurements were normalised against the reaction mixture with 0 mM DCPIP.

### 2.3.2. Preparation of resting cells and membrane fractions

Pre-cultures of *E. coli, C. necator* or *G. diazotrophicus* (2.1.4) were used to inoculate 100 ml suitable media and grown until the $OD_{600}$ reached 1.6-2.0 (*E. coli, C. necato*r) or 1.2-1.4 (*G. diazotrophicus*). Cells were harvested by centrifugation (6000 ×g, 15 min, 4°C) and resuspended in 17 ml phosphate buffered saline (PBS) (8.01 g $l^{-1}$ NaCl, 1.44g $l^{-1}$ $Na_2HPO_4$, 0.2 g $l^{-1}$ KCl, 0.27 $g^{-1}$ $KH_2PO_4$, pH 7.2 with HCl). 1 ml of this suspension was transferred into a 2 ml microcentrifuge tube and centrifuged at 10,000 ×g for 1 min before resuspension to OD 0.6 using PBS. These were stored on ice and used as resting cells (Whole cell, WC).

The remaining 15 ml of cells were transferred to a 30 ml universal tube, and sonicated on ice (10 min, 15 s on/ 30 s off, 40% amplitude) using Fisherbrand™ 505 sonicator (Thermo Fisher Scientific) with a Qsonica CL-334 probe (Qsonica), The lysate was cleared using centrifugation (2000 ×g, 25 min, 4°C). 2 ml of the lysate was kept on ice and used as cleared lysate (CL).

The remaining lysate was centrifuged at 33,500 ×g for 2 h at 4°C, the supernatant was decanted and stored on ice to be used as the soluble fraction (SF). The pellet was resuspended in 10 ml PBS and spun again as before, followed by resuspension in 1 ml PBS, this was stored on ice and used as the membrane fraction (MF). All fractions were ideally used on the day of generation but were on some occasions snap-frozen in liquid nitrogen and stored at -80°C for later use, even though some sample degradation may have occurred. When using on the same day, all samples were stored on ice. When necessary, the fraction was supplemented with PQQ (2 μM) and incubated on ice for at least 30 min before starting measurements.

### 2.3.3. Determining protein content

Protein content of each sample was measuring using the Pierce™ dilution-free™ rapid gold BCA protein assay kit (Thermo Fisher Scientific) in the microplate format according to the manufacturer's instructions. Serial dilutions of each sample ($10^{-3}$) were first made ensuring enough for triplicate measurements.

### 2.3.4. PMS/DCPIP assay

The artificial electron mediator phenazine methosulphate (PMS) coupled to the redox dye sodium 2,6-dichloroindophenolate (DCPIP) was used to measure the activity of mGDH from samples prepared in the presence of glucose.

Firstly, a 2x reaction master mix was made the same day to prevent degradation: 53 mg $l^{-1}$ DCPIP, 0.612 g $l^{-1}$ PMS, 54 mg $l^{-1}$ $CaCl_2$ in PBS. The protein content of each fraction from extraction was determined (2.3.3) for downstream calculations. Prior to measurements, half of each fraction is supplemented with PQQ to 2 µM and incubated on ice for a minimum of 30 min.
A 0.4 M substrate (glucose) stock solution was made. The final reaction was set up in 1 cm gap plastic cuvettes (Sigma Aldrich) : 500 µl 2X reaction master mix, 300 µl protein stock, 150 µl PBS, and incubated at 30°C for a minimum of 8 minutes prior to the addition of substrate.

The assay was run in at 30°C in a Specord 250 spectrophotometer (Analytik Jena, Göttingen, Germany) by measuring change in $OD_{600}$ every 0.5 sec for 4 min, measurements were started with the addition of 50 µl sugar stock (20 mM final concentration). The measurements were blanked against the reaction mixture excluding DCPIP. Final results were normalised to account for different starting $OD_{600}$ values, and activity calculated using the extinction coefficient of DCPIP (18.05 $mM^{-1}$ $cm^{-1}$ at pH 7; this study). The average activity was calculated from a minimum of two technical replicates. One unit was defined as amount of enzyme activity required for 1 µmol of substrate turnover per minute.

## 2.4. Measurement of *rfp* reporter activity, for PqqU production

The production of PqqU was assessed using a translational fusion of the predicted *C. necator pqqU* promoter region (200bp) and start of *pqqU* coding sequence (70 bp) with the red fluorescent protein (RFP) gene, as present on plasmid pMTL71301_pPqqU_RFP in *C. necator* H16. Seed cultures (2.1.4) were used to inoculate 10 ml F-MM +/- 2 mM PQQ to an $OD_{600}$ of 0.01 in 50 ml falcon tubes (Greiner, Bio-one). 1 ml samples of this were taken at appropriate intervals, these were centrifuged (10,000 xg, 2 min) and re-suspended in 1 ml PBS, centrifuged as before and resuspended in 1 ml PBS. Samples were not stored, with measurements being taken immediately after each collection, 100 µl of each sample was dispensed in triplicate into wells of a clear bottom, black wall 96-well plate (Greiner Bio-One, Cat. No 655090).

Fluorescence was measured ($l_{ex}$: 585 nm, $l_{em}$: 620 nm) in an Infinite® M1000 PRO micro plate reader (Tecan), gain was set automatically . Each sample was measured alongside a sterile medium blank, and a plasmid-less control, with the $OD_{600}$ of all samples also being measured. The mean fluorescence of technical replicates was divided by $OD_{600}$ for normalisation, before the average of the blank replicates was subtracted to give normalised relative fluorescence.

## 2.5. Phenotypic Analysis

### 2.5.1. Optical Density measurements

Absorbance at 600 nm was used to quantify cell culture growth for all species. This was carried out using 1-cm gap plastic cuvette (Sigma Aldrich) and a BioMate 3 spectrophotometer (Thermo Fisher Scientific). Sterile medium was used as blank, Samples with OD > 0.8 were diluted tenfold and remeasured.

### 2.5.2. High-performance Liquid chromatography (HPLC)

For the determination of the amount of PQQ in a sample, HPLC was employed. 10 µl samples were chromatographed (Ultimate 3000; Thermo Scientific) in reversed-phase mode (Ascentis C18 2.7 µm, 3.0 x 100 mm; Supelco, Pennsylvania, USA) at 0.35 mL $min^{-1}$, using a binary gradient of acetonitrile in 0.1 % (v/v) TFA (water) with UV absorbance detection (280 nm and 320 nm). Instrument control and data processing used Chromeleon software (Thermo Scientific; 7.2.10).

### 2.5.3. Growth curve determination

Manual growth curves were carried out in 250 ml membrane filtered shake flasks (Duran®), unless otherwise stated seed cultures (2.1.4) were used to inoculate a maximum 50 ml of the relevant medium to a target $OD_{600}$ 0.01. The flasks were incubated at 30 °C with shaking (200 rpm) with $OD_{600}$ measurements taken every 2 h until growth is observed to plateau (2.5.1).
Growth curves in microtiter plates were carried out in 48 well polystyrene cell culture plates (Greiner Bio One, Cat. No 677180). Unless stated otherwise, seed cultures (2.1.4) were used to inoculate relevant media to an $OD_{600}$ of 0.01, with the final volume per well being 0.3 ml. $OD_{600}$ was measured hourly for 48 h using a CLARIOstar (BMG Labtech). Programme was set to incubate at 30°C with 15 s orbital shaking (200rpm) every 2 min, and 15 s orbital shaking

(200 rpm) before each measurement. All growth curves utilised three biological replicates, occasionally utilising multiple technical repeats for each biological replicate.

## 2.6. In-silico methods and analysis

### 2.6.1. In-Silico DNA analysis and manipulation

For the analysis, design, and theoretical manipulation of DNA and target constructs the software Benchling was employed (https://www.benchling.com/)

### 2.6.2. BLAST analysis

BLAST software available from the NCBI website was used to analyse sequences and identify homologous sequences. Nucleotide BLAST (BLASTn, https://blast.ncbi.nlm.nih.gov/Blast.cgi?PROGRAM=blastn&BLAST_SPEC=GeoBlast&PAGE_TYPE=BlastSearch) optimised for highly similar sequences (Megablast), using the coreNT database, was used to analyse DNA sequences and identify homologous genes based on DNA sequence similarity. Protein Blast (blastp, https://blast.ncbi.nlm.nih.gov/Blast.cgi?PAGE=Proteins), using the ClusteredNR database, was used to analyse peptide and protein sequences and identify homologous proteins based on amino acid sequence similarity.

Finally, for the design or primers, and their screening for specificity against relevant genomes, primer-BLAST was employed (https://www.ncbi.nlm.nih.gov/tools/primer-blast/) .

### *2.6.3.* Predicting promoter region for *pqqU*

The *pqqU* promoter region was predicted using multiple software: SoftBerry BPROM (http://www.softberry.com/berry.phtml?topic=bprom&group=programs&subgroup=gfindb); sapphire (*Pseudomonas*). (https://sapphire.biw.kuleuven.be/); BDGP neural network promoter prediction (https://www.fruitfly.org/seq_tools/promoter.html), ProPr V2.0 (http://ppp.molgenrug.nl/)

Towards this goal, a query sequence consisting of PqqU and the genes immediately upstream and downstream of this was ran through the software mentioned, the potential hits were depicted on a sequence map constructed within Benchling for further analysis (2.6.1).

### 2.6.4. Statistical analysis

Tabulations and calculations of data was carried out in Excel. Graphs were created using GraphPad Prism (https://www.graphpad.com/features), statistical significance and standard deviations were calculated using GraphPad Prism.

### 2.6.5. Computer aided colony counts

For plates which needed colonies quantified but were too numerous to count by hand, the open-source software openCFU (https://opencfu.sourceforge.net/) was employed. The majority of measurements used an inverted threshold with a value of 2. The minimum radius was determined individually for each plate to best capture all colonies present.

### 2.6.6. PyMol

For the visualisation of known and predicted protein structures, and structural alignments PyMol 3.1 was employed (https://www.pymol.org/).

### 2.6.7. AlphaFold

For the prediction of non-experimentally confirmed protein structures based off sequence homology and protein folding kinetics the AlphaFold server (https://alphafoldserver.com/) was used (153).

# 3. Results

The PQQ dependent enzyme mGDH (WP_183115461) from *G. diazotrophicus* was chosen as a model for quinoprotein production in the potential chassis *C. necator* H16. As opposed to native quinoproteins, mGDH provides a well-characterised, easily quantifiable, and selectable marker on account of it bestowing *C. necator* H16 with glucose utilisation abilities (147, 148). Moreover, unlike most other quinoproteins, the product of mGDH is a favourable substrate and would not require further engineering to limit toxicity as would be the case for PQQ dependent methanol dehydrogenase oxidising methanol to produce formaldehyde (154). The activity of mGDH is dependent on the presence of intracellular PQQ, mGDH confers glucose utilisation through the reduction of D-glucose to gluconolactone, which is spontaneously converted to the preferred substrate gluconate in the presence of water.

The resultant strategy was as follows, for any functional quinoprotein production intracellular PQQ is required which can be garnered through over-expression of the native PQQ operon or by supplementing the growth medium with PQQ. The former was to be achieved through the chromosomal insertion of a medium strength constitutive promoter (P21) (62) via suicide plasmid mediated homologous recombination-based knock-in. P21 was selected as this provided a medium level of expression, minimising the possibility of toxicity from excessive metabolic burden whilst still allowing the production of significant levels of PQQ (62). The suitability of growth media supplementation was to be assessed through the identification and characterisation of a putative PQQ import system, widespread in gram-negative bacteria (146). The mGDH encoding gene was introduced into *C. necator* on a broad-host range vector under the control of the native constitutive promoter $P_{phaC}$ for the 'rapid' analysis of mGDH production. In parallel, the mGDH encoding gene was inserted onto a suicide plasmid for homologous recombination-based gene knock-in. The goal was to obtain a strain with at least low levels of glucose utilisation through the activity of mGDH which can be subjected to adaptive laboratory evolution (ALE) for optimisation and identification of bottlenecks. Given that *C. necator* H16 is capable of acquiring mutations for glucose import allowing assimilation by existing internal pathways (40, 75), it was necessary to establish the incidence of this occurring in various genetic backgrounds in conditions relevant to this study, and utilising this information to determine suitable starting strains and mutations necessary to curb these pathways.

## 3.1. Establishing growth profiles of *Cupriavidus necator* strains

### 3.1.1. *C. necator* growth profile in LB and SL7 F-MM

The growth profiles for *C. necator* H16 WT and Δ*nagR* grown in standard F-MM (20 mM fructose) was determined and compared against LB medium (2.1.3, 2.5.3) . LB is routinely used for seed cultures and applications where a defined medium is not necessary; MM on the other hand provides a defined medium for the comparison of mutants and phenotypic properties when grown on a singular carbon source (148). 3 Biological replicate pre-cultures grown in F-MM were used to inoculate LB or F-MM to an $OD_{600}$ of 0.01, 300 µl of each biological replicate was added in triplicate into wells of a polystyrene 48 well cell culture plate (see Figure 3.1).

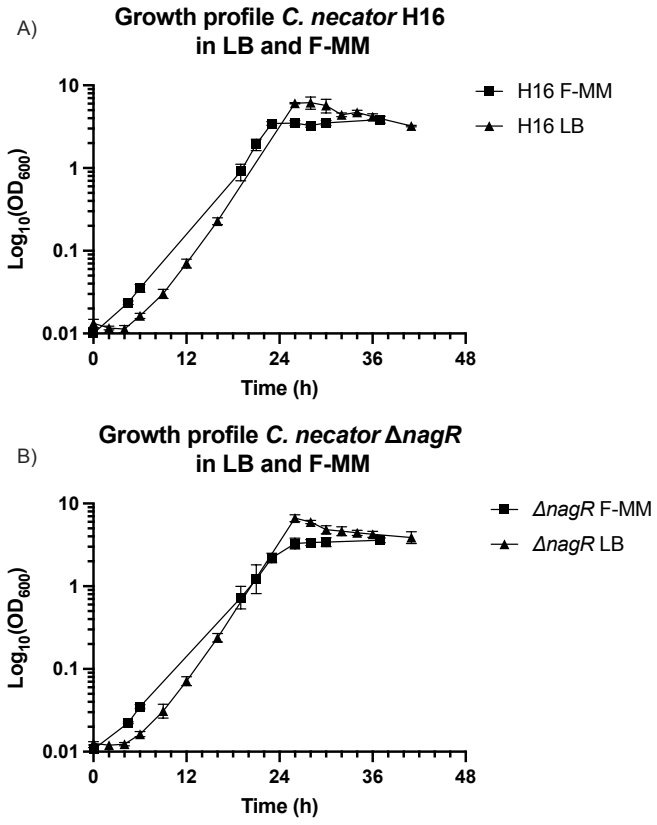


*Figure 3.1*: ***C. necator* WT and Δ*nagR* growth profiles in LB and F-MM.** A) Growth profile of *C. necator* H16 WT (A) and Δ*nagR* (B) in F-MM (20 mM fructose) (squares) and LB (triangles). Values shown represent the mean $OD_{600}$ of technical triplicates from 3 biological replicate pre-cultures with error bars showing standard deviation.

As seen above, there is no noticeable difference in growth rate or maximum cell density for either strain grown in F-MM, with both growing exponentially before plateauing and reaching a maximum $OD_{600} \approx 3.3$ in 26 h. A distinct lag phase does not appear for the WT and Δ*nagR* strains in F-MM as the seed culture was grown in F-MM meaning no acclimatization was necessary. In the case of LB, a roughly 6 h lag period is observed before log growth until a maximum $OD_{600} \approx 6.4$ is reached at 26 h. The doubling time for both strains in both media can be seen in Table 3.1.

Table 3.1: **Doubling time for *C. necator* WT and Δ*nagR* in LB and F-MM during log growth.**

| | Doubling time | |
|---|---|---|
| Strain | LB | F-MM |
| WT | 2 h 20 min (± 1 min) | 2 h 34 min (± 1 min) |
| *nagR* | 2 h 18 min (± 2 min) | 2 h 42 min (± 4 min) |

Comparison of the growth profiles two strain in a specific medium show there to be no significant difference in lag phase, doubling time, or final $OD_{600}$ suggesting the *ΔnagR* mutation does not affect basic metabolic function in LB and F-MM.

### 3.1.2. *C. necator* growth in fructose limiting minimal media (F-MM)

Once the target mutations are implemented the strains were to be subjected to ALE, consisting of a continuous bacterial cultivation under a glucose selective pressure in an effort to optimise the resultant system. The ensuing mutations could provide valuable insights for further rational engineering. Certain strains, for example those harbouring mGDH but with little or no constitutive PQQ biosynthesis, would be unable to grow on G-MM (2.1.3.5) due to the lack of endogenous glucose transport system (78, 155) therefore the growth profiles of *C. necator* H16 WT and Δ*nagR* were determined for SL7 MM supplemented with a range of fructose concentrations. Firstly, an endpoint titration was carried out using *C. necator* H16 WT, Δ*nagR*, and *nagE_G265R_ΔnagR* as a glucose-positive control. This consisted of biological triplicate colonies grown in 20 mM F-MM (2.1.4) sub-cultured to an $OD_{600}$ 0.01 into 10 ml minimal medium (MM) with varying concentrations of fructose (20 mM, 10 mM, 5 mM, 2.5 mM, 1.25 mM, 0 mM) in 50 ml falcon tubes, these were grown under standard conditions for 48 h before measuring $OD_{600}$ (2.5.1).

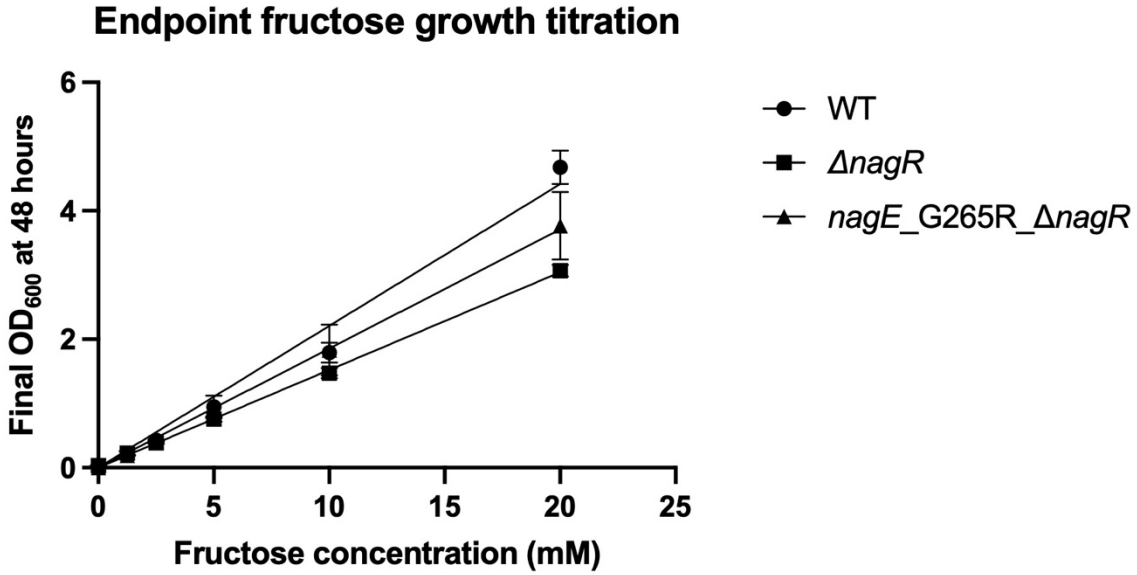


*Figure 3.2*: ***C. necator* H16 (WT, Δ*nagR*, *nagE_G265R_ΔnagR*) grown in SL7 MM across a fructose gradient (0 mM – 20 mM).** Values represent average $OD_{600}$ of three biological replicate seed cultures for each strain (WT, Δ*nagR*, *nagE_G265R_ΔnagR).*

As expected, final optical density of these cultures presented a roughly linear relationship to the applied fructose limitation (Figure 3.2). For greater efficiency in the subsequent ALE process, it may be useful to be able to visually assess the growth of the cultures (I.e. for mutated cultures to have a visually distinctive culture density compared to that of unmutated cultures due to enhanced growth).
Analysing the various samples qualitatively found growth on 2.5 mM F-MM to result in a final culture density significantly visually distinctive from any of the higher concentrations of fructose.

Concurrently, the growth profiles of the three strains in varying concentrations of fructose (20 mM, 5 mM, 2.5 mM, 1.25 mM, 0 mM) were determined using a microplate reader (2.5.3; see Figure 3.3).

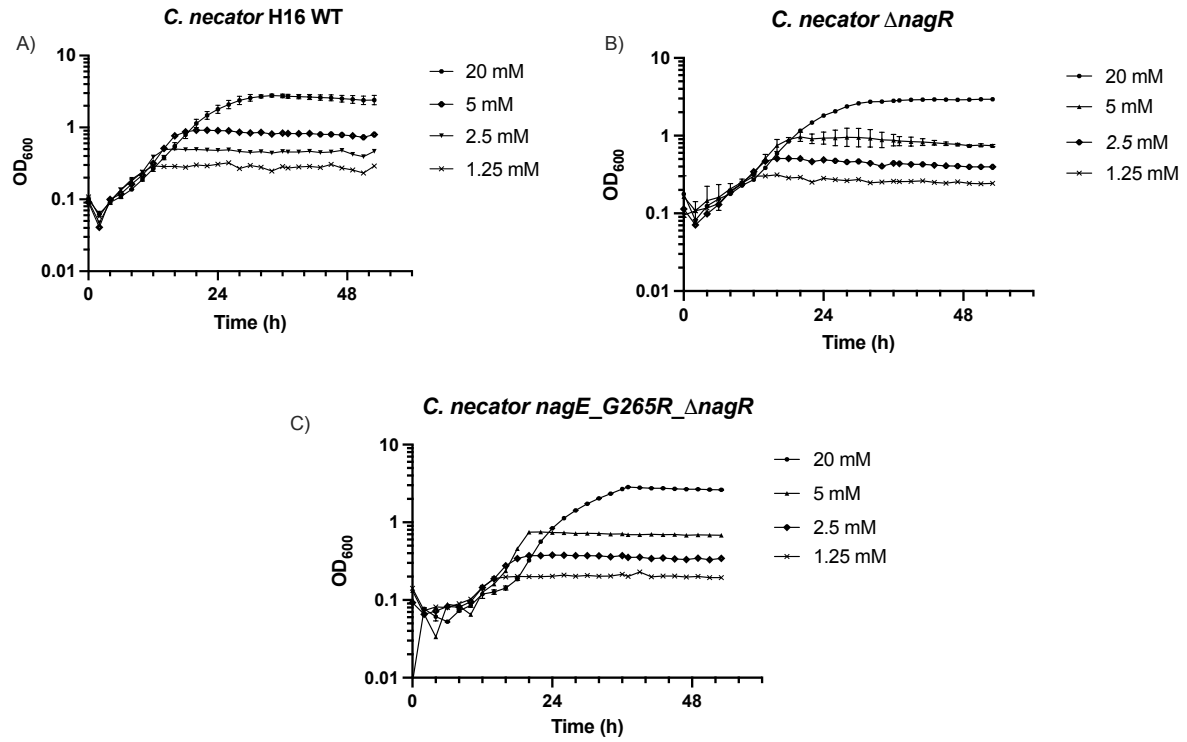


*Figure 3.3*: **Log growth curves of *C. necator* H16 WT (A), Δ*nagR* (B), *nagE_G265R_*Δ*nagR* (C) in MM supplemented with varying fructose concentrations (20 mM, 5 mM, 2.5 mM, 1.25 mM).** Values represent the mean of technical triplicates; error bars signify standard deviation.

As expected, the data above showed the final $OD_{600}$ reached by *C. necator* in F-MM to be linearly related to the fructose concentration regardless of strain. Moreover, the microtiter plate data shows fructose concentration has no effect on the lag phase, with limiting concentrations resulting in a shorter log phase and thus lower final $OD_{600}$. In conjunction with the prior qualitative observations, 2.5 mM fructose was chosen as the concentration for fructose limitation in mutation acquisition (3.2.3) and ALE experiments as this results in significant growth, whilst also limiting final culture density such that *C. necator* H16 variants which present glucose utilisation will result in a visually distinctive final culture densities. This provides a rapid method of identifying mutated strains which would then be validated and characterised with more robust methods.

## 3.2. Incidence of spontaneous glucose assimilation capabilities in *C. necator* WT and Δ*nagR*

As mentioned prior, once the target mutations were achieved the resultant strains were to be submitted to ALE in a glucose minimal medium for optimisation and guidance for future rational engineering. Previous studies upon *C. necator* H16 generated mutants capable of glucose utilisation through chemical mutagenesis (156), UV mutagenesis (76, 157), and spontaneous generation (75). In particular, prior work on the spontaneous generation of a glucose utilising phenotype to occur readily, with the rate of incidence being directly linked to the concentration of glucose found in the medium (75). In order to account for potential interference from spontaneous glucose assimilation mutations, it was therefore necessary to characterise the incidence rate of this arising when grown in media compositions relevant to this study, namely on solid G-MM agar plates; liquid G-MM (20 mM glucose); and in a fructose limiting G-MM (2.5 mM fructose, 20 mM glucose).

### 3.2.1. Spontaneous glucose assimilation on G-MM agar

Biological triplicate seed cultures of *C. necator* WT and Δ*nagR* (2.1.4) were sub-cultured into 5 ml F-MM and grown until mid to late logarithmic growth was reached. They were washed twice in G-MM by centrifugation in a tabletop centrifuge, followed by resuspension in 5 ml G-MM. 100 µl of each undiluted sample was spread onto G-MM agar, repeated to produce 6 technical replicates for each biological replicate. In tandem to establish a colony forming unit (cfu) count, each culture was serially diluted down to $10^{-6}$, with the final two dilutions being plated onto F-MM (2.6.5). All plates were then incubated at 30°C, the F-MM plates were taken out the once distinct colonies were present and used to estimate the number of cells plated on G-MM (2.6.5). The G-MM plates were checked every 2 days with their appearance noted, and any distinct colonies found, picked and re-streaked onto a separate G-MM plate and incubated at 30°C until notable growth was seen (48-72 h). Colonies which showed growth after re-streaking were subjected to colony PCR (2.2.10) using primers targeting *nagR*, *nagE,* and the *phaC* promoter (2.1.1) the former to confirm strain identity, and the latter two to confirm *C. necator* identity. An example of a positive identification is shown in Figure 3.4.

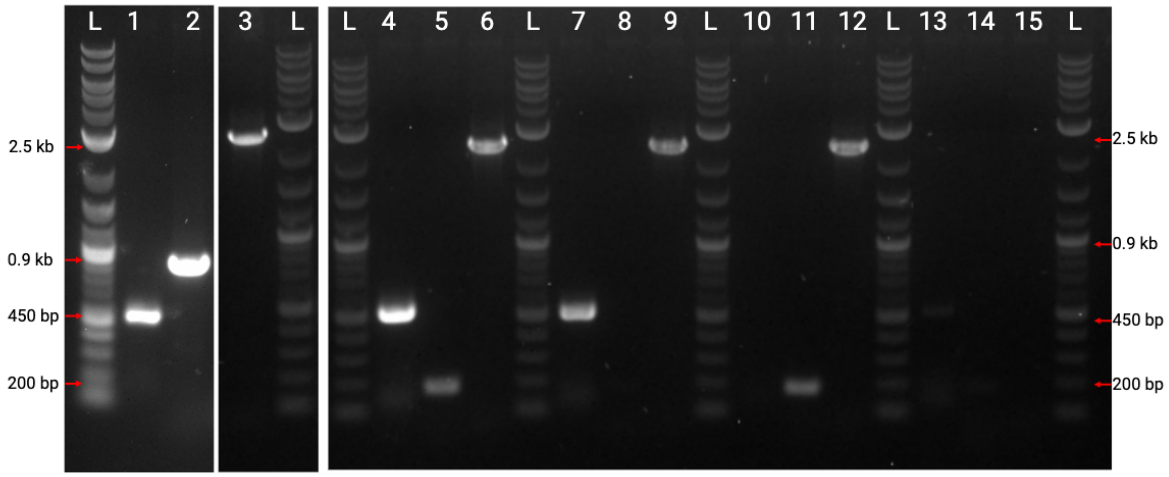


*Figure 3.4*: **Example of positive *C. necator* identification for colonies picked from G-MM plates.** Screened are *C. necator* WT (lanes 1-3) and *ΔnagR* (lanes 4-6) picked from G-MM plates after incubation at 30 °C for 24 days or between 4-20 days, respectively. Also screened are *C. necator* WT (lanes 7-9) and Δ*nagR* (lanes 10-12) picked from LB gentamicin plates, and *E. coli* S17 pMTL71301_$P_{psts}$_*rfp* (lanes 13-15) acting as a negative control. Each candidate was screened using primers targeting $P_{phaC}$ (450 bp), *nagR* (WT: 900 bp, Δ*nagR*: 200 bp) and *nagE* (2.5 kb) which were loaded into the first second and third lane of each section respectively. Expected fragment sizes shown by red arrows. Negative results in lanes 8 and 10 were likely due to interference from colony PCR, the results observed were enough to confirm both *C. necator* identity and strain identity.

As mentioned, undiluted cultures spread on G-MM plates were checked every 2 days for any new developments; no growth was observed for *C. necator* WT until day 20, whereupon numerous very small colonies became visible, too small to count. These were left incubating for a further 4 days at 30°C until the colonies to grew to an appropriate size. All colonies across all plates were identical in colour and differed only in size (*Figure 3.5*). Interestingly all of these initially arose within the span of 2 days of each other, and no new colonies appeared thereafter. Two colonies from each repeat were re-streaked onto new G-MM agar for subsequent PCR identification (2.2.10), all colonies tested returned positive for *C. necator* H16. On the other hand, *C. necator* Δ*nagR* on G-MM agar showed confluent growth on all undiluted G-MM plates within the first two days. However, this was not substantial growth being barely visible at first and growing to only a haze after 18 days (Figure 3.5.C), this low basal growth was expected due to the de-repression of the *nag* operon combined with the low affinity of the unmutated NagE permease towards glucose (79). As time progressed, but starting at day 4, small distinct colonies appeared on some of the G-MM agar, with all plates showing at least 1

colony by day 10, no new colonies appeared thereafter. The frequency at which these appeared over time is shown in Figure 3.6. For each plate, only the first two colonies to form were re-streaked for colony PCR identification assuming all following colonies looked identical, no abnormal colonies were spotted. The incidence rate of spontaneous glucose utilisation arising was calculated using the total number of colonies present after 20 days incubation, results of which are shown in Table 3.2.

A) B)

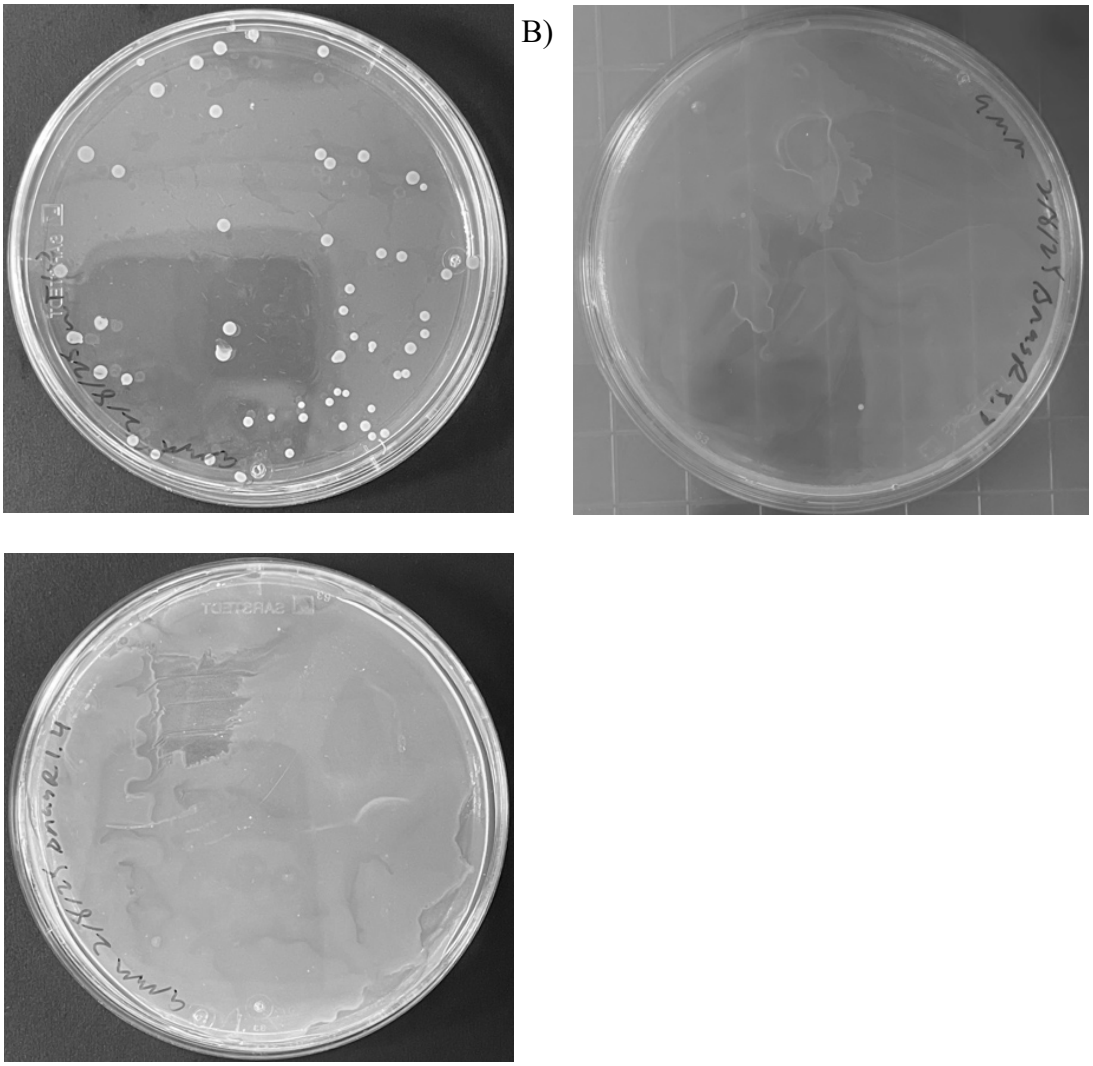

C)



*Figure 3.5*: **Spontaneous growth of *C. necator* H16 WT and Δ*nagR* on G-MM agar incubated for up to 18 days at 30°C.** A) *C. necator* H16 inoculated onto G-MM agar following 24 days incubation at 30°C B) *C. necator* Δ*nagR* inoculated onto G-MM agar and incubated at 30°C, shown is a plate after 4 days of incubation with one distinct colony. C) Shown is *C. necator* Δ*nagR* undiluted on G-MM after incubation for 20 days, present are several small but distinct colonies in addition to substantial background growth.

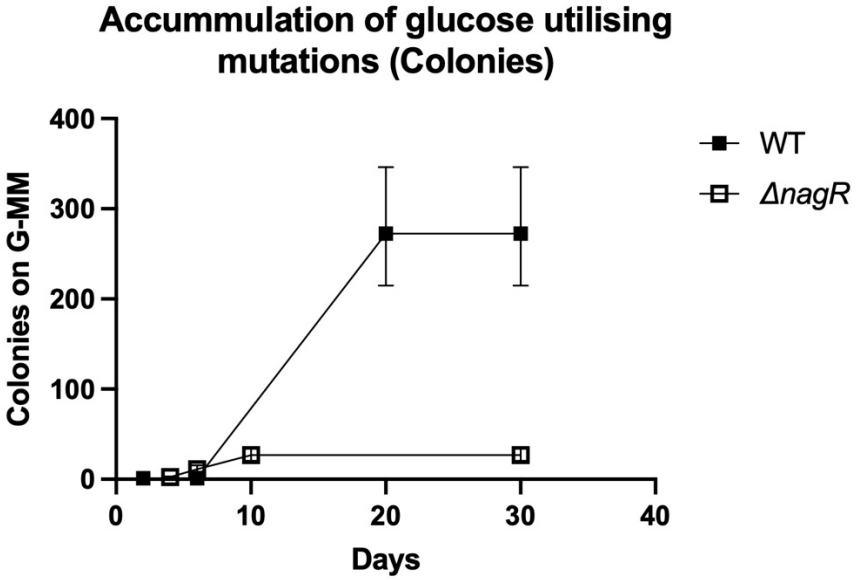


*Figure 3.6*: **Accumulation of distinct colonies on G-MM agar over time.** 100 µl from 3 biological replicate seed cultures was spread onto G-MM agar giving 6 technical repeats of each biological replicate and incubated at 30°C for up to 30 days being checked every 2 days. This graph shows the cumulative frequency of distinct colonies that appeared on G-MM agar for *C. necator* WT (Full square) and Δ*nagR* (Empty square) over time. The data shows the averaged total of each repeat over time, with error bars signifying standard deviation.

For a more representative comparison, the cell count plates onto G-MM was determined using the colony count of the F-MM plates inoculated in tandem (2.6.5), this was used to normalise results as the incidence of mutation acquisition per 100,000 colonies (See Table 3.2).

| | Biological replicate | | | |
|---|---|---|---|---|
| Strains | 1 | 2 | 3 | Average (± standard dev.) |
| WT | 0.27 | 0.34 | 1.5 | 0.73 (± 0.69) |
| Δ*nagR* | 0.025 | 0.058 | 0.037 | 0.040 (± 0.016) |

*Table 3.2*: **Incidence rate of glucose utilisation spontaneously arising in *C. necator* WT and Δ*nagR* plated on G-MM.** 3 Biological replicate seed cultures for each strain were spread onto 6 G-MM agar plates (100 µl) and incubated for up to 30 days at 30°C. The CFU count was established from serial dilutions ($10^{-6}$) spread onto F-MM agar (100 µl) and incubated overnight at 30°C, which were counted using openCFU (2.6.5). The incidence rate represents the number of colonies present on G-MM per $10^6$ cells initially plated (2 significant figures).

The wild-type strain saw a 20-day lag phase before observable colonies developed at an average incidence of $0.76 \times 10^{-6}$ ($\pm 0.69$). The Δ*nagR* mutant saw a low level of basal growth presenting as a 'lawn'; with a 4-day lag phase for the first distinct colonies to appear, with no more new colonies appearing after day 10 for a final incidence of $0.04 \times 10^{-6}$ ($\pm 0.016$)

### 3.2.2. Spontaneous glucose assimilation in G-MM (liquid)

*C. necator* WT and Δ*nagR* have both been shown to spontaneously acquire or improve glucose utilisation abilities when grown on G-MM agar. It was therefore tested to what extend this occurred in liquid medium, i.e. how it manifested itself in in terms of measurable $OD_{600}$ differences.

5 ml seed cultures of each strain (2.1.4) were centrifuged and resuspended in 5 ml G-MM, this was repeated twice before being used to inoculate in triplicate 25 ml G-MM to an $OD_{600}$ of 0.01). These cultures were incubated at 30°C with $OD_{600}$ measured every 48 h over a period of 14 days. Results are shown in Figure 3.7.

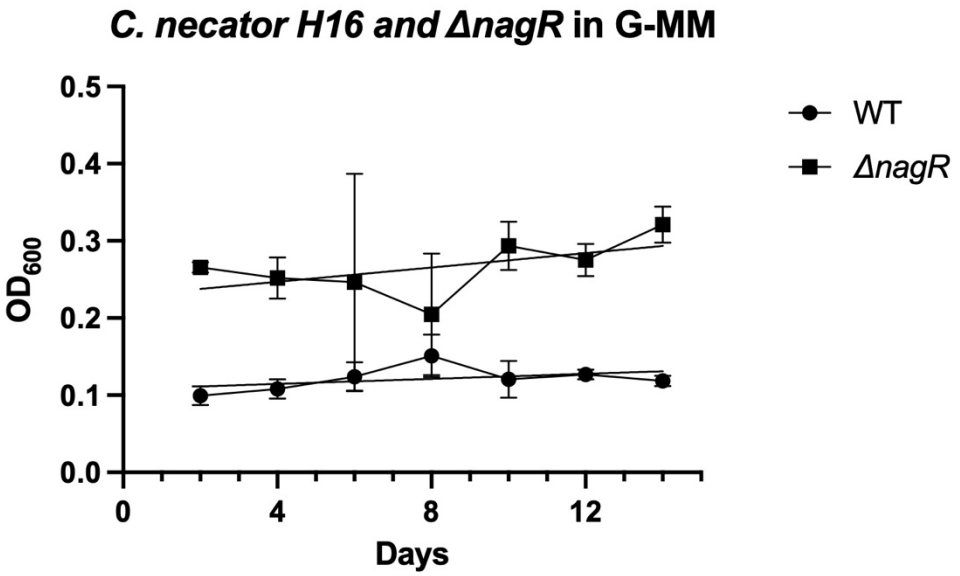


*Figure 3.7*: **The change in final $OD_{600}$ of *C. necator* WT and Δ*nagR* in G-MM.** *C. necator* WT and Δ*nagR* seed cultures were used to inoculate 25 ml G-MM to an $OD_{600}$ 0.1, and incubated at 30°C with $OD_{600}$ measurements taken every 48 h for 14 days. Data represents means of values of 3 technical replicates, with error bars representing standard deviation. Linear regression is plotted and was used to calculate statistic significance (WT: $Y = 0.001637x + 0.1081$ P > 0.05; Δ*nagR*: $Y = 0.004643x + 0.2284$ P > 0.05).

Over the course of the 14 days of measurement, a slight increase is seen in the final $OD_{600}$ for both WT and Δ*nagR* incubated in G-MM (See Figure 3.7), however this was not statistically significant for either strain within the timeframe observed (P > 0.05). However, as expected due to the low affinity of active NagE towards glucose, the Δ*nagR* strain has a significantly higher $OD_{600}$ (P: 0.0006).

### 3.2.3. Spontaneous glucose assimilation in G-MM (liquid) containing 2.5 mM fructose

Downstream ALE would be carried out using fructose limiting G-MM as this offered a medium where evolving glucose utilising strains should show a distinct difference (increase) in final $OD_{600}$ compared to non-glucose utilising strains. This is useful, for example, in the case of *C. necator* carrying the mGDH encoding gene, when selecting for improved native PQQ production. However, as shown earlier (3.2) glucose utilisation can arise spontaneously in *C. necator* cultured on solid and liquid minimal media supplemented with glucose. These mutations would be undesirable e.g. within *C. necator* strains harbouring the mGDH encoding

gene, as they would interfere with downstream ALE. It was therefore important to assess how growth-limiting amounts of fructose impact on the accumulation of glucose utilising strains in WT and Δ*nagR* populations across repeated sub-culturing.

Seed cultures for each strain (2.1.4) were used to inoculate, in triplicate, 25 ml fructose limiting G-MM to $OD_{600}$ 0.01. Following incubation at 30°C for 48 h the $OD_{600}$ was measured (2.5.1) for each sample, each was then sub-cultured into fresh fructose limiting G-MM (100 µl culture in 25 ml medium) . This was repeated for a total of 7 passes, over 14 days. The change in final $OD_{600}$ across this process can be seen in Figure 3.8.

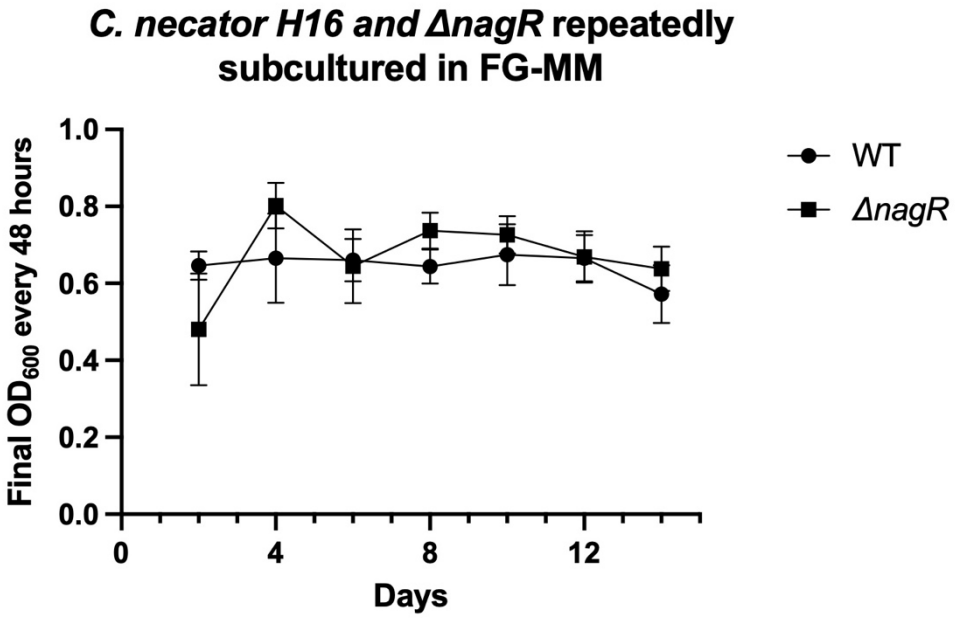


*Figure 3.8*: **The change in final $OD_{600}$ across repeated subculturing of *C. necator* WT and Δ*nagR* in fructose limiting G-MM.** *C. necator* WT (Black circle) and Δ*nagR (Black square)* seed cultures were used to inoculate 25 ml G-MM containing 2.5 mM fructose to $OD_{600}$ 0.01, and incubated at 30°C for 48 h. Final ODs were measured before subculturing (100 µl culture into 25 ml fresh medium). This was repeated 7 times, with graphs showing the mean change in final $OD_{600}$ across technical replicates ($n$ = 3), with error bars representing standard deviation.

No change in final OD is observed over the course of the observed period for both WT and the Δ*nagR* strain. Concurrent with the fructose titration (3.1.2), final $OD_{600}$ before subculturing every 2 days reached ≈ 0.7.

## 3.3. Heterologous expression of mGDH in *C. necator*

The membrane bound PQQ dependent glucose dehydrogenase (mGDH, UniProt: A9H4Z4) from *G. diazotrophicus* belongs to the oxidoreductase family of proteins and is responsible for the oxidation of D-glucose to D-glucono-1,5-lactone in the periplasm, and facilitating the subsequent transfer of electrons into the bacterial electron transport chain through direct interaction with ubiquinone ($Q_{10}$) on the cytoplasmic membrane (74, 86). This enzyme was chosen to assess the suitability of *C. necator* as a quinoprotein platform strain for its selectability and non-toxicity of products; *C. necator* H16 WT does not possess glucose assimilation abilities, whereas the product of mGDH: D-glucono-1,5-lactone is hydrolysed to gluconate spontaneously in the presence of water and readily used as a favourable carbon source (79, 158). The mGDH encoding gene from *G. diazotrophicus* was to be cloned into *C. necator* first using a broad-host range vector to preliminarily assess the suitability of the gene in in this organism, this would then be followed by a transformation of *C. necator* WT using a suicide vector containing the mGDH encoding gene for homologous recombination based knock-in. Broad-host range vector-based testing of quinoprotein functionality should not-present issues as long as the medium contains a carbon source other than glucose, preventing the acquisition of glucose utilising mutations (75). Chromosomal insertion of the mGDH gene prior to ALE experiments requires more considerations which are explored shortly (3.3.2)

### 3.3.1. Construction of pMTL71301_$P_{phaC}$_mGDH

The broad host vector employed for the constitutive heterologous expression of the mGDH encoding gene was the medium to low copy number plasmid pMTL71301 (2.1.1). This was first linearised using NdeI and HindIII and purified for HiFi as described earlier (2.2.8). The mGDH encoding gene from *G. diazotrophicus* was amplified via PCR (2.2.4) using the primers HiFi_71301_mGDH fwd/rev (2.1.1) using gDNA from *G. diazotrophicus* as the template (2.2.3), these produced a truncated gene excluding the native transcription terminator region in favour of the plasmid contained terminator. The mGDH encoding gene would be placed under the control of the *phaC* promoter ($P_{phaC}$) ensuring weak constitutive expression in *C. necator,* (Figure 3.9) (62, 159). This was amplified from gDNA extracted from *C. necator* H16 (2.2.3, 2.2.4) using the primers HiFi_71301_phaC fwd/rev (2.1.1). All fragments were prepared and assembled as described earlier (2.2.8) to form pMTL71301_$P_{phaC}$_mGDH, before

transformation into *E. coli* DH5a for storage and validation (2.2.9) by double digest and (Figure 3.10) and Sanger sequencing (Eurofins genomics).

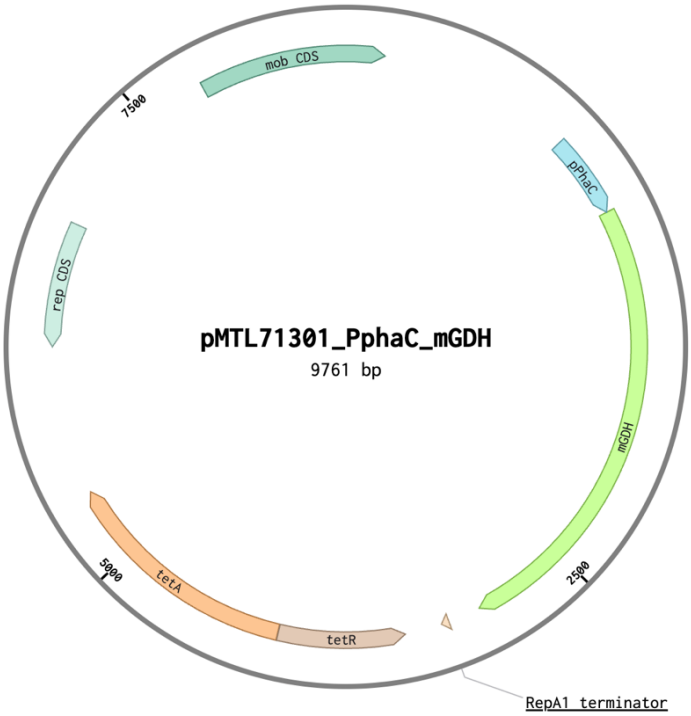


*Figure 3.9*: **pMTL71301_P$_{phaC}$_mGDH plasmid map.** pMTL71301 was digested using NdeI and HindIII. P$_{phaC}$ and mGDH were amplified from *C. necator and G. diazotrophicus* respectively using Q5 High fidelity polymerase. The final plasmid was assembled via HiFi assembly as described in section. *tetA, tetR*, Tetracycline resistance cassette; rep CDS, pBBR1 replicase coding sequence. MOB, for mobilisation of plasmid during bacterial conjugation.

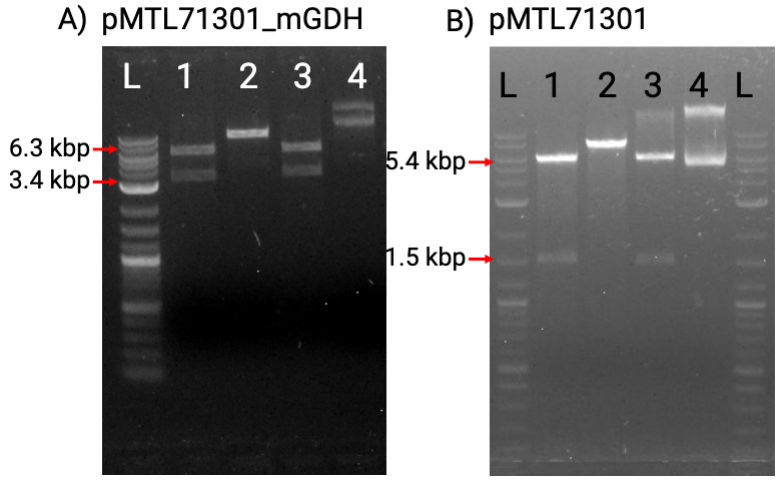


*Figure 3.10*: **pMTL71301_P$_{phaC}$_mGDH validation**. A) pMTL71301_P$_{phaC}$_mGDH and B) pMTL71301 isolated from *E. coli* DH5a storage strains subjected to restriction digest using Eco32I and SalI. The enzymes were chosen such that there is at least one cut site locates within the mGDH encoding gene. Expected lane sizes for double digest identified by red arrows. For A,B: L: NEB 1 kb plus ladder. Lane 1: plasmid + both enzymes; Lane 2: plasmid + SalI; Lane 3: Plasmid + Eco32I; Lane 4: plasmid only.

Transfer of pMTL71301_P$_{phaC}$_mGDH into *C. necator* was achieved by way of electroporation (2.1.8) for the strains WT, Δ*nagR*, and p21_*pqqA*_Δ*nagR*, the latter of which contains a medium strength synthetic promoter knocked-in upstream of the native *pqqA* (see section 3.4 for further details). Individual colonies were re-streaked onto F-MM-tetracycline (12.5 µg ml$^{-1}$) and used for colony PCR (2.2.10) screening for plasmid presence using the primers 71301_*tet* fwd/rev (2.1.1). Positive identification of the plasmid in *C. necator* WT, Δ*nagR,* p21_*pqqA*_Δ*nagR* can be seen in Figure 3.11

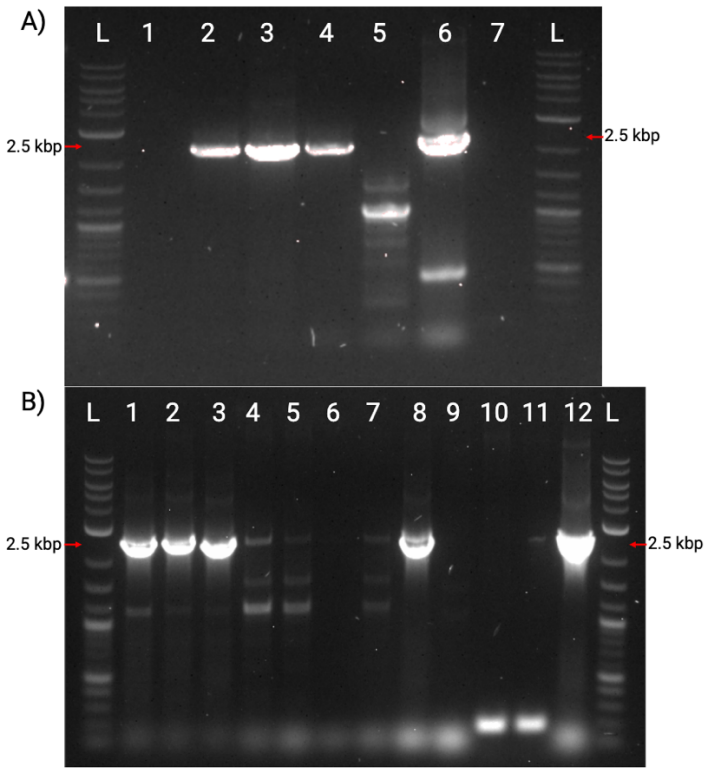


*Figure 3.11*: **Colony PCR confirming plasmid presence (pMTL71301_P$_{phaC}$_mGDH) in *C. necator* H16 WT, Δ*nagR*, and p21_*pqqA*_Δ*nagR*.** A) Colony PCR on potential *C. necator* WT transformants using the primers HiFi_71301_mGDH fwd/rev. Lanes 1-4: *C. necator* transformants ; Lane 5: primers *nagR* fwd/rev used on random colony, selected from those being screened, to confirm strain identity (WT: 900 bp); Lane 6: plasmid pMTL71301_P$_{phaC}$_mGDH used as template; Lane 7: *C. necator* WT colony used as template. Expected PCR fragment sizes for positive identification shown with red arrows. Colonies represented by lanes 2 and 4 (*C. necator* pMTL71301_P$_{phaC}$_mGDH) were kept for stocks and downstream applications. B) Colony PCR on *C. necator* Δ*nagR* and p21_*pqqA*_Δ*nagR* transformed with pMTL71301_P$_{phaC}$_mGDH for plasmid presence using primers HiFi_71301_mGDH fwd/rev. Lanes 1-4: *C. necator* p21_*pqqA*_Δ*nagR* transformants; Lane 5-8: *C. necator* Δ*nagR* transformants. Lane 9: *C. necator* Δ*nagR* gDNA used as template; Lanes 10,11: Colony PCR on random colony, selected from those being screened, from *C. necator* p21_*pqqA*_Δ*nagR* (10) and ΔnagR (11) transformants using the primers *nagR* fwd/rev to confirm strain identity (Δ*nagR*: 200 bp). Expected PCR fragment sizes for positive identification shown with red arrows. Colonies represented by lane 1 (*C. necator* p21_*pqqA*_Δ*nagR* pMTL71301_P$_{phaC}$_mGDH) and lane 8 (*C. necator Δnag*R pMTL71301_P$_{phaC}$_mGDH) were kept for stocks and downstream applications .

### 3.3.2. Construction of pMTL70641_*sacB3*_mGDH_Δ*nagE*

Glucose assimilation spontaneously developing in *C. necator* WT was explored in UV mutagenesis studies which elucidated various derivatives of *C. necator* H16 capable of growing on glucose. These were found to be imparted by mutations in the *N*-acetylglucosamine phosphotransferase system ($PTS^{nag}$), specifically a loss of function mutation in the transcriptional repressor (*nagR*) leading to overexpression of the *nag* operon, and various possible missense mutations in the membrane component (*nagE*) conveying greater glucose specificity (78, 155).

The incidence of glucose utilisation being acquired spontaneously in a medium with glucose as the sole carbon source was inspected earlier (3.2) and found to occur readily. The mutations responsible for these instances were not elucidated in this study, however a prior study employing a similar method of culturing *C. necator* in minimal media supplemented with glucose found that, for every independent mutant studied, deletion of the *nagFEC* genes resulted in a loss of glucose assimilation (75). This was the case for mutagenesis studies also (78, 155), thus the same was assumed for this study.

In order to mitigate interference from this occurrence downstream, it was decided to target the mGDH encoding gene knock-in to the *nagE* locus, replacing it (Figure 3.12). Moreover, when introduced into a *nagR* deficient strain this would ensure constitutive expression of mGDH, as opposed to inserting mGDH into a *nagFEC* deficient strain which would require further considerations and engineering to achieve mGDH expression (79). Allelic replacement would be achieved through suicide plasmid based homologous recombination driven by sucrose counter selection using the suicide plasmid pMTL70641_*sacB3 (60)*.

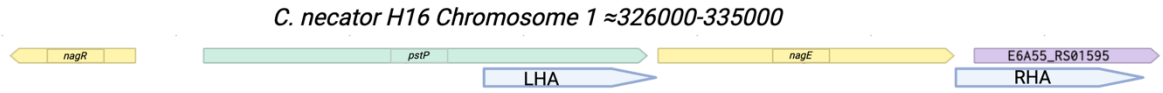


*Figure 3.12*: **Location of homology arms for pMTL70641_sacB3_mGDH_Δ*nagE* on *C. necator* H16 chromosome 1.** Most glucose utilising *C. necator* H16 phenotypes presented with one or multiple mutations in the *nag* system. To mitigate this from interfering with mGDH establishment downstream it was decided to replace the *nagE* locus, as such the homology arms were determined to be roughly 1 kb either side of *nagE*. (NCBI ref: NZ_CP039287.1).

To this end, the suicide plasmid linearised with NotI and XhoI was assembled (2.2.8) with the mGDH encoding gene from *G. diazotrophicus* and the pair of homology arms (≈1 kb) targeted to flank the *nagE* locus (Figure 3.13). For PCR amplification of the mGDH encoding gene the primer HiFi_70641_mGDH was used which preserved the native transcription terminator region (2.1.1); Left and right homology arms were amplified using the primers HiFi_70641_mGDH_LHA fwd/rev and HiFi_70641_mGDH_LHA fwd/rev respectively (2.1.1). The resultant suicide plasmid, pMTL70641_*sacB3*_mGDH_Δ*nagE*, contained in *E. coli* DH5a was validated (2.2.9) by double digest (See Figure 3.14) and Sanger sequencing before being electroporated into *E. coli* S17 for downstream conjugations.

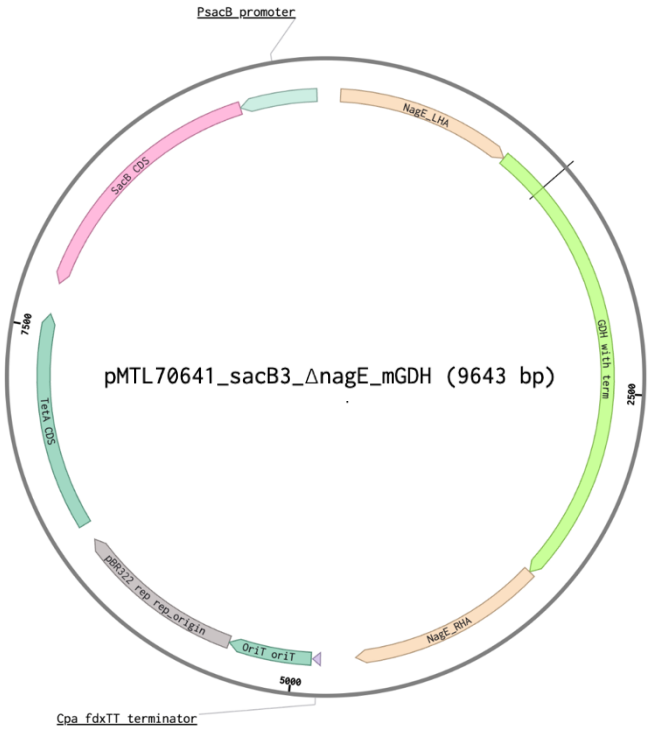


*Figure 3.13*: **Map of pMTL70641_sacB3_mGDH_Δ*nagE*.** The mGDH encoding gene (lime green) is nested between homology arms (≈ 1 kb, beige) which target this to the endogenous *nagE* locus. The plasmid confers tetracycline resistance (*tetA*), and carries a levansucrase (SacB) encoding gene (pink), which converts sucrose to the polysaccharide levan which is toxic to *C. necator* H16 when accumulated (160). This drives a second crossover event by promoting colonies which loose the plasmid backbone. (*OriT*: origin of transfer; pBR322 rep: pBR322 derived origin of replication.

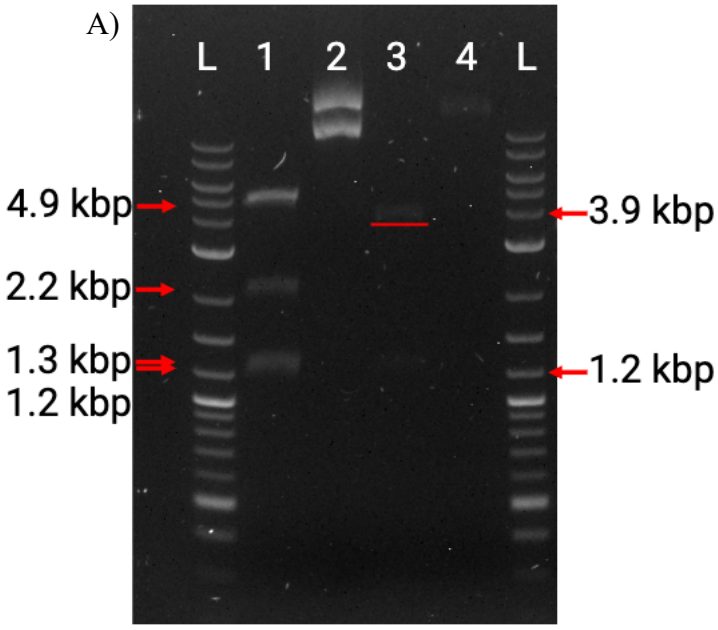


*Figure 3.14*: **Validation for pMTL70641_sacB3_mGDH_Δ*nagE* via double digest and Sanger sequencing** A) pMTL70641_*sacB3*_mGDH_Δ*nagE* (lane 1,2) and pMTL70641_*sacB3* (Lane 3,4) digested with Eco32I. Lanes 1 and 3 represent the digested sample, lanes 2 and 4 consist of undigested plasmid. Red arrows designate the expected PCR fragment sizes for a positive identification. A red line highlights one of the pMTL70641_*sacB3* bands as this is very faint.

#### 3.3.2.1. Screening for single and double crossover events and mutant validation

With the suicide plasmid carrying mGDH assembled, construction of the strains *C. necator*::mGDH_Δ*nagE and C. necator*_mGDH_Δ*nagE*_Δ*nagR* would begin with conjugal transfer of the plasmid into *C. necator* WT and Δ*nagR* strains respectively (2.1.9, 2.1.8.) with only the WT allelic replacement yielding successful potential mutants during the available time-frame. Colonies present after re-streaking onto tetracycline selective plates suggest a homologous recombination event occurred, as the vector does not possess a *C. necator* replicon meaning antibiotic resistance would not be conferred unless integrated into the chromosome as the plasmid cannot replicate and would be lost in subsequent generations. These colonies were screened via colony PCR to determine the location of the integration, either left or right-handed (upstream or downstream of *nagE*). Two sets of primers ('Upstream linked', and 'downstream linked') were used to determine this, each pair consisting of one primer targeting outside of the homology arms, and another targeting within the mGDH encoding gene (Figure 3.15).Each set of primers would only give a result if the integration it was targeting occurred, as the template length would otherwise be too long, the results from this screening can be seen in Figure 3.12. there were troubles with getting a positive result with the upstream linked primers despite

trouble shooting with multiple PCR variations and primer re-designs. Ultimately the 4 positive results with the downstream linked primers, and the tetracycline resistance observed with the colonies, was enough evidence to move forward with allelic replacement.

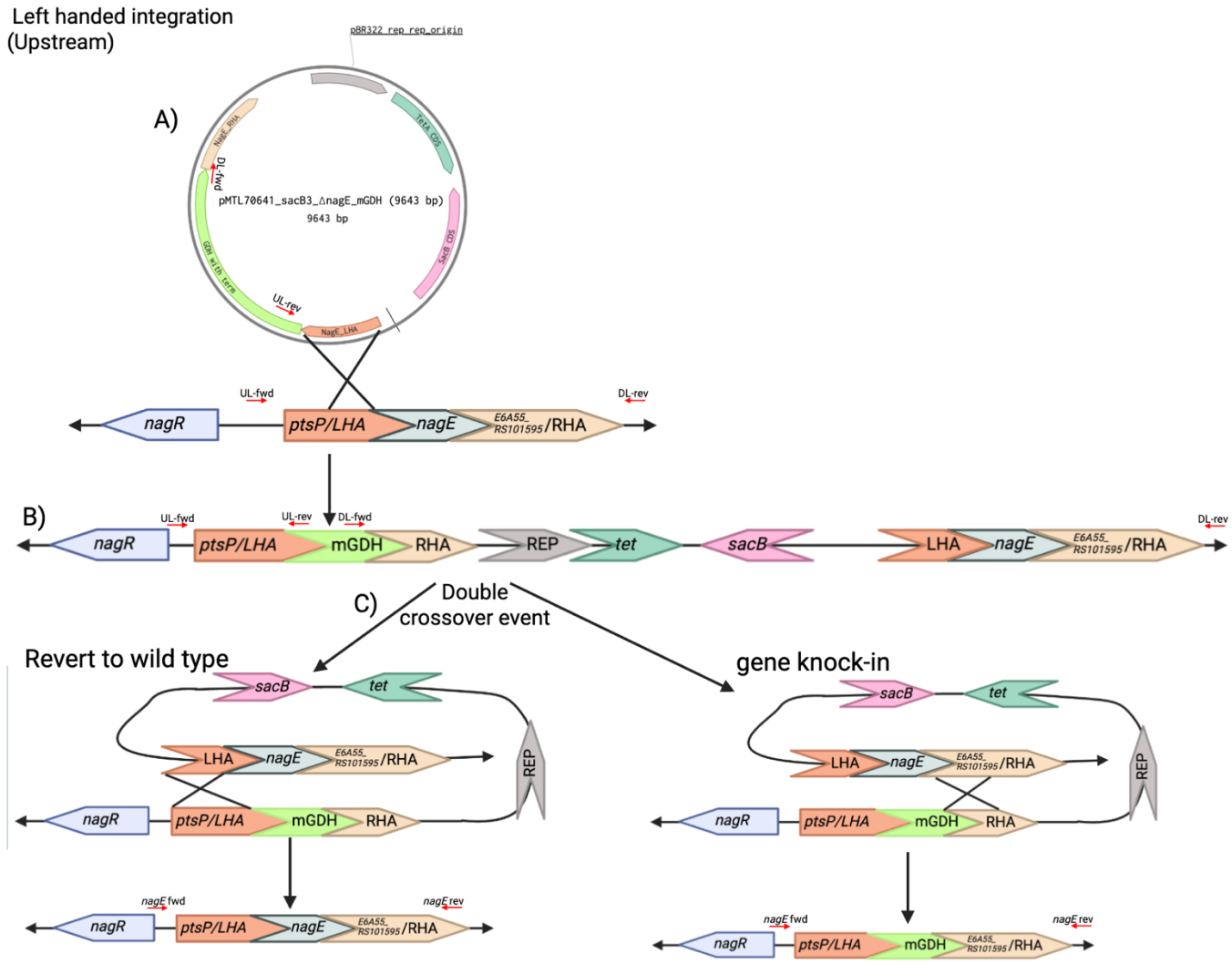


*Figure 3.15*: **Schematic of homologous recombination mediated gene knock-in via upstream integration, and position of screening primers on DNA.** A) pMTL70641_*sacB*_mGDH_Δ*nagE* aligns to chromosome via either homology arm, shown here is using the left homology arm, and initiates a crossover event. LHA results in insertion of the vector upstream of target locus, the opposite is true for RHA integration. B) Single crossovers are screened for using two sets of primers, UL_mGDH fwd/rev (UL fwd/rev) and DL_mGDH fwd/rev (DL fwd/rev), their positions are signalled by red arrows. Two separate PCR reactions are run, one for each primer pair. Only the pair corresponding to the integration that took place would show a result as the latter target would be too large for amplification, as shown above (B) with DL_mGDH encompassing a region ≈ 14 kb. C) colonies positive for a single crossover event are subjected to sucrose selection, post plating on selective agar colonies would have undergone a second homologous recombination event, losing the plasmid backbone and tetracycline resistance. This second event will result in cells reverting to wild type, or result in gene knock-in depending on whether recombination took place at the same or the opposite homology arm as the first event, respectively. PCR screening using the primers *nagE* fwd/rev (see red arrows), with the mutated cells showing a higher band compared to the wild type.

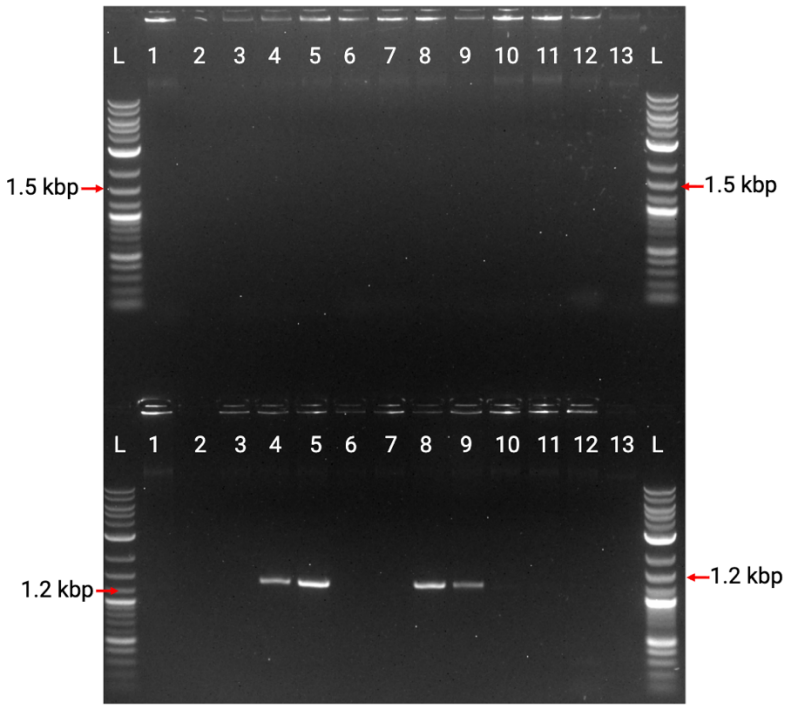


*Figure 3.16*: **Single crossover screening for *C. necator* pMTL70641_*sacB3*_mGDH_Δ*nagE*.** Colony PCR was carried out on colonies re-streaked onto F-MM-tetracycline (12.5 µg $ml^{-1}$). Lanes 1-12 represent respective colonies; Lane 13 represents a negative control using gDNA obtained from *C. necator* WT; the top row of reactions used the primers UL_mGDH fwd/rev, the lower row used DL_mGDH fwd/rev (2.1.1). Colonies represented by lanes 5 and 8 (*C. necator* pMTL70641_*sacB*3_mGDH_Δ*nagE*) were stored (2.1.5) and used downstream.

Colonies with confirmed single crossover events were then inoculated into 5 ml LSLB-MOPS-tetracycline (12.5 µg $ml^{-1}$) and grown overnight (2.1.3, 2.1.4), this was sub-cultured into 5 ml LSLB-MOPS ($OD_{600}$ 0.1) supplemented with 20% sucrose (w/v) and incubated overnight at 30°C with shaking (200 rpm) to select for double crossover events. The following day serial dilutions (down to $10^{-3}$) were plated on LSLB-MOPS agar supplemented with 20% sucrose (w/v). These were incubated at 30°C until colonies appeared (48-72 h), after which individual colonies were replica spotted onto LB-tetracycline agar (12.5 µg $ml^{-1}$) and LB agar, respectively. Colonies which grew exclusively on LB were screened via colony PCR using the primers *nagE* fwd/rev (2.1.1) for mGDH insertion and *nagE* loss; confirmed by a band size of ≈ 3.2 kb for the mutant, instead of ≈ 2.4 kb as observed in the wild type (Figure 3.17). As mentioned earlier, pMTL70641_*sacB3*_mGDH_Δ*nagE* conjugation was attempted into *C. necator* H16 and *C.* necator H16 Δ*nagR* (See section 3.4) multiple times, each being

unsuccessful in that either no colonies appeared on the initial selective plates, or any colony screened for single crossover events came back negative.

A)

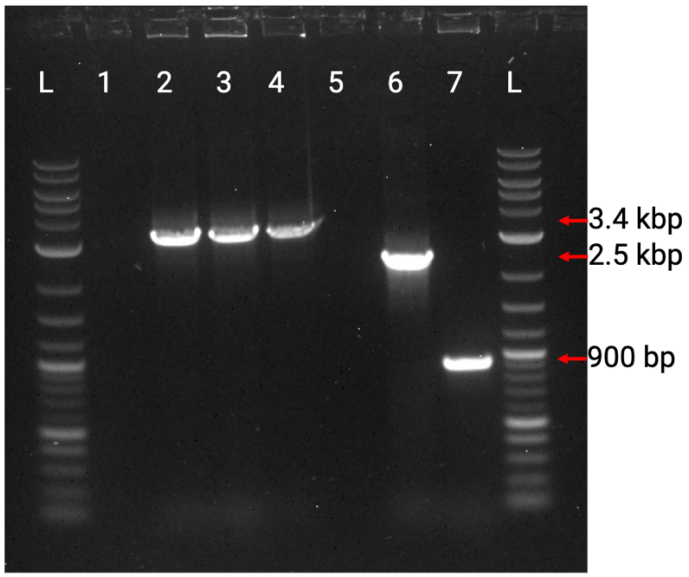


Figure 3.17: **Double crossover screening for *C. necator* pMTL70641_*sacB3*_mGDH_Δ*nagE*.** A) Colony PCR was carried out using primers *nagE* fwd/rev . Lanes 1-4 represent respective colonies; lane 5 is blank; lane 6 was carried out using *C. necator* gDNA as a template; lane 7 used a random colony with the primer *nagR* fwd/rev to confirm strain identity (*C. necator* H16 WT : 920 bp). PCR conditions: Tm- 61°C, Ext- 3 min. Colonies represented by lanes 2 and 3 (*C. necator::*mGDH_Δ*nagE*) were stored (2.1.5) and used downstream.

### 3.3.3. Measuring mGDH activity using a phenazine methosulphate (PMS), 2,6-dichloroindophenol assay.

Once the above described mGDH carrying strains and mutants were constructed, the activity of mGDH within *C. necator* was to be measured using a phenazine methosulphate (PMS)/ 2,6-dichloroindophenolate (DCPIP) assay. The oxidation of glucose by mGDH results in the transfer of two electron to DCPIP mediated by PMS, the reduction of DCPIP results in a distinct colour change which can be followed by measuring change in $OD_{600}$. (161). The PMS/DCPIP assay was to be carried out as laid out earlier (2.3.4), however firstly the extinction co-efficient of DCPIP under reaction conditions was determined (Figure 3.18) as it has been shown that this can vary quite significantly across reaction setups mainly due to effects of pH (161).

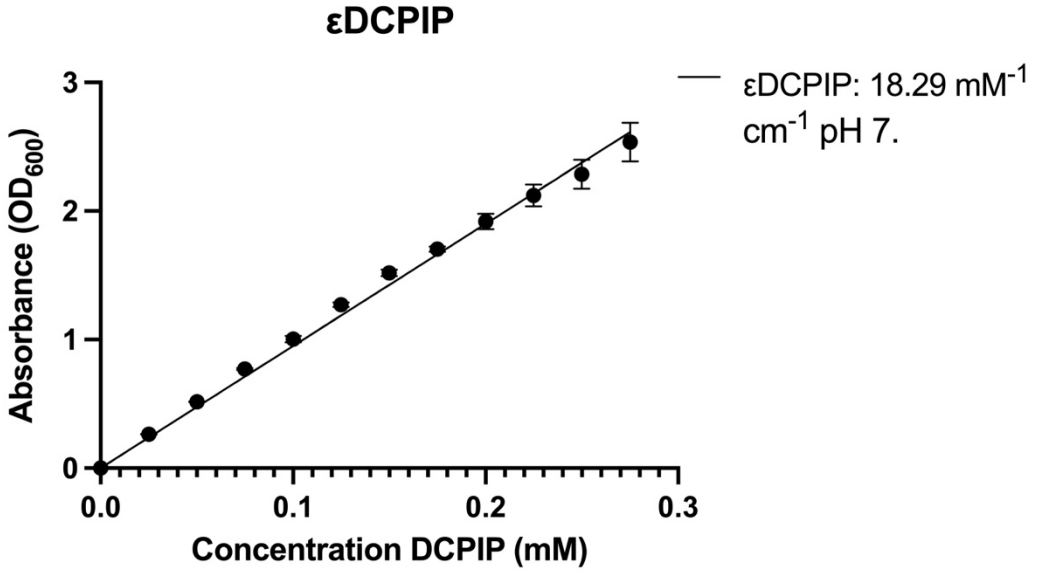


*Figure 3.18*: **Relationship between absorbance at 600 nm and DCPIP concentration under assay conditions.** Plotted are the mean values of triplicate measurements of the $OD_{600}$ of various concentrations of the oxidised form of DCPIP under assay conditions. A linear regression analysis constrained to intercept at (0,0) determined the slope as $y = 18.29x$, and $r^2 = 0.995$. Error bars represent standard deviation.

The extinction coefficient for DCPIP determined at 600 nm under experimental conditions aligns with published values in similar set-ups (161). Thus, the assay was employed to test for active mGDH in the constructed strains: *C. necator* mGDH_Δ*nagE, C. necator* pMTL71301_$P_{phaC}$_mGDH, and *C. necator* Δ*nagR* pMTL71301_$P_{phaC}$_mGDH; with *C. necator* H16 and *G. diazotrophicus* Pal 5 employed as negative and positive controls respectively. Whole cell samples, crude cell lysate, soluble proteins, and the membrane fraction, were prepared as described earlier (2.3.2), the protein content of all fractions except the whole cell were quantified with a commercial assay as described prior (2.3.3), and used to dilute protein mixtures to 1 mg $ml^{-1}$ protein content. This assay was also run with the fractions incubated with 2 µM PQQ in the event that mGDH was produced as the apo-enzyme. This concentration is in great excess of what was shown to be required for PQQ import independent activation of mGDH in *E. coli* (135) in order to ensure presence of PQQ within whole cells. Moreover, we have observed that PQQ supplemented to the medium has no impact on growth kinetics of *C. necator* H16 at concentrations exceeding 10 µM (data not shown).

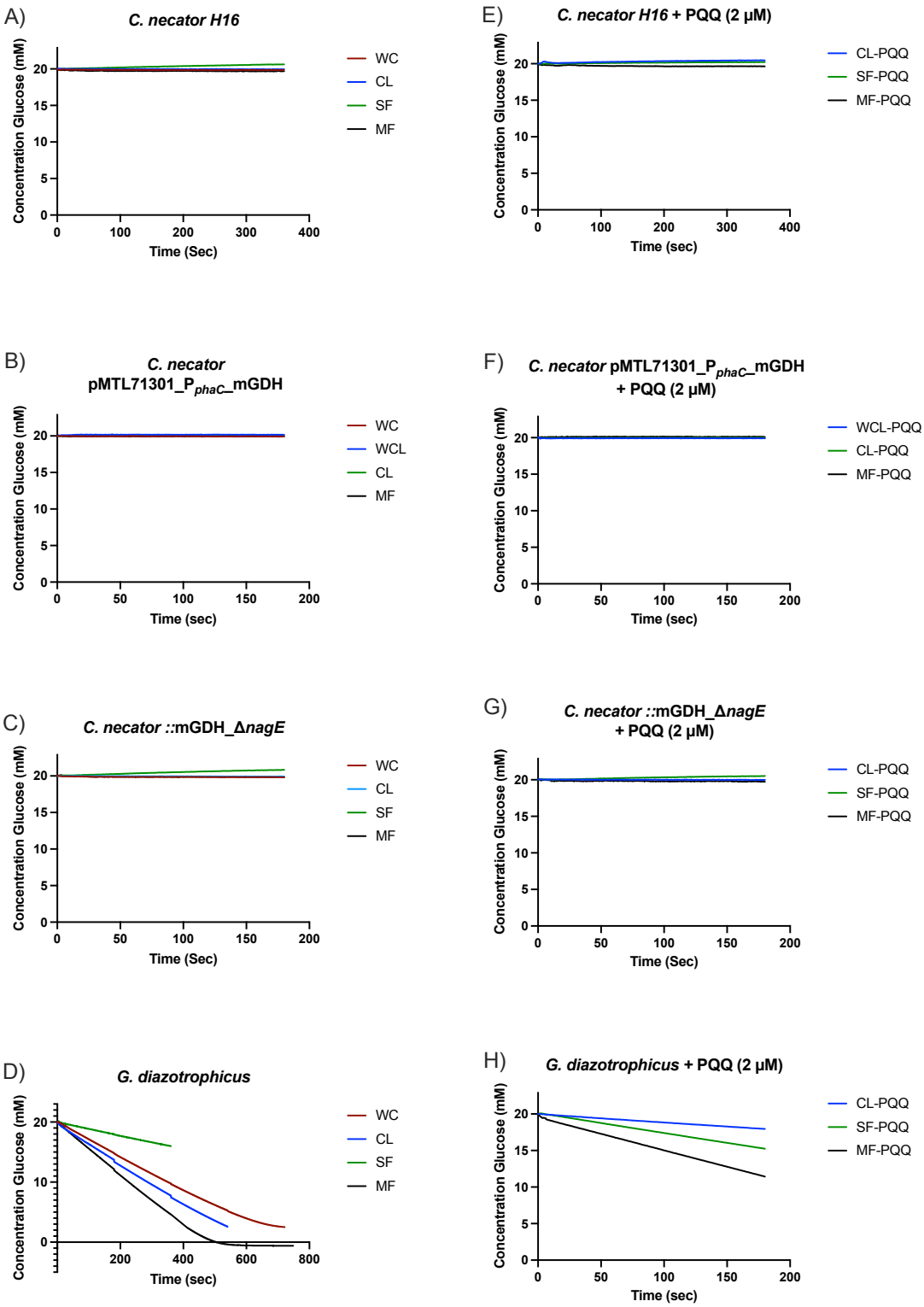


*Figure 3.19*: **Determining mGDH activity in *C. necator* H16 WT, *C. necator* pMTL71301_P$_{phaC}$_mGDH, and *C. necator::*mGDH_Δ*nagE*; with *G. diazotrophicus* PAL5 as positive control.** Assay was carried out in a 1 cm cuvette at a volume of 1 ml and consisted of 500 µl 2x reaction mixture, 150 µl PBS, and 300 µl whole cell or protein fraction (0.33 mg ml$^{-1}$ protein in final reaction), the assay was initiated by the addition and brief mixing of 50 µl substrate stock. This was run twice for each fraction, plotted are the mean changes in glucose concentration in the medium over

time (technical replicates), calculated by relating εDCPIP to $\Delta OD_{600}$. (A,E) *C. necator* H16; (B,F) *C. necator pMTL71301_*$P_{phaC}$_mGDH*;* (C,G) *C. necator*::mGDH_ Δ*nag*E*;* (D,H) *G. diazotrophicus* Pal5. Panels on the left represent samples without supplemented PQQ, the panels on the right represent samples with added PQQ (2 µM). WC- whole cell; CL- cleared lysate; SF- soluble fraction; MF- membrane fraction.

As the graphs in Figure 3.19 indicate, no mGDH activity was measured for any of the *C. necator* pMTL71301_$P_{phaC}$_mGDH and *C. necator*::mGDH_Δ*nagE* fractions regardless of supplemented PQQ. However, the positive control, *G. diazotrophicus,* showed activity for all tested fractions, with highest activities seen, as expected, in the membrane fraction, the specific activities can be seen in Figure 3.20

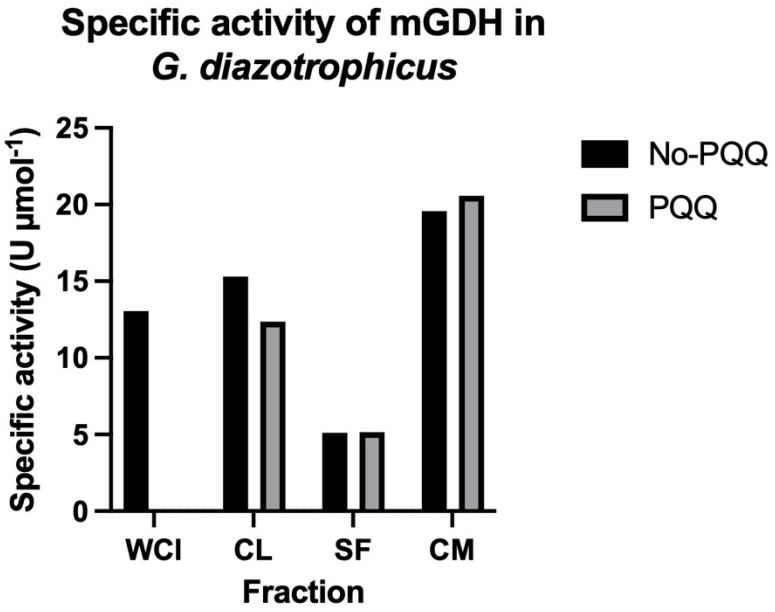


Figure 3.20: **Specific activity of mGDH from *G. diazotrophicus* with and without supplemented PQQ**. One unit is defined as the enzyme activity required for the conversion of 1 µmol D-glucose per minute. Graph is based on data from Figure 3.19.

## 3.4. Establishing constitutive PQQ biosynthesis

*C. necator* possesses *pqq*ABCDE on chromosome 2 (NCBI ref: NZ_CP039288) however lacks an obvious *pqq*F terminal peptidase gene (Figure 3.21-A). In *Acinetobacter calcoaceticus* PQQ biosynthesis ability is present, but an absence of *pqq*F shows that a dedicated PQQ terminal peptidase gene is not essential in all organisms (112, 162). Using this information, it was decided that the existing *pqq* operon would be utilised as the basis for establishing constitutive PQQ biosynthesis, a prerequisite for producing active mGDH under standard growth conditions.

### 3.4.1. Plasmid construction for P21 promoter knock-in upstream of *pqqA*

A synthetic promoter with medium strength constitutive transcriptional activity (P21) was selected to be reconstituted instead of the native promoter (62). This was to be assembled into a suicide plasmid for the knock-in of the promoter upstream of *pqqA*, replacing the native promoter. P21 was chosen to provide a balance between significant PQQ biosynthesis and the potential for metabolic burden.

To this end, the pMTL70641_*sacB3* suicide vector backbone was employed. Homology arms (≈ 1 kb) targeting a region slightly upstream of the ribosome binding site (RBS) of the *pqqA* promoter were identified and used to create the HiFi primers required. As the promoter to be inserted was too short to be amplified and assembled as its own fragment, the promoter sequence was split and tagged onto relevant HiFi primers to introduce the promoter into the fragments during the amplification of the homology arms from *C. necator* gDNA (Figure 3.21-B,C) The primers for this were designed manually.

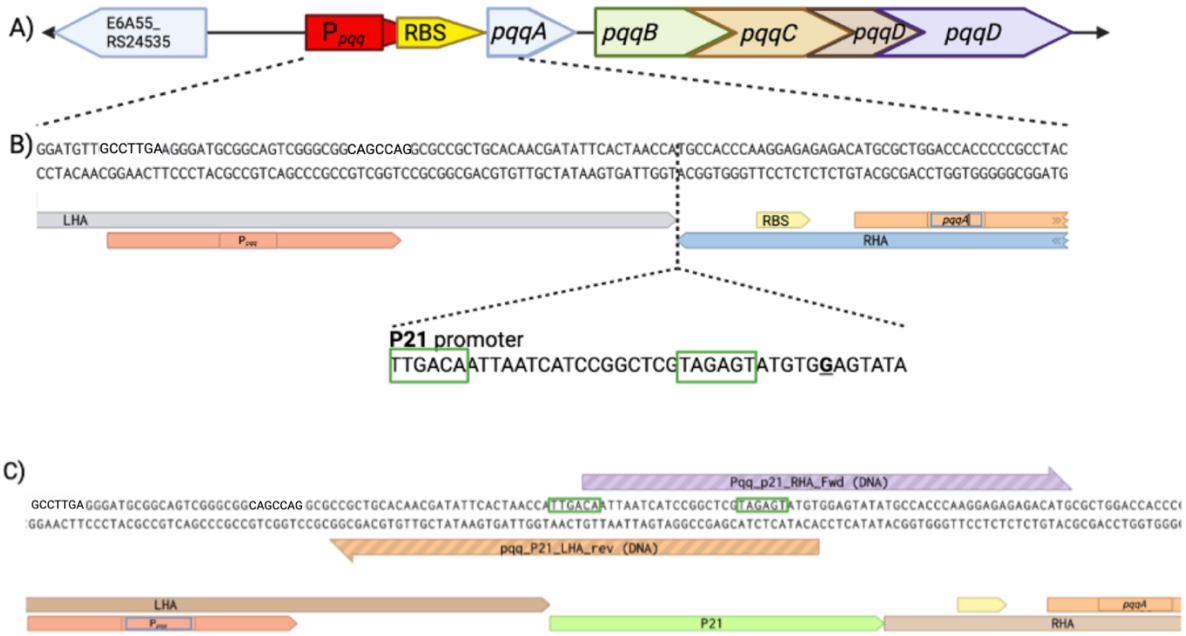


*Figure 3.21*: **Strategy for integrating the P21 synthetic promoter into *pqq*A homology arms for knock-in upstream of *pqqA*.** A) Structure of the *pqq* operon and surrounding genes in *C. necator* (NZ_CP039288). *pqq* native promoter and RBS shown in red and yellow respectively. B) The homology arms (length ≈1 kb) were targeted to between the native promoter and ribosome binding site. The dotted line represents site of P21 insertion, P21 sequence also shown; highlighted in green are the -10 and -35 elements, the underlined G represents the transcription start site. C) Schematic of HiFi primers covering P21 overlaid on target construct. The promoter was divided across the LHA_rev and RHA_fwd primers each carrying 33-37 bp of the promoter resulting in a 29 bp overlap as required for assembly. The full 41 bp promoter would be present once the fragments are assembled. The complementary primer for each homology arm was designed using the NEBuilder calculator (New England Biolabs), defining the LHA_fwd and RHA_rev primers as those designed manually.

The plasmid backbone (pMTL70641_sacB3) was prepared via double digest using NotI and Xho1 (2.2.7), the right homology arm was prepared via PCR (2.2.8). Due to the design constraints imposed by introducing P21 on the HiFi primers, the LHA could not be amplified by standard PCR as a great degree of non-specific binding occurred. Therefore, a nested approach was employed using the primers N_70641_P21_LHA fwd/rev which amplified the target LHA plus 50-150 bp extra on each side to allow for optimal primer binding. This fragment was purified and ran in a second reaction using HiFi_70641_P21_LHA fwd/rev (Figure 3.22). Once prepared, the linearised plasmid and both homology arms were assembled to form pMTL70641_P21 (2.2.8) (Figure 3.23). This was introduced into *E. coli* DH5α (2.1.7)

for storage and validation (2.2.9) (Figure 3.22). Once confirmed, pMTL70641_P21 was transferred into *E. coli* S17 for subsequent conjugal transfer into *C. necator* (2.1.9).

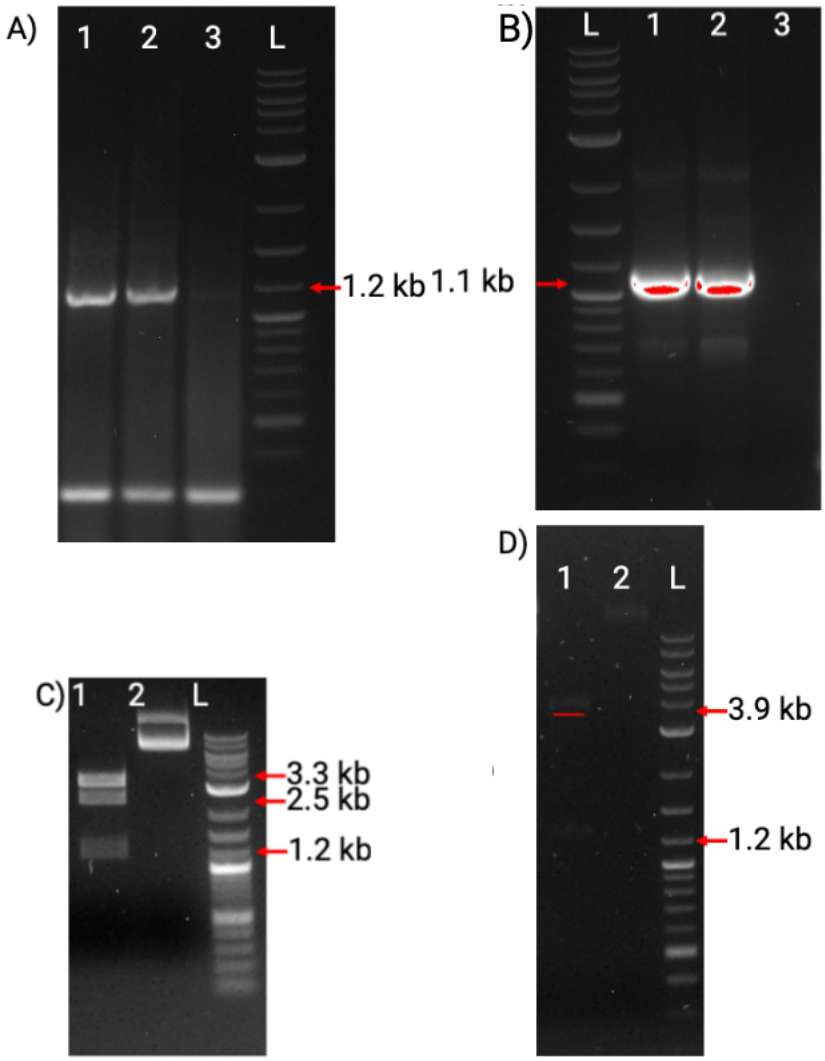


*Figure 3.22*: **Amplification of P21_LHA and Validation of pMTl70641_*sacB*3_p21.** P21_LHA was amplified using a nested PCR due non-specific binding of HiFi primers; both reactions used the same conditions: final Tm: 72°C; extension: 1:30 min, expected fragment sizes designated by red arrows A) reaction 1 used primers N_70641_P21_LHA fwd/rev (2.1.1), Lanes 1,2: gDNA template from *C. necator*; Lane 3: No template material. B) Reaction 2 used primers HiFi_70641_P21_LHA fwd/rev (2.1.1), Lanes 1,2: Template was purified products from lanes 1 and 2 of reaction 1; Lane 3: no template material. Products of reaction 2 from lanes 1,2 were purified (2.2.6) and pooled prior to use in assembly. Restriction digest of (C) pMTl70641_*sacB*3_p21 and (D) pMTL70641_*sacB3* using Eco32I. lane 1 represents digest; lane 2 represents undigested plasmid. Expected fragment sizes for a positive identification digest shown with red arrows.

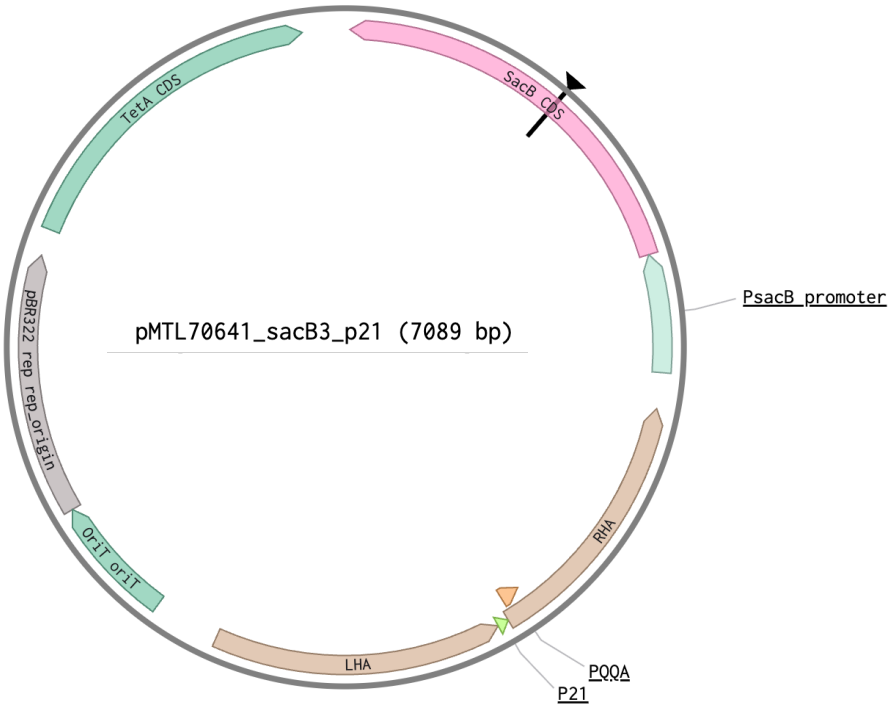


*Figure 3.23*: **pMTl70641_*sacB*3_p21 plasmid map.** The P21 synthetic promoter is targeted to be inserted upstream of *pqqA* using the plasmid pMTL70641_*sacB*3_P21; which confers tetracycline resistance (*tetA)* and harbours *sacB* encoding a levansucrase gene allowing for sucrose counter selection of a second crossover event. Other features: *oriT*- origin of transfer; pBR322 rep- *E. coli* specific origin of replication derived from pBR322.

### 3.4.2. Screening of single and double crossover events and validation of putative mutants

Validated pMTL70641_*sacB3*_P21 was transferred into *E. coli* S17-1 (2.1.7) and the resultant strain was used for conjugal transfer of the suicide vector into *C. necator* WT and Δ*nagR* mutant (*2.1.9*). However, this was only successfully achieved for *C. necator ΔnagR.* The selection process for single and double crossover events was identical to the one described earlier (3.3.2.1), with screening primers in the same relative positions (Figures 3.15, 3.24).

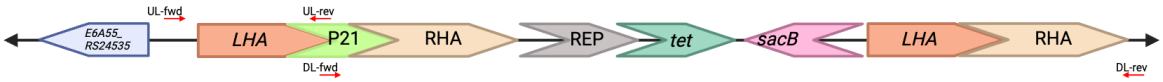


*Figure 3.24*: **Schematic of a left homology arm mediated single crossover event for pMTL70641_*sacB3*_P21 in *C. necator* and screening primer location.** The locations of the two primer pairs UL_P21 fwd/rev (UL fwd/rev) and DL_P21 fwd/rev (DL fwd/rev) are designated by red arrows. Each set of primers would only produce a product if an integration took place in orientation it screens for as the target region would otherwise be too long, as seen here for DL fwd/rev.

Screening for single and subsequent double mutants was carried out by colony PCR (2.2.10) using the two primer pairs UL_p21 fwd/rev and DL_P21 fwd/rev (2.1.1); results for this are shown in Figure 3.25. Despite troubleshooting by using multiple variations of the PCR, and slight re-designs for the primers, a positive result was not observed for the downstream linked primers. This may in part be due to the short P21 sequence (41 bp) offering limited potential targets littered with strong self-complementarity.

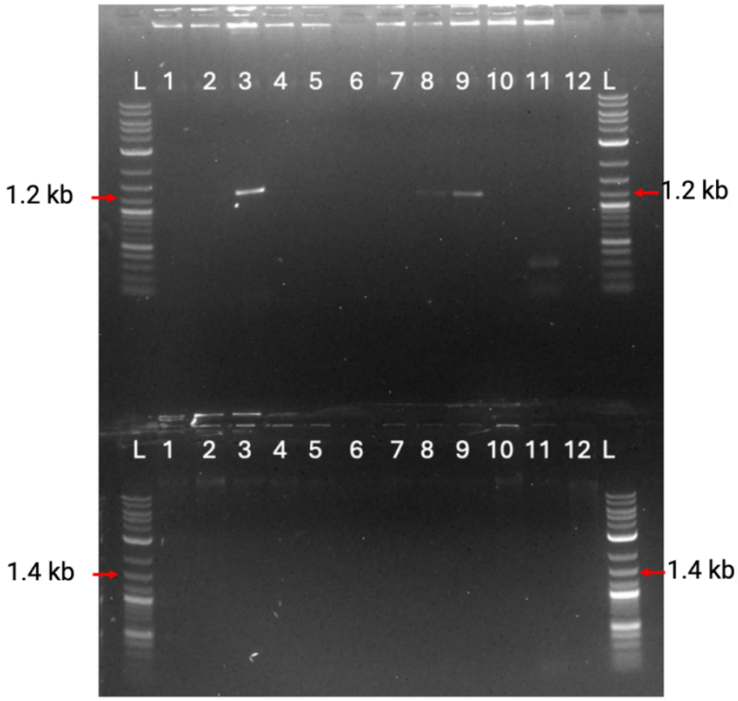


*Figure 3.25*: **Single crossover screening for pMTL70641_*sacB3*_P21 in *C. necator* Δ*nagR*.** Lanes 1-10 represent respective colonies. Lane 11 represents a random colony using the primers *nagR* fwd/rev to confirm strain identity. Lane 12 was an empty PCR rection. The top row used primer UL_P21 fwd/rev whilst the lower row used DL_p21 fwd/rev (2.1.1) Expected PCR fragment sizes for positive identification shown with red arrows. Colonies corresponding to lanes 3 and 9 (*C. necator* Δ*nagR* pMTL70641_*sacB3*_P21) were used for stocks (2.1.5) and downstream sucrose selection.

Colonies first identified as having undergone a single crossover event were taken through sucrose selection (3.3.2.1). Resulting colonies present exclusively on LB $^{-}$ after replica patching were then screened for double crossover events via colony PCR (2.2.10) using the primers UL_P21 fwd/rev and DL_P21_ fwd/rev (See Figure 3.26). Unfortunately, this was achieved with little time remaining to analyse the expression of *pqq*ABCDE under the P21 promoter.

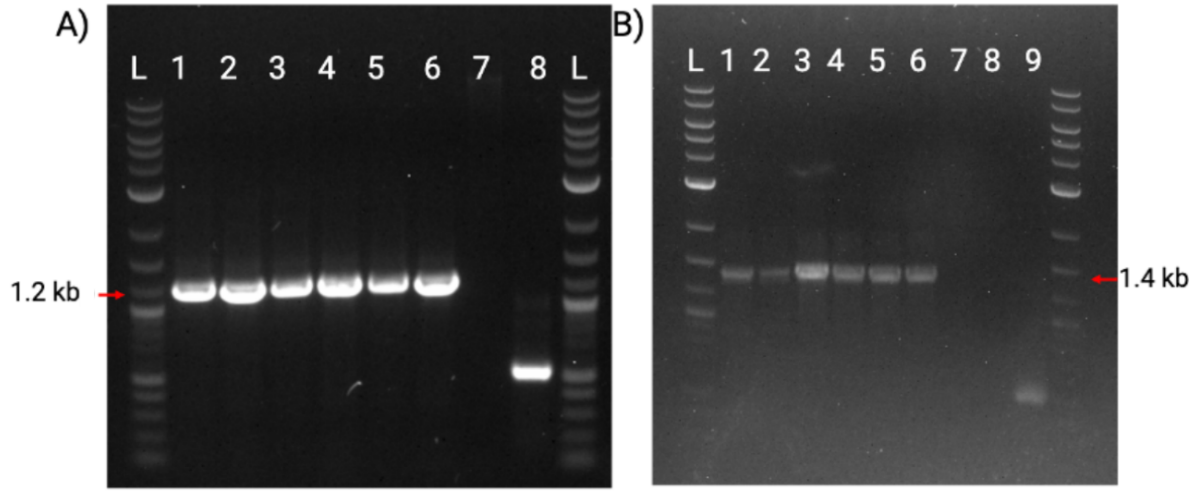


*Figure 3.26*: **Screening double crossover events for pMTL70641_*sacB3*_P21 in *C. necator* Δ*nagR*.** Putative double crossover events were screened for using the same primers as for single crossover events, with both pairs expected to give a positive result. Templates were colonies post-sucrose selection growing exclusively on LB without antibiotic after replica patching. A) Colony PCR carried out using UL_P21 fwd/rev; lanes 1-6: respective colony; lane 7: no template; lane 8: Random colony chosen for PCR using the primers *nagR* fwd/rev to confirm strain identity. B) Colony PCR carried out using DL_P21 fwd/rev; lane 1-6: respective colony; lane 7,8: no template; lane 9: Random colony chosen for PCR using the primers *nagR* fwd/rev to confirm strain identity. Expected PCR fragment sizes shown with red arrows. Colonies 1 and 3 (*C. necator* p21_*pqqA*_Δ*nagR*) were kept for stocks and used for downstream applications.

## 3.5. Translationally linked *rfp* reporter for the putative promoter region of *pqqU* in *C. necator*

PQQ biosynthesis is a complicated and energy intensive process. With the molecular mass of PQQ being only 330.2 g $mol^{-1}$ (330 Da) it lies under the diffusion limit for Gram-negative bacteria outer membrane porins and is often secreted into the environment by PQQ producing bacteria (137, 163). Making use of this are species such as *E. coli* which do not possess an endogenous PQQ biosynthetic operon but nevertheless contain genes encoding for various quinoproteins (135). Whilst diffusion through the membrane is possible, for uptake from the environment this would be highly inefficient unless a relatively high PQQ concentration is present; PQQ released into the medium by bacteria in studies optimising PQQ production reached titres between 0.3 nM to 3 μM (163).

To overcome the need for a high diffusion potential, many Gram-negative bacteria possess a gene encoding a PQQ import protein, namely *pqqU* which was shown to be active at PQQ concentrations as low as 1 nM within *E. coli* (135, 146), whereas a *pqqU* deficient *E. coli* mutant only started showing stunted growth at 100 nM (135).

### 3.5.1. Identification of putative *pqqU* in *C. necator* H16

The possibility of supplying exogenous PQQ to the growth medium of *C. necator* for the production of functional mGDH was assessed through the characterisation of a putative PQQ import system; *pqqU* has been shown to be prevalent amongst Gram-negative bacteria (146). To see whether it can be found specifically in *C. necator,* the PqqU amino acid sequence from *E. coli* K12 (UniProt: P76115; NP_415968.1) was subjected to a protein BLAST analysis (2.6.2) filtered to *C. necator* H16 (taxID: 6), this used the ClusteredNR database which clusters proteins from multiple species based on sequence identity and length similarity. The search yielded 5 proteins from *C. necator* H16, each in a separate cluster but all being part of the Ton-B dependent outer membrane receptor protein family.

A prior study identified amino acids essential for PQQ import and successfully used this to map *pqqU* presence across gram-negative bacteria (146), the same amino acids and their positions were compared against all *C. necator* H16 hits, with only the top result (WP_011617650.1) possessing the essential residues at the correct position (see Figure 3.27).

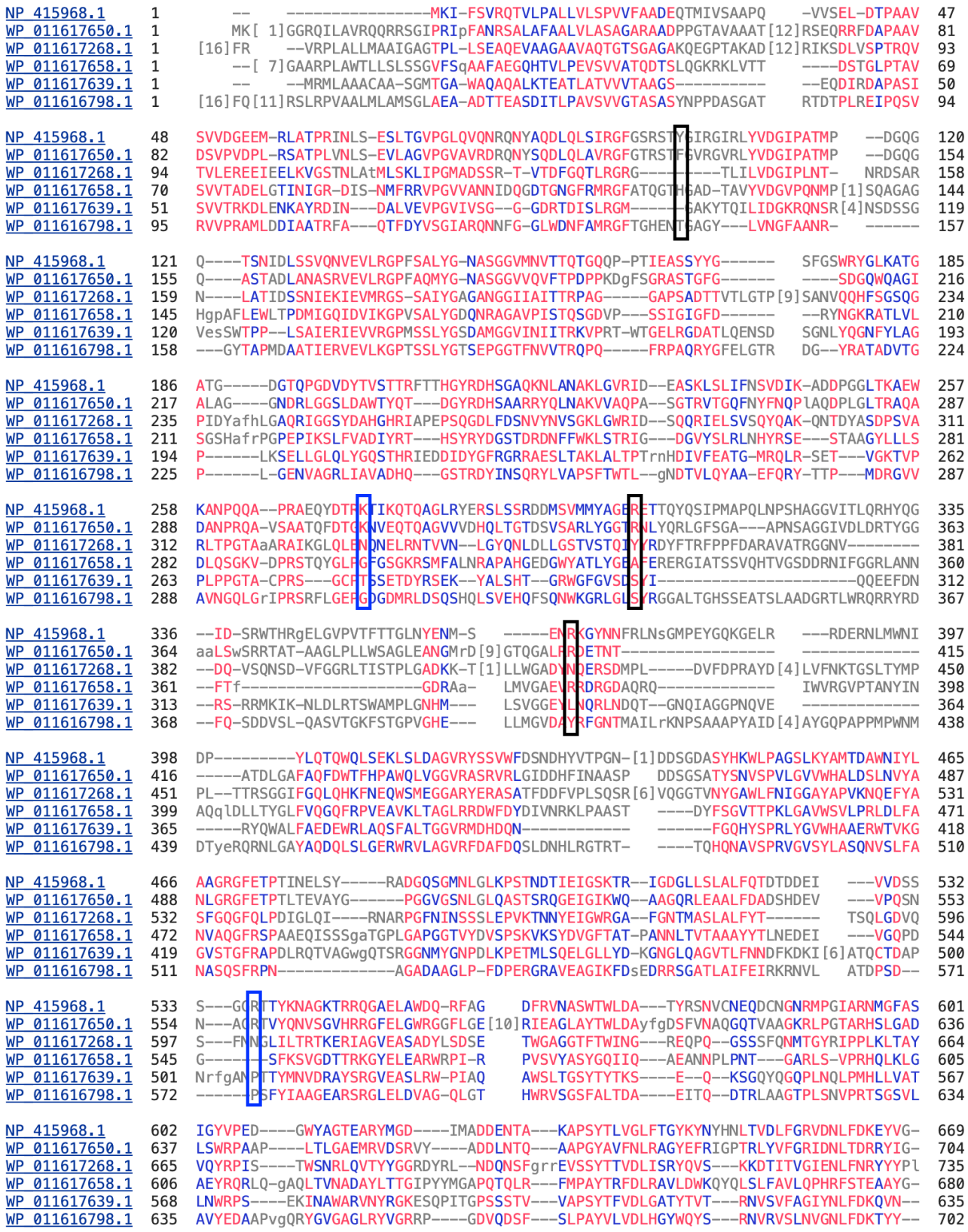

*Figure 3.27*: **Multiple sequence alignment comparing PqqU from *E. coli* K12 against the most similar proteins from *C. necator* H16.** All five results from the BLASTp analysis (2.6.2) were aligned against the sequence of PqqU from *E. coli* K12 (NP_415968.1). Outlined in black are residues essential

for PQQ binding and conserved across all species, Y99, R304, R365. Y99 is responsible for p-p interactions with PQQ, as such tryptophan (W) or phenylalanine (F) would also be accepted in this position. Outlined in blue are residues considered essential for PqqU function in *E. coli* K12, but not entirely conserved across Gram-negative bacteria. Only the top hit (WP_011617650.1) possesses the essential residues with F99 instead of Y99, also observed at the correct relative positions are the residues not entirely conserved across all Gram-negative bacteria.

| Accession Tag | Query cover (%) | Percentage identity (%) | Percentage similarity (%) |
|---|---|---|---|
| WP_011617650.1 | 95 | 41 | 56 |
| WP_011617268.1 | 93 | 24 | 41 |
| WP_011617658.1 | 77 | 22 | 38 |
| WP_011617639.1 | 19 | 32 | 55 |
| WP_011616798.1 | 15 | 30 | 50 |

*Table 3.3*: **Query cover, percentage identity, and similarity of proteins identified from blast of PqqU against *C. necator* H16.** Values were obtained from BLASTp analysis conducted earlier (3.5.1)

Despite an unassuming percentage identity and similarity (Table 3.3), it is likely the identified protein (WP_011617650.1) could likely be a PqqU homologue based on the aforementioned amino acid presence, and very high structural similarity to PqqU from *E. coli* K12 (PyMol RMSD: 0.659 Å) (Figure 3.28). Further investigations would be required to confirm PqqU identity, however as these were beyond the scope of this study it was decided to assume the identified protein was a PqqU homologue based off the structural similarity and conserved residues.

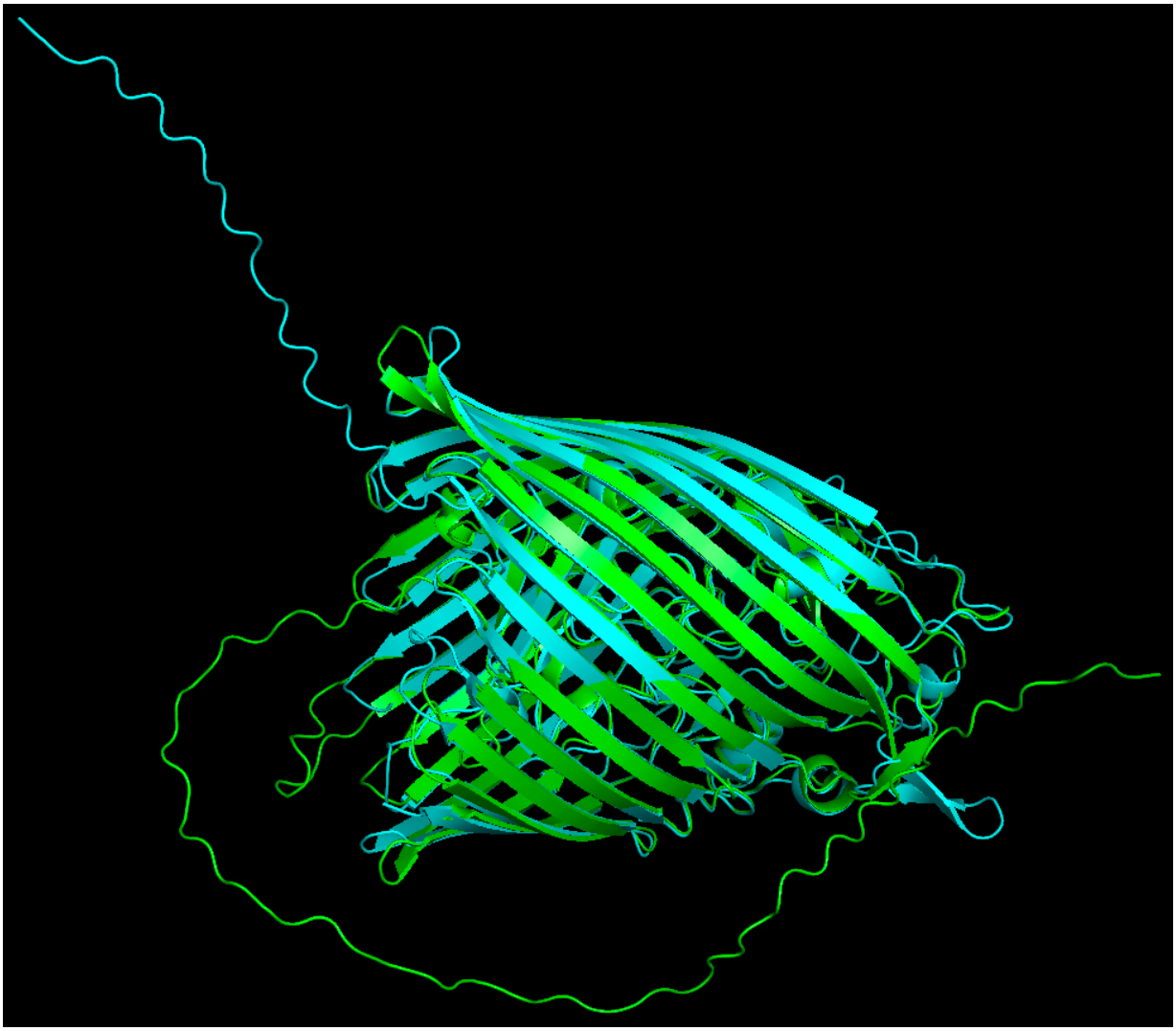

*Figure 3.28*: **PyMol alignment of top BLASTp result (WP_011617650.1) against PqqU from *E. coli* K12 (2.6.6).** The structures for PqqU from *E. coli* K12 (NP_415968.1) and the putative Ton-B dependent receptor protein from *C. necator* H16 (WP_011617650.1) were obtained from the AlphaFold database (https://alphafold.ebi.ac.uk/) as linked to from the UniProt (https://www.uniprot.org/) entries of the two proteins. The two structures were aligned using the PyMol feature (2.6.6), the root-mean squared deviation value indicates the average deviation of atoms of the superimposed models and was calculated to be 0.659 Å after accounting for outliers. These outliers were found to be the long unstructured C-terminal tails.

### *3.5.2.* Predicting a promoter region for the putative *C. necator pqqU* homologue

It was decided to investigate the expression of the putative *pqqU* gene within *C. necator* grown in media of interest, this being F-MM with and without PQQ. The promoter of the putative *pqqU* gene was not known, therefore the intergenic region upstream of the gene was run through various bacterial promoter prediction software to generate a map of potential promoter regions (2.6.3) (Figure 3.29). In this regard, the map yielded two "hotspots" upstream of *pqqU*, with the one further upstream seemingly responsible for an upstream located gene encoding a putative flavodoxin family protein (WP_018308768.1). It therefore appeared that the promoter for *pqqU* lies within 200 bp of the start codon.


*Figure 3.29*: **Map of predicted promoter regions in the upstream intergenic region of the putative *pqqU* from *C. necator* H16.** The sequence of the intergenic region (496 bp) upstream of the putative *pqqU* plus 1 kb flanking regions was run through various bacterial promoter prediction software (2.6.3). Predicted promoters from each software are represented by the colours: brown (SAPPHIRE), blue (BPROM), pink (BDGP, prokaryote), and purple (ProPR), with arrow direction indicating orientation.

As the goal was to elucidate the expression patterns of *pqqU*, the region used to construct this reporter encompassed the first 70 bp of *pqqU* with an additional 260 bp upstream from the start codon (Figure 3.29). This isolated sequence was used in conjunction with the sequence for pMTL71301_$P_{psts}$_*rfp* to generate HiFi primers (2.2.8) resulting in a construct where *rfp* is in-frame to the *pqqU* start codon and thus *rfp* expression is linked to *pqqU* translation (Figure 3.30).

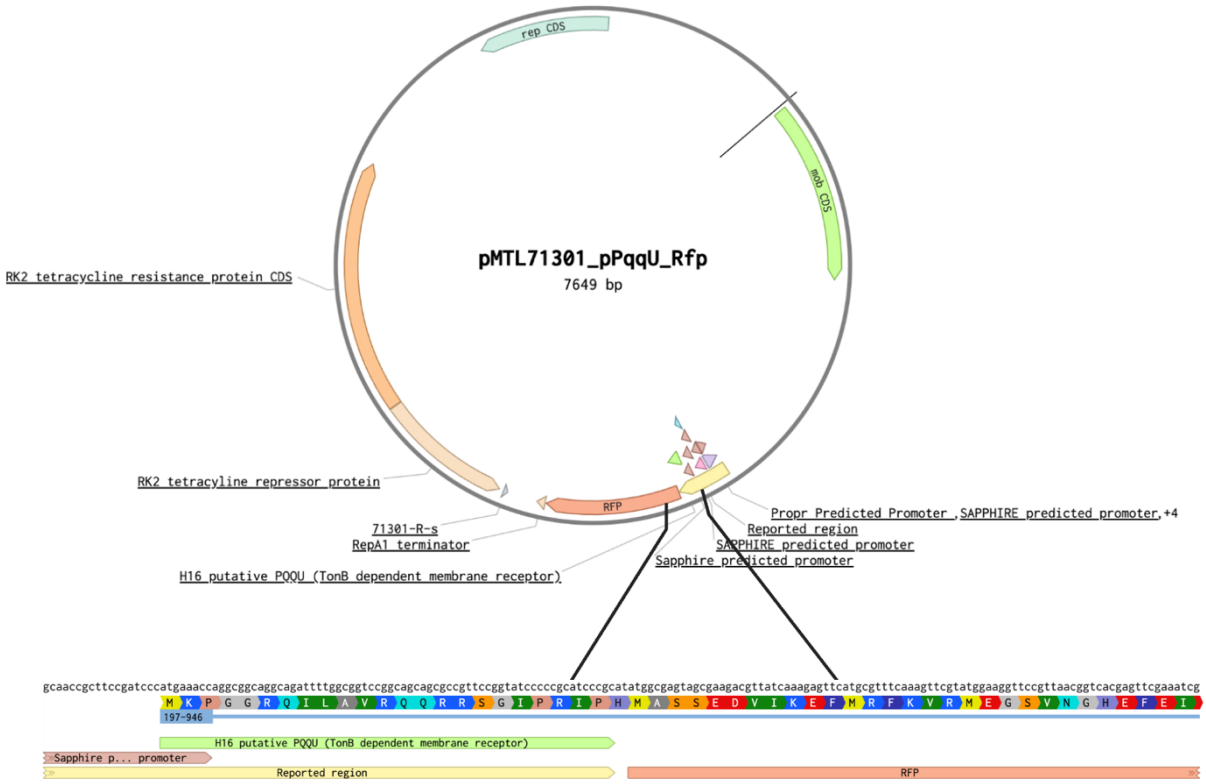


*Figure 3.30*: **pMTL71301_P$_{pqqU}$_*rfp* plasmid map.** The region determined earlier (here on designated P$_{pqqU}$) was assembled onto the broad host range vector pMTL71301 in frame to the *rfp* encoding sequence. Shown is the theoretical construct used to design primers for HiFi assembly (2.1.1, 2.2.8), the enlarged section presents a hypothetical translation showing *rfp* fused to the start of the putative *pqqU*. Mob CDS: sequence for mobility protein used in bacterial conjugation; rep CDS- pBBR1 derived replicase coding sequence ; RK2 tetracycline resistant/repressor proteins confer tetracycline resistance.

In order to assemble the plasmid, pMTL71301_P$_{psts}$_*rfp* was subjected to double digest using NotI and NdeI (2.2.7). P$_{pqqU}$ was amplified using the primers HiFi_71301_P$_{pqqU}$ fwd/rev (2.1.1) from *C. necator* derived gDNA (2.2.3). All fragments were prepared as described earlier (2.2.8) and assembled via HiFi, resulting in pMTL71301_P$_{pqqU}$_*rfp* which was introduced into *E. coli DH5a* for storage and validation (2.2.9; Figure 3.31) before transfer into *E. coli* S17 for subsequent conjugal transfer into *C. necator* (2.1.9).

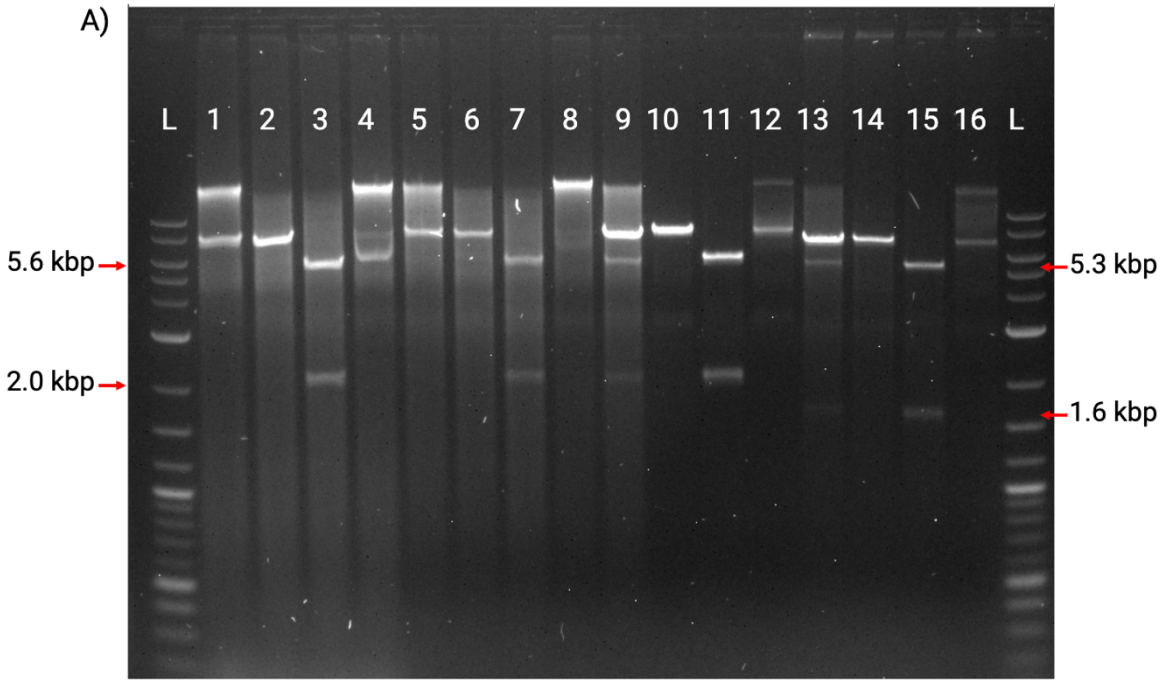


*Figure 3.31*: **pMTL71301_P$_{pqqU}$_*rfp* validation via digest and Sanger sequencing.** A) Restriction digest of pMTL71301_P$_{pqqU}$_*rfp from C. necator* WT (lanes 1-4), Δ*nagR* (lanes 5-8), *E. coli* S17-1 (lanes 9-12), and pMTL71301 using Eco32I and NdeI (2.2.7). Each sample is arranged with the first lane being NdeI only, the second lane Eco32I only, the third lane both enzymes, and the fourth lane being undigested plasmid. The red arrows on the left depict expected fragment sizes for double-digested pMTL71301_P$_{pqqU}$_*rfp*. The red arrows on the right depict the expected fragment sizes for the empty pMTL71301.

The reporter was introduced into *C. necator* WT and Δ*nagR* mutant via electroporation and bacterial conjugation, respectively (2.1.8, 2.1.9). The transformation was confirmed by first re-streaking a random colony from the selective plate post-transformation, and using this to isolate the plasmid from the two strains (2.2.1), before subjecting this to a restriction digest using NdeI and Eco32I (2.2.7; Figure 3.30). Those same colonies were then used to create stocks (2.1.5) and for downstream applications.

### 3.5.3. Measuring *pqqU* expression in minimal media supplemented with PQQ

Using the reporter constructed, the production of *rfp* was linked to the production of the putative PqqU, the fluorescence of which could be measured using a spectrophotometer. The experiment was carried out as outlined earlier (2.4), using *C. necator* WT, *C. necator* pMTL71301_P$_{pqqU}$_*rfp*, and *E. coli* S17-1 pMTL71301_P$_{psts}$_*rfp*. Samples were taken at 4 h,

10 h, 15 h, and 30 h from cultures grown in F-MM with and without PQQ (2 µM); RFP fluorescence was determined in microtiter format as outlined earlier (2.4) ($\lambda_{ex}$: 585 nm, $\lambda_{em}$: 620 nm), the results can be seen in Figure 3.32.

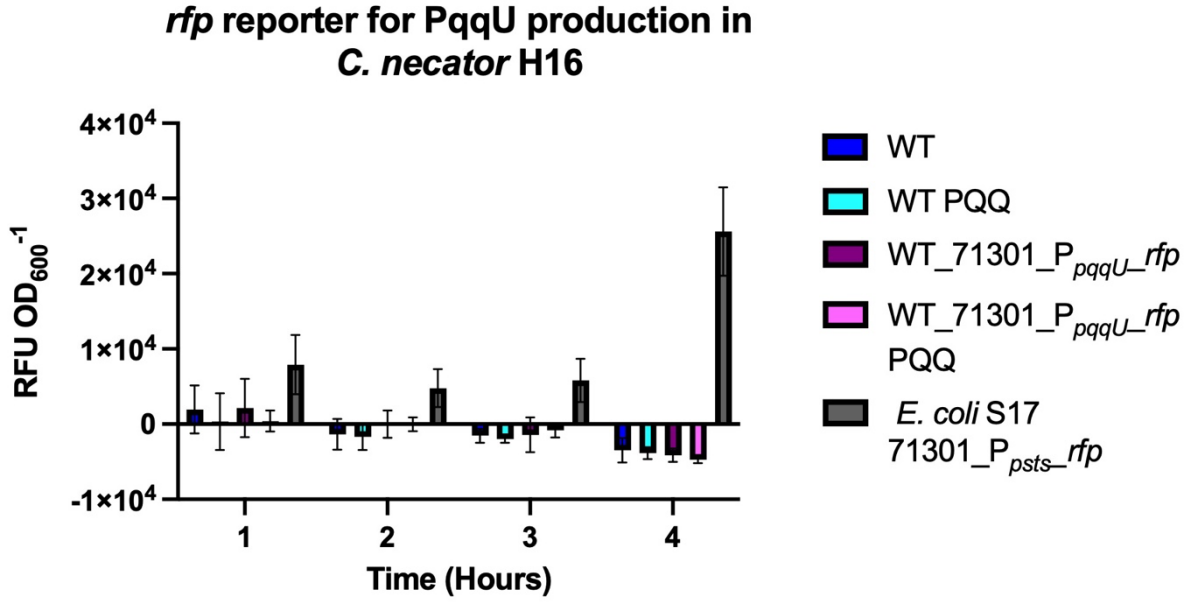


*Figure 3.32*: ***pqqU*** **expression in *C. necator* H16 grown in F-MM with and without supplemented PQQ (2 µM).** The assay was carried out as described earlier (2.4). corrected, $OD_{600}$ normalised results (3 technical replicates). Error bars represent standard deviation. No difference is seen between the *rfp* reporter and plasmid-less control (All p values > 0.05) indicating the reporter is not active under the investigated conditions. Moreover, no statistical significance is observed between *C. necator* carrying the *rfp* reporter in F-MM versus F-MM with PQQ (2 µM, all p values > 0.05), showing PQQ presence in the medium does not trigger a transcription response at the investigated locus. Statistical significance calculated using Mann-Whitney test.

As can be seen from the graph above, no significant difference is observed between the reporter and plasmid-less control, nor between the reporter cultured in F-MM and F-MM PQQ (2 µM). This indicates that A) there is no constitutive transcriptional activity at the investigated locus; and B) the addition of PQQ to the medium does not promote transcriptional activity at this locus. Further investigation would be needed using a similar experiment but supplementing the medium with known quino-protein substrates or their metabolites to investigate whether the putative *pqqU* is transcribed in response to substrate presence.

# 4. Discussion

*C. necator* H16 provides an attractive chassis for use in microbial cell factories due to a highly redundant and robust metabolism, as well as a growing repertoire of molecular biology tools. Part of employing an organism for this purpose might involve engineering towards a specific feedstock for ecologic or economic reasons, to this purpose a largely unexplored class of enzymes prevalent in gram negative bacteria may help in expanding the range of feedstocks available. The PQQ dependent enzymes, or quinoproteins, utilise the cofactor PQQ for the primary oxidation of various alcohols and sugars, an attractive member of this family is the methanol dehydrogenase found throughout methylotrophic bacteria, used with preference over NAD+ dehydrogenases and methanol oxidases likely due to preferential kinetics allowing for quicker clearance of methanol from the medium at the expense of greater reduction potentials (68). Another well studied example of quinoproteins, and the one chosen for this study, is the membrane bound glucose dehydrogenase (mGDH)(77, 84–87, 89, 147, 148, 154). This was selected over other quinoproteins for the non-toxicity of the enzymatic products, and the easily selectable glucose utilising phenotype as *C. necator* cannot natively utilise glucose due to a lack of proper importer. However, it has been shown to spontaneously acquire the ability when subjected to mutagenesis or a glucose selective pressure (40, 75, 76, 79), as such the incidence of this happening under relevant conditions was explored to inform how to best avoid interference.

The aforementioned overall aims of this study were the introduction of mGDH from *G. diazotrophicus* into *C. necator* H16, and contributing to functionality through the over-expression of the native PQQ biosynthetic operon through implementation of a medium strength synthetic promoter (62). This would confer glucose utilisation due to the activity of mGDH converting D-glucose to gluconolactone, which spontaneously hydrolyses to the favourable feedstock gluconate in the presence of water (135, 147).

Spontaneous acquisition of glucose utilisation is conferred by mutations in the $PTS_{nag}$, specifically a missense mutation in the repressor *nagR*, which results in de-repression and constitutive production of the porin NagE, on its own conferring minimal glucose assimilation due to low affinity for glucose (79). However, a further point mutation in *nagE* alters the active site conferring high affinity to glucose, and thus greater glucose assimilation (40, 75, 79).

Therefore, it was necessary to characterise the incidence of this occurring under conditions relevant to this study. *C. necator* H16 and the Δ*nagR* mutant both spontaneously acquired glucose utilisation mutations taking the form of distinct colonies observed when pre-cultures were inoculated onto G-MM agar and incubated at 30°C, in this the WT saw a considerably longer lag phase before the appearance of distinct colonies (20 days) compared to the Δ*nagR* mutant (4 days). The ability of *C. necator* H16 to evolve glucose utilisation was in accordance with earlier work employing mutagenesis or spontaneous generation (40, 75, 76, 156). This work observed a longer lag phase compared to the spontaneous generation study for a similar concentration of glucose; this may be explained by the differences in minimal media composition (75), specifically this study used 300 % $Na_2HPO_4.2H_2$, 65 % $KH_2PO_4$, and a significantly more dilute trace element solution compared to the study by Franz et. al. (75).

Further assessment of the acquisition of glucose utilisation phenotypes arising was carried out in liquid mediums. For *C. necator* H16 WT and Δ*nagR* mutants, no change in $OD_{600}$ or final $OD_{600}$ in G or FG-MM respectively was observed over the 14-day period. For G-MM this likely explained by an insufficient observation period, as indicated by the 20-day lag phase observed for the WT strain on G-MM agar. For FG-MM however, it has been shown that the time taken for glucose utilisation phenotypes to arise is linked to the length of time spent incubated with glucose as sole carbon source, independent of any starvation period prior to glucose supplementation (75). As shown in this study, a considerable (4-20 day) lag phase is required for glucose utilisation mutations to arise, which is simply not achieved through the repetitive subculturing of this investigation. The growth phase in 2.5 mM F-MM is 16 hours (Figure 3.2), meaning at most 32 hours is spent in a glucose exclusive medium, which should theoretically annul, or significantly hamper the development of glucose utilisation (75).

As the quinoprotein of interest was a glucose dehydrogenase and intended downstream applications included ALE against a glucose selective pressure, it was decided for the genome insertion approach to also remove the main gene responsible for conferring glucose utilisation (*nagE*). This was achieved in a single step via allelic replacement using homology arms which flanked the *nagE* locus, targeting the mGDH encoding gene in frame with to the original gene (79). Normally, *nagE* is under the control of a constitutively expressed repressor, NagR (79); therefore, to circumvent the need of employing a new promoter, the strain *C. necator* Δ*nagR* was employed such that mGDH encoding gene insertion at the *nagE* locus would place it under

a constitutively active promoter, which would have been useful for further studies. Unfortunately, mGDH could not be inserted into *C. necator* Δ*nagR* in the timeframe of this study.

The mGDH encoding gene from *G. diazotrophicus* Pal5 was successfully incorporated onto a broad-host range plasmid under the control of the *phaC* promoter and introduced into *C. necator* H16 and Δ*nagR* mutant. On the other hand, genetic introduction of the mGDH encoding gene by suicide plasmid based homologous recombination was only successful for the wild type strain, placing it under an active repressor controlled by a metabolite of the *N*-acetylglucosamine pathway, of which the importer was replaced by mGDH . The intention was to subject this strain to ALE against a glucose selective pressure, this could be achieved through two methods. The former employing repeated subculturing, and the latter a continuous culture; both in a medium with a limiting concentration of fructose or gluconate (2.5 mM), and excess glucose (> 20 mM) to select for glucose utilising mutants (164). The specific aspiration was natural acquisition of a mutation on *nagR* resulting in mGDH production. Unfortunately, time constraints inhibited this, though future work could explore this further.

*C. necator* pMTL71301_$P_{phaC}$_mGDH and *C. necator* H16::mGDH were assayed for mGDH activity using a PMS/DCPIP assay (94, 148, 161), with *G. diazotrophicus* Pal5 and *C. necator* H16 as positive and negative controls, respectively. Two assays were carried out on the same samples, with and without PQQ. The controls behaved as expected with mGDH activity observed for all *G. diazotrophicus* fractions upon the addition of glucose, and no activity for *C. necator* H16 under any conditions (Figure 3.19, 3.20). The assay also showed that no mGDH activity was observed for both *C. necator* pMTL71301_$P_{phaC}$_mGDH and *C. necator* H16::mGDH_Δ*nagE* regardless of PQQ supplementation indicating no form mGDH is being produced, of course this was expected for *C. necator* H16::mGDH_Δ*nagE* as it is located under an active repressor (NagR). One concern may be the lack of adequate transport machinery for mGDH to the inner membrane, however no mGDH activity was found within the lysed cell either. Further work would be needed to elucidate the reasons for lack of mGDH production, this could first take the shape of RT-qPCR to analyse expression levels under $P_{phaC}$ the only apparent issue with this may be its low strength and not actual control of transcription as $P_{phaC}$ has been successfully used for homologous and heterologous expression in *C. necator* H16 (165–167). If this shows adequate transcription, then an RFP linked translational fusion could be used to establish translation levels. One possible problem may be an inadequate

ribosome binding site (RBS) resulting in little or no mGDH translation. The same symptoms may also be caused by improper codon usage demand on the mGDH encoding gene resulting in stunted or inhibited translation (168). However, if RFP activity is observed then focus can shift to troubleshooting proper folding and transport of the enzyme to the cell membrane; one hindrance may lie in incompatibility with native chaperon systems (169). Past work on heterologous expression of quinoproteins from *Gluconacetobacter oxydans* found that inclusion of the 5' untranslated region can lead to greater expression levels, this may be worth exploring also (170).

Insofar as establishing constitutive PQQ biosynthesis through the coupling of the natively contained *pqq* operon with a synthetic constitutive promoter (P21). Despite attempted optimisation of the conjugation protocol, and attempts with electroporation, P21 was successfully introduced only into the Δ*nagR* mutant, but not into the wild type during the timeframe of this study. Very low efficiency was observed for all conjugations involving the pMTL70641 suicide plasmid, at least partially due to requirement for potential transconjugants to have to successfully undergone a double crossover event. As successful introduction of P21 upstream of pqqA in *C. necator* Δ*nagR* was achieved late into the duration of this study, no time was left for investigation into the effectiveness of this alteration beyond confirmation of its introduction. Future work should, at the very least, check whether PQQ is constitutively produced through this approach. However, it may be useful for later work to also attempt to identify the PqqF homologue in *C. necator* H16 as this is missing from the PQQ operon. *pqqF* is often found independent of *pqqABCDE* and its promoter, with some organisms lacking a *pqqF* homologue entirely yet still capable of PQQ biosynthesis. As the protease action of PqqF is essential to PQQ biosynthesis this may hint at possible redundancy with an unidentified enzyme potentially being employed for this purpose. While ultimately this protein may not be exclusively responsible for the trimming of the *PqqADE*, its regulation may have an effect on the level of PQQ biosynthesis (102, 104, 106, 123, 129), and should be elucidated in *C. necator* H16 for the purpose of fine tuning PQQ biosynthesis.

The investigated promoter region of the putative *pqqU* gene was shown to not be active when *C. necator* H16 pMTL71301_$P_{pqqU}$_*rfp* was grown in F-MM neither with nor without PQQ supplemented at 2 μM. This does not exclude this gene from encoding a PQQ importer, however the elucidation of this would require an in-depth study, perhaps where a *pqqU*

knockout and *pqqU* overexpressing strain are cultured in PQQ supplemented media at a range of molar to sub-molar concentrations followed by comparison of intracellular PQQ concentrations. This however was beyond the scope of this study, as such a concentration of PQQ (2 μM) known to diffuse sufficiently through Gram-negative outer membranes to reconstitute quinoprotein apo-enzymes was employed for cultures and assays where quinoprotein activity was measured (135). On the assumption the identified gene is indeed *pqqU*, a similar experiment to the one conducted in this study could be employed but supplementing the medium with known quino-protein substrates to investigate whether *pqqU* is transcribed in response to substrate presence.

In conclusion, the incidence of glucose utilisation in *C. necator* H16 was assessed and found to be significant enough to warrant genetic modifications to remove the locus responsible. This was achieved by replacing the *nagE* locus with the mGDH encoding gene. To circumvent the requirement for a custom promoter , the Δ*nagR* strain was also employed such that mGDH insertion will place it under a constitutively active promoter. Unfortunately, mGDH was chromosomally inserted only into *C. necator* H16 WT. On the other hand, mGDH cloned into a broad-host range vector was introduced into both H16 strains. The activity of mGDH was tested using a PMS/DCPIP assay which found no functional mGDH in any strain regardless of exogenous PQQ supplementation. Coupling of *pqqABCDE* to the synthetic promoter P21 was successful only in *C. necator* H16 Δ*nagR,* but could not be validated due to time constraints . Further work should validate constitutive PQQ biosynthesis, and attempt to locate the PqqF, or protein responsible for this step. Moreover, mGDH expression and production should be assessed potentially via by RT-qPCR and a translationally linked RFP reporter, which will elucidate whether the problem lies in expression, or folding and intracellular transport.

Although production of active mGDH in *C. necator* H16 in this study was unsuccessful, quinoproteins represent a wide range of recently discovered proteins with significant implications in native methylotrophy, and other activities such as catalysing the oxidation of a very wide variety of molecules including aromatics, sugars, and alcohols (73, 98, 101, 142, 171, 172). As such the establishment of a quinoprotein platform in *C. necator* would be of great benefit in unlocking a wide variety of substrates commonly considered polluters, for use in an organism already promising for waste valorisation due to an incredibly diverse and robust

metabolism. Continuation of this study may first verify constitutive PQQ biosynthesis, and attempt to troubleshoot the expression of mGDH. Characterisation of the putative PQQ import system in *C. necator* may yield that it is indeed present and active under relevant conditions. This could be used to develop a co-culturing method of industrial chemical production whereby cofactor biosynthesis is relinquished to a highly specialised organism in order to lighten the metabolic burden on *C. necator*, although this is unlikely to be required due to the small amounts of PQQ actually needed (135). Equally speculatively, *C. necator* may be able to sustain both cofactor biosynthesis and chemical production, as indicated by a *C. necator* strain endogenously harbouring a quinoprotein system (73).

Ultimately this work presents the basis for establishing functional quinoprotein production in *C. necator* H16, highlights the fundamental species-specific problems which may hamper heterologous quinoprotein expression, provides valuable characterisation of spontaneous glucose utilisation mutations in *C. necator*, and informs avenues future studies should explore in order to expand feedstocks. Namely effort should concentrate on elucidating the reason inhibiting mGDH production, or investigating whether the same limitation applies to variants of mGDH or other quinoproteins. Followed by assessments into endogenous PQQ production, and whether supplementation may be more appropriate.

The expansion of available feedstocks may greatly increase the suitability of *C. necator* H16 for use in key chemical production by limiting input constraints, or by unlocking more environmentally friendly feedstocks (E.g. glucose, sorbitol, methanol, and various other alcohols, etc. (142, 171, 172)).

# 5. Bibliography


1. Filonchyk, M., Peterson, M. P., Zhang, L., Hurynovich, V., and He, Y. (2024) Greenhouse gases emissions and global climate change: Examining the influence of CO2, CH4, and N2O. *Science of The Total Environment*. **935**, 173359
2. NOAA National Centers for Environmental Information (2025) Monthly Global Climate Report for Annual 2024. *NOAA National Centers for Environmental Information*. [online] https://www.ncei.noaa.gov/access/monitoring/monthly-report/global/202413 (Accessed November 3, 2025)
3. Rebecca Lindsey (2023) Climate Change: Global Sea Level. *Climate.gov*. [online] https://www.climate.gov/news-features/understanding-climate/climate-change-global-sea-level (Accessed November 2, 2025)
4. Boyin Huang, Peter W. Thorne, Viva F. Banzon, Tim Boyer, Gennady Chepurin, Jay H. Lawrimore, Matthew J. Menne, Thomas M. Smith, Russell S. Vose, and Huai-Min Zhang (2017) NOAA Extended Reconstructed Sea Surface Temperature (ERSST), Version 5. *National oceanic and Atmospheric Association*. [online] https://www.ncei.noaa.gov/access/metadata/landing-page/bin/iso?id=gov.noaa.ncdc:C00927 (Accessed November 2, 2025)
5. Lenton, T. M., Milkoreit, M., Willcock, S., Abrams, J. F., Armstrong McKay, D. I., Buxton, J. E., Donges, J. F., Loriani, S., Wunderling, N., Alkemade, F., Barrett, M., Constantino, S., Powell, T., Smith, S. R., Boulton, C. A., Pinho, P., Dijkstra, H. A., Pearce-Kelly, P., RomanCuesta, R. M., and Dennis, D. (2025) *Global Tipping Points Report 2025*, Exeter
6. *Historical GHG Emissions* (2025) Washington DC, [online] https://www.climatewatchdata.org/ghg-emissions (Accessed November 2, 2025)
7. Li, L., Awada, T., Shi, Y., Jin, V. L., and Kaiser, M. (2025) Global Greenhouse Gas Emissions From Agriculture: Pathways to Sustainable Reductions. *Global Change Biology* **31**, e70015
8. Tickner, J., Geiser, K., and Baima, S. (2021) Transitioning the Chemical Industry: The Case for Addressing the Climate, Toxics, and Plastics Crises. *Environment: Science and Policy for Sustainable Development*. **63**, 4–15
9. Carus, M., Dammer, L., Raschka, A., and Skoczinski, P. (2020) Renewable carbon: Key to a sustainable and future-oriented chemical and plastic industry: Definition, strategy, measures and potential. *Greenhouse Gases: Science and Technology*. **10**, 488–505
10. Morseletto, P. (2020) Targets for a circular economy. *Resources Conservation and Recycling* **153**, 104553
11. Corvellec, H., Stowell, A. F., and Johansson, N. (2022) Critiques of the circular economy. *Journal of Industrial Ecology* **26**, 421–432
12. Slootweg, J. C. (2024) Sustainable chemistry: Green, circular, and safe-by-design. *One Earth*. **7**, 754–758
13. Gavrilescu, M. (2024) From pollutants to products: Microbial cell factories driving sustainable biomanufacturing and environmental conservation. *Chemical Engineering Journal*. **500**, 157152
14. Lee, J. W., Na, D., Park, J. M., Lee, J., Choi, S., and Lee, S. Y. (2012) Systems metabolic engineering of microorganisms for natural and non-natural chemicals. *Nature Chemical Biology* **8**, 536–546

15. Cho, J. S., Kim, G. B., Eun, H., Moon, C. W., and Lee, S. Y. (2022) Designing Microbial Cell Factories for the Production of Chemicals. *JACS Au*. **2**, 1781–1799
16. Gurdo, N., Volke, D. C., McCloskey, D., and Nikel, P. I. (2023) Automating the design-build-test-learn cycle towards next-generation bacterial cell factories. *New Biotechnology* **74**, 1–15
17. *FAQ: Microbes Make the Cheese* (2013) 10.1128/AAMCol.June.2014
18. Poehlein, A., Solano, J. D. M., Flitsch, S. K., Krabben, P., Winzer, K., Reid, S. J., Jones, D. T., Green, E., Minton, N. P., Daniel, R., and Dürre, P. (2017) Microbial solvent formation revisited by comparative genome analysis. *Biotechnology for Biofuels*. **10**, 58
19. Verma, A. S., Agrahari, S., Rastogi, S., and Singh, A. (2011) Biotechnology in the realm of history. *Journal of Pharmacy and Bioallied Science* **3**, 321–3
20. Radde, N., Mortensen, G. A., Bhat, D., Shah, S., Clements, J. J., Leonard, S. P., McGuffie, M. J., Mishler, D. M., and Barrick, J. E. (2024) Measuring the burden of hundreds of BioBricks defines an evolutionary limit on constructability in synthetic biology. *Nature Communications* **15**, 6242
21. Ingelman, H., Heffernan, J. K., Harris, A., Brown, S. D., Shaikh, K. M., Saqib, A. Y., Pinheiro, M. J., de Lima, L. A., Martinez, K. R., Gonzalez-Garcia, R. A., Hawkins, G., Daleiden, J., Tran, L., Zeleznik, H., Jensen, R. O., Reynoso, V., Schindel, H., Jänes, J., Simpson, S. D., Köpke, M., Marcellin, E., and Valgepea, K. (2024) Autotrophic adaptive laboratory evolution of the acetogen Clostridium autoethanogenum delivers the gas-fermenting strain LAbrini with superior growth, products, and robustness. *New Biotechnology* **83**, 1–15
22. Makkar, N. S., and Casida, L. E. (1987) Cupriavidus necator gen. Nov. sp. Nov.; a Nonobligate Bacterial Predator of Bacteria in Soil. *International Journal of Systemic Bacteriology.* **37**, 323–326
23. Diana H. Davis, Michael Doudoroff, Roger Y. Stanier, and Manley Mandel (1969) Proposal to reject the genus hydrogenomonas: taxonomic implications. *International Journal of Systems Bacteriology* **19**, 375–390
24. Yabuuchi, E., Kosako, Y., Yano, I., Hotta, H., and Nishiuchi, Y. (1995) Transfer of Two *Burkholderia* and An *Alcaligenes* Species to *Ralstonia* Gen. Nov. *Microbiology and Immunology* **39**, 897–904
25. Vaneechoutte, M., Kämpfer, P., De Baere, T., Falsen, E., and Verschraegen, G. (2004) Wautersia gen. nov., a novel genus accommodating the phylogenetic lineage including Ralstonia eutropha and related species, and proposal of Ralstonia [Pseudomonas] syzygii (Roberts et al. 1990) comb. nov. *International Journal of Systematic and Evolutionary Microbiology* **54**, 317–327
26. Parte, A. C., Sardà Carbasse, J., Meier-Kolthoff, J. P., Reimer, L. C., and Göker, M. (2020) List of Prokaryotic names with Standing in Nomenclature (LPSN) moves to the DSMZ. *International Journal of Systematic and Evolutionary Microbiology.* **70**, 5607–5612
27. Reinecke, F., and Steinbüchel, A. (2009) Ralstonia eutropha Strain H16 as Model Organism for PHA Metabolism and for Biotechnological Production of Technically Interesting Biopolymers. *Microbial Physiology* **16**, 91–108
28. Schwartz, E., Henne, A., Cramm, R., Eitinger, T., Friedrich, B., and Gottschalk, G. (2003) Complete Nucleotide Sequence of pHG1: A Ralstonia eutropha H16 Megaplasmid Encoding Key Enzymes of H2-based Lithoautotrophy and Anaerobiosis. *Journal of Molecular Biology* **332**, 369–383

29. Vičević, R., Ceronja, E. Š., Šakić, R., Šalić, A., Tušek, A. J., and Zelić, B. (2025) Separation and characterisation of crude hydrogenase from Cupriavidus necator H16 grown on waste glycerol. *Carbon Resources Conversion*. 10.1016/j.crcon.2025.100394
30. Pfitzner, J., and Schlegel, H. G. (1973) Denitrifikation bei Hydrogenomonas eutropha Stamm H16. *Archiv für Mikrobiologie*. **90**, 199–211
31. Holmes, E. C., Bleem, A. C., Johnson, C. W., and Beckham, G. T. (2024) Adaptive laboratory evolution and metabolic engineering of Cupriavidus necator for improved catabolism of volatile fatty acids. *Metabolic Engineering* **86**, 262–273
32. Kohlmann, Y., Pohlmann, A., Schwartz, E., Zühlke, D., Otto, A., Albrecht, D., Grimmler, C., Ehrenreich, A., Voigt, B., Becher, D., Hecker, M., Friedrich, B., and Cramm, R. (2014) Coping with Anoxia: A Comprehensive Proteomic and Transcriptomic Survey of Denitrification. *Journal of Proteome Research* **13**, 4325–4338
33. Morlino, M. S., Serna García, R., Savio, F., Zampieri, G., Morosinotto, T., Treu, L., and Campanaro, S. (2023) Cupriavidus necator as a platform for polyhydroxyalkanoate production: An overview of strains, metabolism, and modeling approaches. *Biotechnology Advances* **69**, 108264
34. Pohlmann, A., Fricke, W. F., Reinecke, F., Kusian, B., Liesegang, H., Cramm, R., Eitinger, T., Ewering, C., Pötter, M., Schwartz, E., Strittmatter, A., Voß, I., Gottschalk, G., Steinbüchel, A., Friedrich, B., and Bowien, B. (2006) Genome sequence of the bioplastic-producing "Knallgas" bacterium Ralstonia eutropha H16. *Natural Biotechnology* **24**, 1257–1262
35. Little, G. T., Ehsaan, M., Arenas-López, C., Jawed, K., Winzer, K., Kovacs, K., and Minton, N. P. (2019) Complete Genome Sequence of Cupriavidus necator H16 (DSM 428). *Microbiology Resource Announcements* 10.1128/MRA.00814-19
36. Alagesan, S., Minton, N. P., and Malys, N. (2018) 13C-assisted metabolic flux analysis to investigate heterotrophic and mixotrophic metabolism in Cupriavidus necator H16. *Metabolomics*. **14**, 9
37. Pérez-Pantoja, D., De la Iglesia, R., Pieper, D. H., and González, B. (2008) Metabolic reconstruction of aromatic compounds degradation from the genome of the amazing pollutant-degrading bacterium *Cupriavidus necator* JMP134. *FEMS Microbiology Reviews* **32**, 736–794
38. Johnson, B. F., and Stanier, R. Y. (1971) Dissimilation of Aromatic Compounds by Alcaligenes eutrophus. *Journal Bacteriology* **107**, 468–475
39. Pearcy, N., Garavaglia, M., Millat, T., Gilbert, J. P., Song, Y., Hartman, H., Woods, C., Tomi-Andrino, C., Reddy Bommareddy, R., Cho, B.-K., Fell, D. A., Poolman, M., King, J. R., Winzer, K., Twycross, J., and Minton, N. P. (2022) A genome-scale metabolic model of Cupriavidus necator H16 integrated with TraDIS and transcriptomic data reveals metabolic insights for biotechnological applications. *PLoS Computational Biology* **18**, e1010106
40. Orita, I., Iwazawa, R., Nakamura, S., and Fukui, T. (2012) Identification of mutation points in Cupriavidus necator NCIMB 11599 and genetic reconstitution of glucose-utilization ability in wild strain H16 for polyhydroxyalkanoate production. *Journal of Biosciences and Bioengineering* **113**, 63–69
41. Tsunedomi, R., Izu, H., Kawai, T., Matsushita, K., Ferenci, T., and Yamada, M. (2003) The Activator of GntII Genes for Gluconate Metabolism, GntH, Exerts Negative Control of GntR-Regulated GntI Genes in *Escherichia coli*. *Journal of Bacteriology* **185**, 1783–1795
42. Strittmatter, C. S., Eggers, J., Biesgen, V., Pauels, I., Becker, F., and Steinbüchel, A. (2022) The reliance of glycerol utilization by Cupriavidus necator on CO2 fixation and

improved glycerol catabolism. *Applied Microbiological Biotechnology* **106**, 2541–2555
43. Fukui, T., Mukoyama, M., Orita, I., and Nakamura, S. (2014) Enhancement of glycerol utilization ability of Ralstonia eutropha H16 for production of polyhydroxyalkanoates. *Applied Microbiological Biotechnology* **98**, 7559–7568
44. Pohlmann, A., Fricke, W. F., Reinecke, F., Kusian, B., Liesegang, H., Cramm, R., Eitinger, T., Ewering, C., Pötter, M., Schwartz, E., Strittmatter, A., Voß, I., Gottschalk, G., Steinbüchel, A., Friedrich, B., and Bowien, B. (2006) Genome sequence of the bioplastic-producing "Knallgas" bacterium Ralstonia eutropha H16. *Natural Biotechnology* **24**, 1257–1262
45. Islam Mozumder, Md. S., Garcia-Gonzalez, L., Wever, H. De, and Volcke, E. I. P. (2015) Poly(3-hydroxybutyrate) (PHB) production from CO2: Model development and process optimization. *Biochemichal Engineering Journal* **98**, 107–116
46. Obruca, S., Benesova, P., Oborna, J., and Marova, I. (2014) Application of protease-hydrolyzed whey as a complex nitrogen source to increase poly(3-hydroxybutyrate) production from oils by Cupriavidus necator. *Biotechnology Letters* **36**, 775–781
47. dos Santos, A. J., Oliveira Dalla Valentina, L. V., Hidalgo Schulz, A. A., and Tomaz Duarte, M. A. (2017) From Obtaining to Degradation of PHB:Material Properties. Part I. *Ingineria y Ciencia* **13**, 269–298
48. Geissdoerfer, M., Savaget, P., Bocken, N. M. P., and Hultink, E. J. (2017) The Circular Economy – A new sustainability paradigm? *Journal of Cleaner Production* **143**, 757–768
49. Nishimura, T. (2015) Chipboard, oriented strand board (OSB) and structural composite lumber. in *Wood Composites*, pp. 103–121, Elsevier, 10.1016/B978-1-78242-454-3.00006-8
50. Guo, M., Stuckey, D. C., and Murphy, R. J. (2013) Is it possible to develop biopolymer production systems independent of fossil fuels? Case study in energy profiling of polyhydroxybutyrate-valerate (PHBV). *Green Chemistry*. **15**, 706
51. Zhou, W., Bergsma, S., Colpa, D. I., Euverink, G.-J. W., and Krooneman, J. (2023) Polyhydroxyalkanoates (PHAs) synthesis and degradation by microbes and applications towards a circular economy. *Journal of Environmental Management* **341**, 118033
52. Ahuja, V., Singh, P. K., Mahata, C., Jeon, J.-M., Kumar, G., Yang, Y.-H., and Bhatia, S. K. (2024) A review on microbes mediated resource recovery and bioplastic (polyhydroxyalkanoates) production from wastewater. *Microbial Cell Factories* **23**, 187
53. Thomas, A. P., Kasa, V. P., Dubey, B. K., Sen, R., and Sarmah, A. K. (2023) Synthesis and commercialization of bioplastics: Organic waste as a sustainable feedstock. *Science of The Total Environment*. **904**, 167243
54. Li, Y., Tao, L., Wang, Q., Wang, F., Li, G., and Song, M. (2023) Potential Health Impact of Microplastics: A Review of Environmental Distribution, Human Exposure, and Toxic Effects. *Environment & Health*. **1**, 249–257
55. Koller, M., Heeney, D., and Mukherjee, A. (2025) Biodegradability of polyhydroxyalkanoate (PHA) biopolyesters in nature: a review. *Biodegradation*. **36**, 76
56. Salinas, A., McGregor, C., Irorere, V., Arenas-López, C., Bommareddy, R. R., Winzer, K., Minton, N. P., and Kovács, K. (2022) Metabolic engineering of Cupriavidus necator H16 for heterotrophic and autotrophic production of 3-hydroxypropionic acid. *Metabolic Engineering* **74**, 178–190

57. Vajente, M., Clerici, R., Ballerstedt, H., Blank, L. M., and Schmidt, S. (2024) Using *Cupriavidus necator* H16 to Provide a Roadmap for Increasing Electroporation Efficiency in Nonmodel Bacteria. *ACS Synthetic Biology* 10.1021/acssynbio.4c00380
58. Kim, S., Jang, Y. J., Gong, G., Lee, S.-M., Um, Y., Kim, K. H., and Ko, J. K. (2022) Engineering Cupriavidus necator H16 for enhanced lithoautotrophic poly(3-hydroxybutyrate) production from CO2. *Microbial Cell Factories* **21**, 231
59. Pan, H., Wang, J., Wu, H., Li, Z., and Lian, J. (2021) Synthetic biology toolkit for engineering Cupriviadus necator H16 as a platform for CO2 valorization. *Biotechnology for Biofuels*. **14**, 212
60. Ehsaan, M., Baker, J., Kovács, K., Malys, N., and Minton, N. P. (2021) The pMTL70000 modular, plasmid vector series for strain engineering in Cupriavidus necator H16. *Journal of Microbiological Methods*. **189**, 106323
61. Arhar, S., Rauter, T., Stolterfoht-Stock, H., Lambauer, V., Kratzer, R., Winkler, M., Karava, M., Kourist, R., and Emmerstorfer-Augustin, A. (2024) CO2-based production of phytase from highly stable expression plasmids in Cupriavidus necator H16. *Microbial Cell Factories* **23**, 9
62. Alagesan, S., Hanko, E. K. R., Malys, N., Ehsaan, M., Winzer, K., and Minton, N. P. (2018) Functional Genetic Elements for Controlling Gene Expression in Cupriavidus necator H16. *Applied Environmental Microbiology* 10.1128/AEM.00878-18
63. Mishra, S., Perkovich, P. M., Mitchell, W. P., Venkataraman, M., and Pfleger, B. F. (2024) Expanding the synthetic biology toolbox of Cupriavidus necator for establishing fatty acid production. *Journal of Industrial Microbiology Biotechnology* 10.1093/jimb/kuae008
64. Friedrich, B., Hogrefe, C., and Schlegel, H. G. (1981) Naturally occurring genetic transfer of hydrogen-oxidizing ability between strains of Alcaligenes eutrophus. *Journal of Bacteriology* **147**, 198–205
65. Raberg, M., Volodina, E., Lin, K., and Steinbüchel, A. (2018) Ralstonia eutropha H16 in progress: Applications beside PHAs and establishment as production platform by advanced genetic tools. *Critical Reviews in Biotechnology* **38**, 494–510
66. Aneja, K. K., Ashby, R. D., and Solaiman, D. K. Y. (2009) Altered composition of Ralstonia eutropha poly(hydroxyalkanoate) through expression of PHA synthase from Allochromatium vinosum ATCC 35206. *Biotechnology Letters* **31**, 1601–1612
67. Tee, K. L., Grinham, J., Othusitse, A. M., González-Villanueva, M., Johnson, A. O., and Wong, T. S. (2017) An Efficient Transformation Method for the Bioplastic-Producing "Knallgas" Bacterium *Ralstonia eutropha* H16. *Biotechnology Journal* 10.1002/biot.201700081
68. Krüsemann, J. L., Rainaldi, V., Cotton, C. A., Claassens, N. J., and Lindner, S. N. (2023) The cofactor challenge in synthetic methylotrophy: bioengineering and industrial applications. *Current Opinions in Biotechnology* **82**, 102953
69. Nielsen, J. R., Weusthuis, R. A., and Huang, W. E. (2023) Growth-coupled enzyme engineering through manipulation of redox cofactor regeneration. *Biotechnology Advances* **63**, 108102
70. Biswal, T., Shadangi, K. P., Sarangi, P. K., and Srivastava, R. K. (2022) Conversion of carbon dioxide to methanol: A comprehensive review. *Chemosphere*. **298**, 134299
71. Chen, F. Y.-H., Jung, H.-W., Tsuei, C.-Y., and Liao, J. C. (2020) Converting Escherichia coli to a Synthetic Methylotroph Growing Solely on Methanol. *Cell*. **182**, 933-946.e14
72. Keller, P., Reiter, M. A., Kiefer, P., Gassler, T., Hemmerle, L., Christen, P., Noor, E., and Vorholt, J. A. (2022) Generation of an Escherichia coli strain growing on methanol via the ribulose monophosphate cycle. *Nature Communications* **13**, 5243

73. Zarnt, G., Schräder, T., and Andreesen, J. R. (1997) Degradation of tetrahydrofurfuryl alcohol by Ralstonia eutropha is initiated by an inducible pyrroloquinoline quinone-dependent alcohol dehydrogenase. *Applied Environmental Microbiology* **63**, 4891–4898
74. Sará-Páez, M., Contreras-Zentella, M., Gómez-Manzo, S., González-Valdez, A. A., Gasca-Licea, R., Mendoza-Hernández, G., Escamilla, J. E., and Reyes-Vivas, H. (2015) Purification and Characterization of the Membrane-Bound Quinoprotein Glucose Dehydrogenase of Gluconacetobacter diazotrophicus PAL 5. *Protein Journal* **34**, 48–59
75. Franz, A., Rehner, R., Kienle, A., and Grammel, H. (2012) Rapid selection of glucose-utilizing variants of the polyhydroxyalkanoate producer Ralstonia eutropha H16 by incubation with high substrate levels. *Letters in Applied Microbiology* **54**, 45–51
76. Schlegel, H. G., and Gottschalk, G. (1965) Utilization of glucose by a mutant of *hydrogenomonas* H16. *Biochemische Zeitschrifte* **341**, 249–59
77. Cozier, G. E., and Anthony, C. (1995) Structure of the quinoprotein glucose dehydrogenase of *Escherichia coli* modelled on that of methanol dehydrogenase from *Methylobacterium extorquens*. *Biochemical Journal*. **312**, 679–685
78. Raberg, M., Peplinski, K., Heiss, S., Ehrenreich, A., Voigt, B., Döring, C., Bömeke, M., Hecker, M., and Steinbüchel, A. (2011) Proteomic and Transcriptomic Elucidation of the Mutant *Ralstonia eutropha* G $^{+}$ 1 with Regard to Glucose Utilization. *Applied Environmental Microbiology* **77**, 2058–2070
79. Raberg, M., Kaddor, C., Kusian, B., Stahlhut, G., Budinova, R., Kolev, N., Bowien, B., and Steinbüchel, A. (2012) Impact of each individual component of the mutated PTSNag on glucose uptake and phosphorylation in Ralstonia eutropha G+1. *Appl. Microbiological Biotechnology* **95**, 735–744
80. Cao, Z., Tan, T., Zhang, Y., Han, L., Hou, X., Ma, H., and Cai, J. (2018) NagRBt Is a Pleiotropic and Dual Transcriptional Regulator in Bacillus thuringiensis. *Frontiers in Microbiology* 10.3389/fmicb.2018.01899
81. Bertram, R., Rigali, S., Wood, N., Lulko, A. T., Kuipers, O. P., and Titgemeyer, F. (2011) Regulon of the N-acetylglucosamine utilization regulator NagR in Bacillus subtilis. *Journal of Bacteriology* **193**, 3525–36
82. Lin, Y., and Ng, I. (2025) Rewiring Cupriavidus necator for Enhanced Polyhydroxybutyrate Production via Genetic Toolkits and Feeding Strategy. *Biotechnology and Bioengineering* **122**, 2535–2545
83. Weng, C., Tang, R., Peng, X., and Han, Y. (2023) Co-conversion of lignocellulose-derived glucose, xylose, and aromatics to polyhydroxybutyrate by metabolically engineered Cupriavidus necator. *Bioresource Technology* **374**, 128762
84. Duine, J. A., Jzn., J. F., and Van Zeeland, J. K. (1979) Glucose dehydrogenase from *Acinetobacter calcoaceticus*. *FEBS Lett.* **108**, 443–446
85. Imanaga, Y., Hirano-Sawatake, Y., Arita-Hashimoto, Y., Itou-Shibouta, Y., and Katoh-Semba, R. (1979) On the cofactor of glucose dehydrogenase of Pseudomonas fluorescens. *Proceedings of the Japan Academy, Series B*. **55**, 264–269
86. Yamada, M., Sumi, K., Matsushita, K., Adachi, O., and Yamada, Y. (1993) Topological analysis of quinoprotein glucose dehydrogenase in Escherichia coli and its ubiquinone-binding site. *Journal of Biological Chemistry* **268**, 12812–7
87. van Schie, B. J., Hellingwerf, K. J., van Dijken, J. P., Elferink, M. G., van Dijl, J. M., Kuenen, J. G., and Konings, W. N. (1985) Energy transduction by electron transfer via a pyrrolo-quinoline quinone-dependent glucose dehydrogenase in Escherichia coli, Pseudomonas aeruginosa, and Acinetobacter calcoaceticus (var. lwoffi). *Journal of Bacteriology* **163**, 493–499

88. Niederpruem, D. J., and Doudoroff, M. (1965) Cofactor-Dependent Aldose Dehydrogenase of *Rhodopseudomonas spheroides*. *Journal of Bacteriology* **89**, 697–705
89. Hauge, J. G. (1964) Glucose Dehydrogenase of Bacterium anitratum: an Enzyme with a Novel Prosthetic Group. *Journal of Biological Chemistry*. **239**, 3630–3639
90. Anthony, C., and Zatman, L. (1964) The microbial oxidation of methanol. 1. Isolation and properties of Pseudomonas sp. M 27. *Biochemical Journal*. **92**, 609–614
91. Duine, J. A. (1999) The PQQ story. *J. Biosci. Bioeng.* **88**, 231–236
92. Anthony, C., and Zatman, L. (1967) The microbial oxidation of methanol. The prosthetic group of the alcohol dehydrogenase of *Pseudomonas* sp. M27: a new oxidoreductase prosthetic group. *Biochemical Journal*. **104**, 960–969
93. Salisbury, S. A., Forrest, H. S., Cruse, W. B. T., And Kennard, O. (1979) A novel coenzyme from bacterial primary alcohol dehydrogenases. *Nature*. **280**, 843–844
94. Duine, J. A., Frank Jzn, J., And Verwiel, P. E. J. (1980) Structure and Activity of the Prosthetic Group of Methanol Dehydrogenase. *European Journal of Biochemistry* **108**, 187–192
95. National Center for Biotechnology Information (2025) PubChem Compound Summary for CID 1024, Pyrroloquinoline Quinone. *PubChem*. [online] https://pubchem.ncbi.nlm.nih.gov/compound/1024 (Accessed October 29, 2025)
96. PubChem Compound Summary for CID 3035424, Tryptophan tryptophylquinone. (2025) *National Center for Biotechnology Information*. [online] https://pubchem.ncbi.nlm.nih.gov/compound/Tryptophan-tryptophylquinone. (Accessed November 8, 2025)
97. PubChem Compound Summary for CID 71464600, Cysteine tryptophylquinone. (2025) *National Center for Biotechnology Information* . [online] https://pubchem.ncbi.nlm.nih.gov/compound/Cysteine-tryptophylquinone.Copy (Accessed November 8, 2025)
98. Satoh, A., Kim, J.-K., Miyahara, I., Devreese, B., Vandenberghe, I., Hacisalihoglu, A., Okajima, T., Kuroda, S., Adachi, O., Duine, J. A., Van Beeumen, J., Tanizawa, K., and Hirotsu, K. (2002) Crystal Structure of Quinohemoprotein Amine Dehydrogenase from Pseudomonas putida. *Journal of Biological Chemistry*. **277**, 2830–2834
99. Davidson, V. L. (2000) Methylamine Dehydrogenase Structure and Function of Electron Transfer Complexes. in *Enzyme-Catalyzed Electron and Radical Transfer*, pp. 119–143, Kluwer academic/ Plenum Publishers, **35**, 119–143
100. Dooley, D. M. (1999) Structure and biogenesis of topaquinone and related cofactors. *JBIC Journal of Biological Inorganic Chemistry*. **4**, 1–11
101. ANTHONY, C. (1996) Quinoprotein-catalysed reactions. *Biochemical Journal*. **320**, 697–711
102. Zhu, W., and Klinman, J. P. (2020) Biogenesis of the peptide-derived redox cofactor pyrroloquinoline quinone. *Current Opinions in Chemistry and Biology* **59**, 93–103
103. Meulenberg, J. (1990) Cloning of Klebsiella pneumoniae pqq genes and PQQ biosynthesis in Escherichia coli. *FEMS Microbiology Letters* **71**, 337–343
104. Goosen, N., Vermaas, D. A., and van de Putte, P. (1987) Cloning of the genes involved in synthesis of coenzyme pyrrolo-quinoline-quinone from Acinetobacter calcoaceticus. *Journal of Bacteriology* **169**, 303–307
105. Biville, F., Mazodier, P., Turlin, E., and Gasser, F. (1989) Mutants of Methylobacterium organophilum unable to synthesize PQQ. *Antonie Van Leeuwenhoek*. **56**, 103–107

106. Biville, F., Turlin, E., and Gasser, F. (1989) Cloning and Genetic Analysis of Six Pyrroloquinoline Quinone Biosynthesis Genes in Methylobacterium organophilum DSM 760. *Microbiology (N. Y).* **135**, 2917–2929
107. Goosen, N., Huinen, R. G., and van de Putte, P. (1992) A 24-amino-acid polypeptide is essential for the biosynthesis of the coenzyme pyrrolo-quinoline-quinone. *Journal of Bacteriology* **174**, 1426–1427
108. Morris, C. J., Biville, F., Turlin, E., Lee, E., Ellermann, K., Fan, W. H., Ramamoorthi, R., Springer, A. L., and Lidstrom, M. E. (1994) Isolation, phenotypic characterization, and complementation analysis of mutants of Methylobacterium extorquens AM1 unable to synthesize pyrroloquinoline quinone and sequences of pqqD, pqqG, and pqqC. *Journal of Bacteriology* **176**, 1746–1755
109. Houck, D. R., Hanners, J. L., Unkefer, C. J., van Kleef, M. A. G., and Duine, J. A. (1989) PQQ: Biosynthetic studies inMethylobacterium AM1 andHyphomicrobium X using specific13C labeling and NMR. *Antonie Van Leeuwenhoek*. **56**, 93–101
110. Velterop, J. S., Sellink, E., Meulenberg, J. J., David, S., Bulder, I., and Postma, P. W. (1995) Synthesis of pyrroloquinoline quinone in vivo and in vitro and detection of an intermediate in the biosynthetic pathway. *Journal of Bacteriology* **177**, 5088–5098
111. Ramamoorthi, R., and Lidstrom, M. E. (1995) Transcriptional analysis of pqqD and study of the regulation of pyrroloquinoline quinone biosynthesis in Methylobacterium extorquens AM1. *Journal of Bacteriology* **177**, 206–211
112. Goosen, N., Horsman, H. P., Huinen, R. G., and van de Putte, P. (1989) Acinetobacter calcoaceticus genes involved in biosynthesis of the coenzyme pyrrolo-quinoline-quinone: nucleotide sequence and expression in Escherichia coli K-12. *Journal of Bacteriology* **171**, 447–455
113. Meulenberg, J. J. M., Sellink, E., Riegman, N. H., and Postma, P. W. (1992) Nucleotide sequence and structure of the Klebsiella pneumoniae pqq operon. *Molecular and General Genetics* **232**, 284–294
114. Wecksler, S. R., Stoll, S., Tran, H., Magnusson, O. T., Wu, S., King, D., Britt, R. D., and Klinman, J. P. (2009) Pyrroloquinoline Quinone Biogenesis: Demonstration That PqqE from *Klebsiella pneumoniae* Is a Radical *S* -Adenosyl- 1-methionine Enzyme. *Biochemistry*. **48**, 10151–10161
115. Yang, H., McDaniel, E. C., Impano, S., Byer, A. S., Jodts, R. J., Yokoyama, K., Broderick, W. E., Broderick, J. B., and Hoffman, B. M. (2019) The Elusive 5′-Deoxyadenosyl Radical: Captured and Characterized by Electron Paramagnetic Resonance and Electron Nuclear Double Resonance Spectroscopies. *Journal of the American Chemical Society* **141**, 12139–12146
116. Boswinkle, K., McKinney, J., and Allen, K. D. (2022) Highlighting the Unique Roles of Radical *S* -Adenosylmethionine Enzymes in Methanogenic Archaea. *Journal of Bacteriology* 10.1128/jb.00197-22
117. Saichana, N., Tanizawa, K., Ueno, H., Pechoušek, J., Novák, P., and Frébortová, J. (2017) Characterization of auxiliary iron–sulfur clusters in a radical *S* -adenosylmethionine enzyme PqqE from *Methylobacterium extorquens* AM1. *FEBS Open Bio*logy **7**, 1864–1879
118. Wecksler, S. R., Stoll, S., Iavarone, A. T., Imsand, E. M., Tran, H., Britt, R. D., and Klinman, J. P. (2010) Interaction of PqqE and PqqD in the pyrroloquinoline quinone (PQQ) biosynthetic pathway links PqqD to the radical SAM superfamily. *Chemical Communications*. **46**, 7031
119. Barr, I., Stich, T. A., Gizzi, A. S., Grove, T. L., Bonanno, J. B., Latham, J. A., Chung, T., Wilmot, C. M., Britt, R. D., Almo, S. C., and Klinman, J. P. (2018) X-ray and EPR

Characterization of the Auxiliary Fe–S Clusters in the Radical SAM Enzyme PqqE. *Biochemistry*. **57**, 1306–1315
120. Grell, T. A. J., Goldman, P. J., and Drennan, C. L. (2015) SPASM and Twitch Domains in S-Adenosylmethionine (SAM) Radical Enzymes. *Journal of Biological Chemistry*. **290**, 3964–3971
121. Zhu, W., Walker, L. M., Tao, L., Iavarone, A. T., Wei, X., Britt, R. D., Elliott, S. J., and Klinman, J. P. (2020) Structural Properties and Catalytic Implications of the SPASM Domain Iron–Sulfur Clusters in *Methylorubrum extorquens* PqqE. *Journal of the Americal Chemical Society* **142**, 12620–12634
122. Zhu, W., Iavarone, A. T., and Klinman, J. P. (2024) Hydrogen–Deuterium Exchange Mass Spectrometry Identifies Local and Long-Distance Interactions within the Multicomponent Radical SAM Enzyme, PqqE. *ACS Central Science* **10**, 251–263
123. Shen, Y.-Q., Bonnot, F., Imsand, E. M., RoseFigura, J. M., Sjölander, K., and Klinman, J. P. (2012) Distribution and Properties of the Genes Encoding the Biosynthesis of the Bacterial Cofactor, Pyrroloquinoline Quinone. *Biochemistry*. **51**, 2265–2275
124. Sonnhammer, E. (1998) Pfam: multiple sequence alignments and HMM-profiles of protein domains. *Nucleic Acids Resources* **26**, 320–322
125. Martins, A. M., Latham, J. A., Martel, P. J., Barr, I., Iavarone, A. T., and Klinman, J. P. (2019) A two-component protease in Methylorubrum extorquens with high activity toward the peptide precursor of the redox cofactor pyrroloquinoline quinone. *Journal of Biological Chemistry*. **294**, 15025–15036
126. Gliese, N., Khodaverdi, V., and Görisch, H. (2010) The PQQ biosynthetic operons and their transcriptional regulation in Pseudomonas aeruginosa. *Archives of Microbiology* **192**, 1–14
127. Tu, X., Latham, J. A., Klema, V. J., Evans, R. L., Li, C., Klinman, J. P., and Wilmot, C. M. (2017) Crystal structures reveal metal-binding plasticity at the metallo-β-lactamase active site of PqqB from Pseudomonas putida. *JBIC Journal of Biological Inorganic Chemistry*. **22**, 1089–1097
128. Koehn, E. M., Latham, J. A., Armand, T., Evans, R. L., Tu, X., Wilmot, C. M., Iavarone, A. T., and Klinman, J. P. (2019) Discovery of Hydroxylase Activity for PqqB Provides a Missing Link in the Pyrroloquinoline Quinone Biosynthetic Pathway. *Journal of the American Chemical Society* **141**, 4398–4405
129. Magnusson, O. T., Toyama, H., Saeki, M., Schwarzenbacher, R., and Klinman, J. P. (2004) The Structure of a Biosynthetic Intermediate of Pyrroloquinoline Quinone (PQQ) and Elucidation of the Final Step of PQQ Biosynthesis. *Journal of the American Chemical Society* **126**, 5342–5343
130. Liu, Y., and Liu, Y. (2022) Computational Study of Aromatic Hydroxylation Catalyzed by the Iron-Dependent Hydroxylase PqqB Involved in the Biosynthesis of Redox Cofactor Pyrroloquinoline Quinone. *Inorganic Chemistry* **61**, 5943–5956
131. Magnusson, O. T., Toyama, H., Saeki, M., Rojas, A., Reed, J. C., Liddington, R. C., Klinman, J. P., and Schwarzenbacher, R. (2004) Quinone biogenesis: Structure and mechanism of PqqC, the final catalyst in the production of pyrroloquinoline quinone. *Proceedings of the National Academy of Sciences of the United States of America* **101**, 7913–8
132. Magnusson, O. Th., RoseFigura, J. M., Toyama, H., Schwarzenbacher, R., and Klinman, J. P. (2007) Pyrroloquinoline Quinone Biogenesis: Characterization of PqqC and Its H84N and H84A Active Site Variants. *Biochemistry*. **46**, 7174–7186
133. Wan, H., Xia, Y., Li, J., Kang, Z., and Zhou, J. (2017) Identification of transporter proteins for PQQ-secretion pathways by transcriptomics and proteomics analysis in

Gluconobacter oxydans WSH-003. *Frontiers in Chemistry Science and Engineering* **11**, 72–88
134. van Kleef, M. A., and Duine, J. A. (1989) Factors relevant in bacterial pyrroloquinoline quinone production. *Applied Environmental Microbiology* **55**, 1209–1213
135. Hantke, K., and Friz, S. (2022) The TonB dependent uptake of pyrroloquinoline-quinone (PQQ) and secretion of gluconate by Escherichia coli K-12. *Molecular Microbiology* **118**, 417–425
136. Ho, J. V., and Cotruvo, J. A. (2019) A Periplasmic Binding Protein for Pyrroloquinoline Quinone. *Biochemistry*. **58**, 2665–2669
137. Nikaido, H. (2003) Molecular Basis of Bacterial Outer Membrane Permeability Revisited. *Microbiology and Molecular Biology Reviews*. **67**, 593–656
138. Thompson, P. J., Boggs, D. G., Wilson, C. A., Bruchs, A. T., Velidandla, U., Bridwell-Rabb, J., and Olshansky, L. (2024) Structure-driven development of a biomimetic rare earth artificial metalloprotein. *Proceedings of the National Academy of Sciences*. 10.1073/pnas.2405836121
139. Ochsner, A. M., Hemmerle, L., Vonderach, T., Nüssli, R., Bortfeld-Miller, M., Hattendorf, B., and Vorholt, J. A. (2019) Use of rare-earth elements in the phyllosphere colonizer *Methylobacterium extorquens* PA1. *Molecular Microbiology* **111**, 1152–1166
140. Saichana, N., Tanizawa, K., Pechoušek, J., Novák, P., Yakushi, T., Toyama, H., and Frébortová, J. (2016) PqqE from Methylobacterium extorquens AM1: a radical S-adenosyl-l-methionine enzyme with an unusual tolerance to oxygen. *Journal of Biochemistry* **159**, 87–99
141. Neijssel, O. M. (1987) PQQ-linked enzymes in enteric bacteria. *Microbiological Science* **4**, 87–90
142. Matsushita, H. T. M. Y. O. K. (2002) Quinoproteins: structure, function, and biotechnological applications. *Appied Microbiology and Biotechnology* **58**, 13–22
143. Matsushita, K., Arents, J. C., Bader, R., Yamada, M., Adachi, O., and Postma, P. W. (1997) Escherichia coli is unable to produce pyrroloquinoline quinone (PQQ). *Microbiology (N. Y).* **143**, 3149–3156
144. McIntire, W. S. (1998) Newly Discovered Redox Cofactors: Possible Nutritional, Medical, and Pharmacological Relevance to Higher Animals. *Annu. Rev. Nutr.* **18**, 145–177
145. Braun, V. (1995) Energy-coupled transport and signal transduction through the Gram-negative outer membrane via TonB-ExbB-ExbD-dependent receptor proteins. *FEMS Microbiology Reviews* **16**, 295–307
146. Munder, F., Voutsinos, M., Hantke, K., Venugopal, H., and Grinter, R. (2025) High-affinity PQQ import is widespread in Gram-negative bacteria. *Science Advances* 10.1126/sciadv.adr2753
147. Sará-Páez, M., Contreras-Zentella, M., Gómez-Manzo, S., González-Valdez, A. A., Gasca-Licea, R., Mendoza-Hernández, G., Escamilla, J. E., and Reyes-Vivas, H. (2015) Purification and Characterization of the Membrane-Bound Quinoprotein Glucose Dehydrogenase of Gluconacetobacter diazotrophicus PAL 5. *Protein journal.* **34**, 48–59
148. Meyer, M., Schweiger, P., and Deppenmeier, U. (2013) Effects of membrane-bound glucose dehydrogenase overproduction on the respiratory chain of Gluconobacter oxydans. *Applied Microbiology and Biotechnology.* **97**, 3457–3466
149. DSMZ Microorganisms 1129. Phototrophic Medium

150. Biebl, H., and Pfennig, N. (1981) Isolation of Members of the Family Rhodospirillaceae. in *The Prokaryotes*, pp. 267–273, *Springer Berlin Heidelberg*, Berlin, Heidelberg, 10.1007/978-3-662-13187-9_14
151. Chester, N., and Marshak, D. R. (1993) Dimethyl Sulfoxide-Mediated Primer Tm Reduction: A Method for Analyzing the Role of Renaturation Temperature in the Polymerase Chain Reaction. *Analitical Biochemistry* **209**, 284–290
152. Sokolova, I. (2018) Re: Determining pathlength for Beer's law with flat bottomed 96 well plates? *https://www.researchgate.net/post/Determining-pathlength-for-Beers-law-with-flat-bottomed-96-well-plates/5aeb0a6af677ba046e2ad70b/citation/download.* . [online] https://www.researchgate.net/post/Determining-pathlength-for-Beers-law-with-flat-bottomed-96-well-plates/5aeb0a6af677ba046e2ad70b/citation/download. (Accessed September 20, 2025)
153. Abramson, J., Adler, J., Dunger, J., Evans, R., Green, T., Pritzel, A., Ronneberger, O., Willmore, L., Ballard, A. J., Bambrick, J., Bodenstein, S. W., Evans, D. A., Hung, C.-C., O'Neill, M., Reiman, D., Tunyasuvunakool, K., Wu, Z., Žemgulytė, A., Arvaniti, E., Beattie, C., Bertolli, O., Bridgland, A., Cherepanov, A., Congreve, M., Cowen-Rivers, A. I., Cowie, A., Figurnov, M., Fuchs, F. B., Gladman, H., Jain, R., Khan, Y. A., Low, C. M. R., Perlin, K., Potapenko, A., Savy, P., Singh, S., Stecula, A., Thillaisundaram, A., Tong, C., Yakneen, S., Zhong, E. D., Zielinski, M., Žídek, A., Bapst, V., Kohli, P., Jaderberg, M., Hassabis, D., and Jumper, J. M. (2024) Accurate structure prediction of biomolecular interactions with AlphaFold 3. *Nature*. **630**, 493–500
154. Anthony, C. (2004) The quinoprotein dehydrogenases for methanol and glucose. *Archives of Biochemistry and Biophysics.* **428**, 2–9
155. Orita, I., Iwazawa, R., Nakamura, S., and Fukui, T. (2012) Identification of mutation points in Cupriavidus necator NCIMB 11599 and genetic reconstitution of glucose-utilization ability in wild strain H16 for polyhydroxyalkanoate production. *Journal of Bioscience and Bioengineering.* **113**, 63–69
156. Hye-Yeon Kim, Jin-Seo Park, Hyun-Dong Shin, and Yong-Hyun Lee (1995) Isolation of Glucose Utilizing Mutant of Alcaligenes eutrophus, its Substrate Selectivity, and Accumulation of Poly-β-hydroxybutyrate. *Journal of Microbiology*. **33**, 51–58
157. Schlegel, H. G., and Trüper, H. G. (1966) Repression of enzyme formation in Hydrogenomonas strain H16G+ by molecular hydrogen and by fructose. *Antonie Van Leeuwenhoek*. **32**, 277–292
158. Volodina, E., Raberg, M., and Steinbüchel, A. (2016) Engineering the heterotrophic carbon sources utilization range of *Ralstonia eutropha* H16 for applications in biotechnology. *Critical Reviews in Biotechnology.* **36**, 978–991
159. Delamarre, S. C., and Batt, C. A. (2006) Comparative study of promoters for the production of polyhydroxyalkanoates in recombinant strains of Wautersia eutropha. *Applied Microbiology and Biotechnology.* **71**, 668–679
160. Zhou, P., G C, B., Hu, B., and Wu, C. (2025) Development of SacB-based counterselection for efficient allelic exchange in Fusobacterium nucleatum. *Microbiology Spectrum.* 10.1128/spectrum.02066-24
161. Jahn, B., Jonasson, N. S. W., Hu, H., Singer, H., Pol, A., Good, N. M., den Camp, H. J. M. O., Martinez-Gomez, N. C., and Daumann, L. J. (2020) Understanding the chemistry of the artificial electron acceptors PES, PMS, DCPIP and Wurster's Blue in methanol dehydrogenase assays. *JBIC Journal of Biological Inorganic Chemistry*. **25**, 199–212

162. Goosen, N., Vermaas, D. A., and van de Putte, P. (1987) 1/ Cloning of the genes involved in synthesis of coenzyme pyrrolo-quinoline-quinone from Acinetobacter calcoaceticus. *Journal of Bacteriology.* **169**, 303–7
163. McIntire, W. S. (1998) NEWLY DISCOVERED REDOX COFACTORS: Possible Nutritional, Medical, and Pharmacological Relevance to Higher Animals. *Annual Review of Nutrition.* **18**, 145–177
164. Wickham-Smith, C., Malys, N., and Winzer, K. (2023) Improving carbon monoxide tolerance of Cupriavidus necator H16 through adaptive laboratory evolution. *Frontiers in Bioengineering and Biotechnology.* 10.3389/fbioe.2023.1178536
165. Park, S. J., Jang, Y.-A., Lee, H., Park, A.-R., Yang, J. E., Shin, J., Oh, Y. H., Song, B. K., Jegal, J., Lee, S. H., and Lee, S. Y. (2013) Metabolic engineering of Ralstonia eutropha for the biosynthesis of 2-hydroxyacid-containing polyhydroxyalkanoates. *Metabolic Engineering.* **20**, 20–28
166. Arikawa, H., and Matsumoto, K. (2016) Evaluation of gene expression cassettes and production of poly(3-hydroxybutyrate-co-3-hydroxyhexanoate) with a fine modulated monomer composition by using it in Cupriavidus necator. *Microbial Cell Factories.* **15**, 184
167. Insomphun, C., Xie, H., Mifune, J., Kawashima, Y., Orita, I., Nakamura, S., and Fukui, T. (2015) Improved artificial pathway for biosynthesis of poly(3-hydroxybutyrate-co-3-hydroxyhexanoate) with high C6-monomer composition from fructose in Ralstonia eutropha. *Metabolic Engineering.* **27**, 38–45
168. Jiang, R., Yuan, S., Zhou, Y., Wei, Y., Li, F., Wang, M., Chen, B., and Yu, H. (2024) Strategies to overcome the challenges of low or no expression of heterologous proteins in Escherichia coli. *Biotechnology Advances.* **75**, 108417
169. Yano, N., Emi, T., Gregory, D. J., and Fedulov, A. V. (2021) Consideration on Efficient Recombinant Protein Production: Focus on Substrate Protein-Specific Compatibility Patterns of Molecular Chaperones. *Protein Journal* **40**, 756–764
170. Yakushi, T., Komatsu, K., Matsutani, M., Kataoka, N., Vangnai, A. S., Toyama, H., Adachi, O., and Matsushita, K. (2018) Improved heterologous expression of the membrane-bound quinoprotein quinate dehydrogenase from Gluconobacter oxydans. *Protein Expression and Purification.* **145**, 100–107
171. Anthony, C. (2001) Pyrroloquinoline Quinone (PQQ) and Quinoprotein Enzymes. *Antioxidants and Redox Signaling.* **3**, 757–774
172. Takeda, K., Ishida, T., Yoshida, M., Samejima, M., Ohno, H., Igarashi, K., and Nakamura, N. (2019) Crystal Structure of the Catalytic and Cytochrome b Domains in a Eukaryotic Pyrroloquinoline Quinone-Dependent Dehydrogenase. *Applied Environmental Microbiology.* 10.1128/AEM.01692-19
173. Gandomkar, S., Rocha, R., Sorgenfrei, F. A., Montero, L. M., Fuchs, M., and Kroutil, W. (2021) PQQ-dependent Dehydrogenase Enables One-pot Bi-enzymatic Enantio-convergent Biocatalytic Amination of Racemic sec -Allylic Alcohols. *ChemCatChem*. **13**, 1290–1293
174. Yamada, M., Elias, M. D., Matsushita, K., Migita, C. T., and Adachi, O. (2003) Escherichia coli PQQ-containing quinoprotein glucose dehydrogenase: its structure comparison with other quinoproteins. *Biochimica et Biophysica Acta (BBA) - Proteins and Proteomics*. **1647**, 185–192